**University of Calgary**

**PRISM Repository** **https://prism.ucalgary.ca**

The Vault Open Theses and Dissertations

2015-03-16

# Experimental and Simulation Study of Relative Permeabilities in Heavy Oil/Water/Gas Systems

Modaresghazani, Jafar

Modaresghazani, J. (2015). Experimental and Simulation Study of Relative Permeabilities in Heavy Oil/Water/Gas Systems (Doctoral thesis, University of Calgary, Calgary, Canada). Retrieved from https://prism.ucalgary.ca. doi:10.11575/PRISM/26055

http://hdl.handle.net/11023/2116

*Downloaded from PRISM Repository, University of Calgary*

UNIVERSITY OF CALGARY

# Experimental and Simulation Study of Relative Permeabilities in Heavy Oil/Water/Gas Systems

by

Jafar Modaresghazani

A THESIS

SUBMITTED TO THE FACULTY OF GRADUATE STUDIES

IN PARTIAL FULFILMENT OF THE REQUIREMENTS FOR THE

DEGREE OF DOCTOR OF PHILOSOPHY

DEPARTMENT OF CHEMICAL AND PETROLEUM ENGINEERING

CALGARY, ALBERTA

MARCH, 2015

© JAFAR MODARESGHAZANI 2015

## ABSTRACT

An experimental study was conducted to investigate the relative permeability behaviour of a typical Canadian bitumen, water and gas. Series of isothermal core flood experiments were conducted on an unconsolidated core composed of cleaned Athabasca sand matrix and relative permeabilities of the involved phases were determined. Athabasca bitumen was used as the oil phase and distilled water and nitrogen were used as the water and gas phases respectively. A vertical sand-pack core-holder of 1.5 inch diameter and 2 feet long was designed and fabricated to perform sequential injection of oil, gas and water at reservoir temperature and pressure, while collecting information on pressure drop across the core and fluid volumes. The history match technique was used to determine relative permeabilities for two-phase and three-phase water/oil/gas systems.

Two-phase oil-water experiments were started with a primary drainage process followed by imbibition process and secondary drainage to assess the possible hysteresis effects on oil-water relative permeability. The secondary drainage process in which the core reaches the residual water saturation, was followed by gas injection till no further liquid was produced.

Three-phase flow was studied by first injecting a slug of oil into a gas flooded core. Then a slug of water was injected which was followed by continuous gas injection to simulate the three-phase flow inside the sand pack. Stone's first and second model and Baker's linear interpolation model were used to calculate the three-phase oil relative permeability in the three-phase flow experiment. Two-phase drainage water/oil and gas/liquid relative permeabilities were used as input for three-phase models to calculate the oil three-phase relative permeability.

Hysteresis was found to exist in both wetting-phase and non-wetting-phase relative permeability in two-phase water/oil systems. Overall, the individual phase relative permeability was higher when its saturation was increasing than when decreasing. Predicted values for oil and water production were in good agreement with experimental results for all drainage and imbibition two-phase oil/water experiments.

Gas/liquid relative permeabilities for gas injection into an oil-flooded core, showed low gas relative permeability compared to the liquid relative permeabilities by around two orders of magnitude. These relative permeabilities resulted in a close match for the produced liquid even though the gas production was slightly over predicted at higher gas saturations.

In three-phase oil/water/gas experiments, two-phase water/oil and liquid/gas relative permeabilities were used to calculate the three-phase oil relative permeabilities. Among the three examined models, Stone's second model produced the best prediction for liquid production and late time gas production even though the prediction of all of the models showed a significant deviation from experimental gas production during the early and middle time of the flood.

## ACKNOWLEDGEMENTS

I would like to thank the kind support and valuable guidance of Dr. R.G. Moore and Dr. S.A. Mehta who provided me a great opportunity to work with them.

I also appreciate the technical support of our former PVT lab manager Mr. Kees Van Fraassen, in designing and fabricating the experimental setup.

My gratitude is also with all the current and former staff of the In Situ Combustion Research Group, particularly with Matt Ursenbach, Mark Hancock, Don Mallory, Elizabeth Zalewski, Ligaya Aguinaldo, Lucy Molinos, George Nerier and Jed Gomes, for their friendship and valuable technical support.

Valuable assistance and technical support received from the engineering machine shop in fabricating the experimental setup is highly appreciated. My appreciation also goes toward the people in the Department of Chemical and Petroleum Engineering for all of their assistance.

This research work would not have been possible without the financial assistance of NSERC (PGS D) and the Department of Chemical and Petroleum Engineering and reservoir simulation software provided by CMG. Financial support received from scholarships including Queen Elizabeth II Graduate Scholarship, Edward Wichert Graduate Scholarship and ASME Pipeline System Division Award during the course of this study are highly appreciated.

Special thanks to Dr. Brij Maini for his instructions at the early stages of this project.

Special thanks to my family for their continuous support and love, especially to my wife Sara and to my parents.

# DEDICATION

To my parents

and

Sara

## TABLE OF CONTENTS

ABSTRACT ..... II

ACKNOWLEDGEMENTS ..... IV

DEDICATION ..... V

TABLE OF CONTENTS ..... VI
List of Tables ..... viii
List of Figures and Illustrations ..... ix
List of Symbols, Abbreviations and Nomenclature ..... xii
List of Subscripts ..... xiii

CHAPTER ONE: INTRODUCTION AND PROBLEM STATEMENT ..... 1
1.1 Introduction ..... 1
1.2 In situ combustion process ..... 2
1.3 Statements of problem and objectives of current study ..... 4
1.4 Organization of the thesis ..... 6

CHAPTER 2: CONCEPTS AND LITERATURE REVIEW ..... 8
2.1 Relative permeability concept ..... 8
2.2 Factors affecting relative permeability ..... 11
2.2.1 Effect of wettability ..... 13
2.2.2 Effect of saturation history ..... 15
2.2.3 Effect of temperature ..... 16
2.3 Measurement of relative permeability ..... 17
2.3.1 Steady state methods ..... 18
2.3.2 Unsteady-state methods ..... 19
2.4 Review of published data on relative permeability of heavy oils and bitumen ..... 25

CHAPTER 3: EXPERIMENTAL SETUP AND PROCEDURES ..... 32
3.1 Experimental apparatus details ..... 32
3.1.1 Description of sand pack and core holder ..... 32
3.1.1.1 Capillary end effects ..... 35
3.1.2 Injection system ..... 36
3.2.3 Pressure measurement and monitoring system ..... 37
3.2.4 Sample storage system ..... 38
3.2.5 Liquid and gas collecting system ..... 38
3.2.6 Data acquisition system ..... 39
3.2 Materials ..... 39
3.2.1 Porous medium ..... 39
3.2.2 Bitumen ..... 40
3.2.3 Water and gas ..... 41
3.3 Dead volume of the sand pack ..... 41
3.4 Porosity measurement ..... 42

3.4.1 Helium injection .....42
3.4.2 Water injection .....43
3.5 Absolute permeability of the sand pack.....44

CHAPTER 4: TWO-PHASE WATER-GAS EXPERIMENTS .....46
4.1 Outlook of water-gas experiments.....46
4.2 Description of experimental and analysis methods .....47
4.2.1 Steady-state method.....47
4.2.2 Unsteady state method.....49
4.2.3 Processing the raw data .....49
4.2.4 Determination of water/gas relative permeabilities by unsteady-state method51
4.2.5 Detailed calculation for a particular water/gas experiment .....52
4.3 Results and discussion .....56

CHAPTER FIVE: OIL/WATER/GAS EXPERIMENTS.....64
5.1 Introduction.....64
5.2 Description of simulation of core flood process .....65
5.2.1 Fluid model description.....66
5.2.2 Simulation model definition .....69
5.2.3 Preparing the field history files .....70
5.3 Two phase oil/water experiments .....71
5.3.1 Primary drainage process .....71
5.3.1.1 Collecting and analyzing the produced fluids.....72
5.3.1.2 Results and discussion .....73
5.3.2 Imbibition process .....80
5.3.2.1 Results and discussion .....81
5.3.3 Secondary drainage process .....84
5.3.4 Concluding remarks on two-phase oil/water experiments .....89
5.3.1 Hysteresis effects .....89
5.3.2 Comparison with literature .....92
5.4 Gas/liquid displacement.....96
5.4.1 Practical difficulties.....97
5.4.2 Results and discussion.....101
5.5 Three-phase water/oil/gas experiment .....103

CHAPTER 6: CONCLUSION AND RECOMMENDATIONS .....114
6.1 Summary.....114
6.2 Conclusions.....116
6.3 Recommendations for future work .....118

REFERENCES .....120

APPENDIX 1: EQUATIONS OF BUILT-IN THREE-PHASE RELATIVE PERMEABILITY MODELS IN CMG STARS .....125

**List of Tables**

Table 3.1 Absolute permeability measurement for sand pack ..... 45

Table 4.1 Viscosity and density of water and nitrogen at pressure of 500psi (3.45 MPa) and three different temperatures ..... 47

Table 4.2 End point saturations for drainage/imbibition processes in water/gas systems at different temperatures ..... 60

Table 4.3 End point relative permeabilities for drainage/imbibition processes in water/gas systems at different temperatures ..... 61

Table 4.4 Typical values and uncertainties of variables that appear in Darcy's equation to calculate the effective permeability of gas at 500 psi (3.45 MPa) ..... 63

Table 5.1 Summary of the two-phase and three-phase water/oil/gas floods ..... 65

Table 5.2 SimDist result for extracted oil sample ..... 67

Table 5.3 Properties of pseudo components used to characterize the oil ..... 68

Table 5.4 Viscosity of oil at 500 psi (3.45 MPa) and different temperatures ..... 69

Table 5.5 Parameters and constant values of Sigmund- McCaffery model for primary drainage at 80$^{o}$C ..... 76

Table 5.6 Mathematical equations of water and oil relative permeabilities from Sigmund-McCaffery model for primary drainage process ..... 77

Table 5.7 Parameters and constant values of Sigmund- McCaffery model for secondary drainage ..... 85

Table 5.8 Mathematical equations of water and oil relative permeabilities from original and modified Sigmund- McCaffery model for secondary drainage process ..... 85

**List of Figures and Illustrations**

Figure 1.1 Schematic diagram of the *in situ* combustion process illustrating how it would ideally occur between two vertical wells (Moore et al., 2007) ..... 3

Figure 2.1 A typical two-phase relative permeability curve for oil-water ..... 12

Figure 2.2 Hysteresis effect on a typical two-phase oil-water system for a strong water-wet reservoir ..... 17

Figure 3.1 Schematic of experimental core-flood apparatus ..... 33

Figure 3.2 Inner-face view of sand pack head showing the installed screen and distribution channels ..... 35

Figure 3.3 Schematic indicating the head of aluminum sleeve and dead volume ..... 42

Figure 4.1-Variation of differential pressure in steady-state experiment for water/gas at 40$^{o}$C .. 52

Figure 4.2 Average water saturation in steady-state experiment for water/gas at 40$^{o}$C ..... 53

Figure 4.3 Average gas saturation inside the core at unsteady state experiment for water/gas at 23$^{o}$C ..... 55

Figure 4.4 Average gas saturation versus number of pore volumes of gas injected at unsteady state experiment for water/gas at 23$^{o}$C ..... 55

Figure 4.5 A plot of 1QwIr vs 1Qw for a gas-water displacement at room temperature. Slope and regression constant are shown by fitting a straight line. ..... 56

Figure 4.6 Drainage relative permeability of water-gas at room temperature from unsteady-state method ..... 57

Figure 4.7 Drainage relative permeability of water-gas at room temperature by steady-state and unsteady-state method ..... 57

Figure 4.8 Drainage relative permeability of water-gas at 40$^{o}$C from unsteady-state method..... 58

Figure 4.9 Drainage relative permeability of water-gas at 40$^{o}$C by steady-state and unsteady-state method ..... 58

Figure 4.10 Drainage relative permeability of water-gas at 80$^{o}$C from unsteady-state method... 59

Figure 4.11 Drainage relative permeability of water-gas at 80$^{o}$C by steady-state and unsteady-state method ..... 59

Figure 4.12 Effect of temperature on relative permeabilities of water/gas ..... 62

Figure 5.1 Density-pressure data of oil measured at 80ºC ..... 68

Figure 5.2 Physical model of sand pack simulated as a cylinder with 56 grid blocks ..... 70

Figure 5.3 Injection and production pressure during oil injection in primary drainage process at 80ºC ..... 72

Figure 5.4 Extrapolation of produced water amount to infinite time ..... 74

Figure 5.5 Relative permeability of oil/water in primary drainage ..... 78

Figure 5.6 History match of water and oil production for primary drainage ..... 79

Figure 5.7 History match of pressure drop for primary drainage process ..... 80

Figure 5.8 Relative permeability of oil/water in imbibition process ..... 81

Figure 5.9 History match of water and oil production for imbibition process ..... 82

Figure 5.10 History match of pressure drop for imbibition process ..... 84

Figure 5.11 Relative permeability of oil/water in secondary drainage process ..... 86

Figure 5.12 History match results for produced oil and water in secondary drainage ..... 87

Figure 5.13 Injection and production pressure at secondary drainage ..... 88

Figure 5.14 Hysteresis of oil relative permeability in drainage and imbibition process ..... 90

Figure 5.15 Hysteresis on water relative permeability for drainage and imbibition process ..... 92

Figure 5.16 Comparison of imbibition relative permeabilities with Bennion's correlations ..... 94

Figure 5.17 Comparison of the water/bitumen relative permeabilities reported by Polikar et al. (1990) with current study ..... 95

Figure 5.18 Variation of injection pressure during liquid displacement by gas injection ..... 99

Figure 5.19 Variation of production pressure during liquid displacement by gas injection ..... 100

Figure 5.20 Relative permeability of gas/liquid in liquid displacement by gas injection at 80ºC ..... 101

Figure 5.21 History match results for produced liquid and gas in gas flood experiment ..... 102

Figure 5.22 Three-phase relative permeability of oil calculated by Stone's first model ..... 105

Figure 5.23 Three-phase relative permeability of oil calculated by Stone's second model ..... 106

Figure 5.24 Three-phase relative permeability of oil calculated by Baker's interpolation method ..... 107

Figure 5.25 Prediction of produced liquid and gas in three-phase system using the Stone's first model to calculate the oil relative permeability ..... 108

Figure 5.26 Prediction of injection pressure in three-phase system using the Stone's first model to calculate the oil relative permeability ..... 108

Figure 5.27 Prediction of produced liquid and gas in three-phase system using the Stone's second model to calculate the oil relative permeability ..... 109

Figure 5.28 Prediction of injection pressure in three-phase system using the Stone's second model to calculate the oil relative permeability ..... 109

Figure 5.29 Prediction of produced liquid and gas in three-phase system using the Bakers interpolation model to calculate the oil relative permeability ..... 110

Figure 5.30 Prediction of injection pressure in three-phase system using the Bakers interpolation model to calculate the oil relative permeability ..... 110

Figure 5.31 Comparison of the predicted values for produced liquid ..... 111

Figure 5.32 Comparison of the predicted values for produced gas ..... 112

## List of Symbols, Abbreviations and Nomenclature

| | |
|---|---|
| A | Cross sectional area of core($cm^2$) |
| D | Darcy, (unit of permeability) |
| f | Fractional flow rate in multiphase flow |
| g | Constant of gravity($cm/s^2$) |
| $I_r$ | Relative injectivity at JBN method |
| K | Absolute permeability (D) |
| $k_{rg}$ | Relative permeability of gas |
| $k_{ro}$ | Relative permeability of oil |
| $k_{rocw}$ | Relative permeability of oil at connate water saturation |
| $k_{rw}$ | Relative permeability of water |
| $k_{rnw}^{o}$ | End point value for relative permeability of non-water phase |
| $k_{rw}^{o}$ | End point value for relative permeability of water |
| L | Length of sand pack(cm) |
| $Q_g$ | Number of injected pore volumes of gas at JBN method |
| $Q_w$ | Number of injected pore volumes of water at JBN method |
| q | Flow rate($cm^3$/min) |
| $q_t$ | superficial velocity of total outlet flow, Buckley and Leverett theory |
| $S_{oir}$ | Irreducible oil saturation |
| $S_{wir}$ | Irreducible water saturation |
| $S_{org}$ | Residual oil saturation at gas flood(%PV) |
| $S_{orw}$ | Residual oil saturation at water flood(%PV) |
| $(s_w)_{min}$ | Irreducible water saturations in Sigmund- McCaffery correlation |
| $(s_w)_{max}$ | Maximum water saturations in Sigmund- McCaffery correlation |
| $s_e$ | Normalized saturation |
| $S_{wc}$ | Connate water saturation(%PV) |
| $s$ | Distance in direction of flow in Darcy's law |
| P | Pressure |
| u | Average velocity of approach toward the inlet of the sand face |

## Greek Symbols

| | |
|---|---|
| $\Delta P$ | Pressure drop |
| $\varepsilon_w$ | Wetting phase parameter in Sigmund -McCaffery correlation |
| $\varepsilon_{nw}$ | Non-wetting phase parameter in Sigmund- McCaffery correlation |
| $\theta$ | Angle of core central axis with horizontal direction |
| $\Phi$ | Fluid potential in general form of Darcy's law |
| $\varphi$ | Porosity |
| $\mu$ | Viscosity(cp) |
| $v$ | Darcy velocity |
| $\rho$ | Density($g/cm^3$) |

**List of Subscripts**

| | |
|---|---|
| w | Water |
| o | Oil |
| g | gas |
| $w_2$ | Water at outlet face of the core |
| $o_2$ | Oil at outlet face of the core |

# CHAPTER ONE: INTRODUCTION AND PROBLEM STATEMENT

## 1.1 Introduction

The Athabasca oil sands reservoir of northeastern Alberta which contains approximately 950 billion barrels of bitumen, is one of the world's largest reserves of accessible hydrocarbons. Although approximately 10 percent of the reservoir can be economically recovered by surface mining, the remainder of the bitumen must be removed from the sand by in situ recovery techniques.

In situ recovery of heavy oils and bitumens from oil sands often involves simultaneous flow of two or three immiscible fluids including oil, water and gas in the oil sands. Examples of recovery processes which involve three-phase flow include: *In Situ* Combustion, Water Alternating Gas injection (WAG), steam drive and Steam Assisted Gravity Drainage (SAGD). A new approach which has been drawing attention, is a hybrid SAGD-Combustion method which more likely is an efficient recovery method for Alberta oil sand reservoirs specially the Athabasca reservoir which has a very viscous bitumen (about one million centipoises) and low temperature of about 12$^{o}$C. In a hybrid SAGD-Combustion process, after running SAGD as primary recovery method, *In Situ* Combustion, runs as a secondary recovery process to produce more residual oil in place.

With continuous improvement in terms of speed and accuracy, computer assisted simulation has become a major tool for evaluating and predicting any typical reservoir performance. By integrating any recovery method into a typical reservoir simulator the feasibility and efficiency

of each recovery method can be evaluated and this would help choosing the most efficient recovery method in terms of economical, practical and environmental aspects.

For the *In Situ* Combustion Research Group (ISCRG) the major focus is on various aspects of the *in situ* combustion process. This recovery process is briefly reviewed in this section as it is required to highlight the relative permeability behavior of flowing phases in this study.

### 1.2 In situ combustion process

The *In Situ* Combustion (ISC) process is basically a burning front that slowly moves from an injection well to one or more production wells. The process is initiated by injecting air into the injection well surrounded by an array of production wells. After permeability development for gas, the burning front starts moving forward to the production wells. Either air or pure oxygen can be used to support burning. Oil is displaced by a vaporizing action of resulting front as well as the sweep provide by combustion product gases and hot water/steam. The process is fuelled by a small fraction of the oil generally believed to be the heavier components, which are burned as fuel by the advancing front. Figure 1.1 shows an idealized schematic of the *in situ* combustion process as it may occur using two vertical wells (Moore et al., 2007). As the combustion front moves away from the injection well, several distinct zones develop in the reservoir and a number of different but intimately related mechanisms start operating.

**Combustion zone:** The crude oil ahead of the high temperature burning front is carbonized to produce a coke-like deposit on the sand grains. This deposit constitutes the principle fuel for the process. The burning front leaves behind hot, clean rock that can be used effectively to heat the injected air. Maximum temperatures of 400 to 900ºC have been observed at the burning front.

**Thermal Cracking:** Further downstream of the burning zone, the temperature is high enough to vaporize the lighter hydrocarbons. These hydrocarbons then move forward into the reservoir and condense in the cold parts ahead. Near the burning front, the high temperature converts the interstitial water to steam. The steam also moves forward and condenses in the cooler sand ahead. Immediately ahead of the burning oil, high temperatures thermally crack the heavy hydrocarbons left on the sand. Products from this cracking are petroleum coke and gaseous hydrocarbons. The hydrocarbon gases move ahead of the front and partially condense in the cooler sand. The petroleum coke is deposited on the sand grains and becomes fuel for the process.

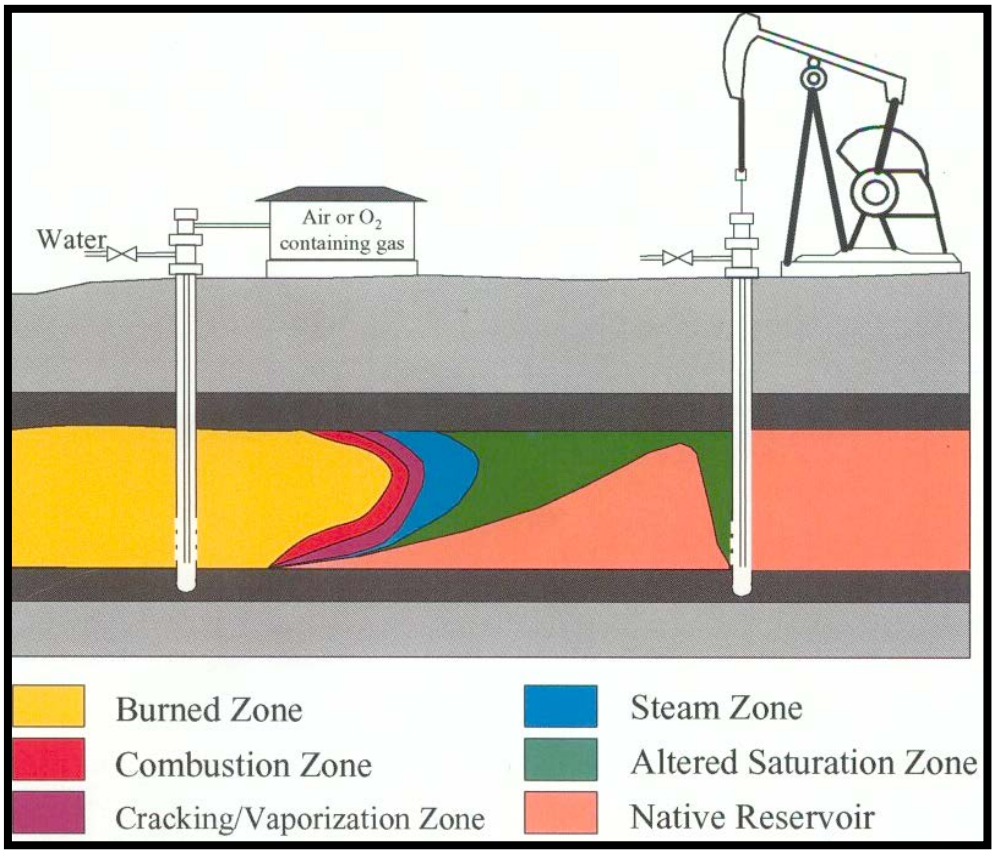


Figure 1.1 Schematic diagram of the *in situ* combustion process illustrating how it would ideally occur between two vertical wells (Moore et al., 2007)

**Condensing steam drive:** As the injected air reacts with the residual fuel at the burning front, steam is one of the products which forms. This steam, along with steam produced from interstitial water evaporation, moves forward and contacts the cooler sand ahead. The steam loses heat rapidly to the formation, and a condensing steam type drive results. The large amount of the latent heat released by the condensing steam imparts substantial energy to the oil in and ahead of the steam zone. The viscosity of the oil decreases greatly and mobility increases, which in turn enhances oil displacement.

**Miscible drive:** Hydrocarbon gases evolved from normal distillation; mix with the hydrocarbon gases formed in the cracking reaction. These streams condense and blend in the oil bank ahead. This blending action and the heat imported to the oil when the gases condense; make the oil more mobile and improves oil displacement.

**Gas drive:** An effective gas drive mechanism forms during the burning process. Combustion gases, generated at the burning front, transfer some heat to the oil. Carbon dioxide partially dissolves in the oil and reduces the viscosity further. The oil bank that forms ahead of the steam zone is displaced physically by combustion gases.

### 1.3 Statements of problem and objectives of current study

In mathematical simulation of any recovery processes the concept of relative permeability is used to describe the characteristics of the multi-phase flow in porous media which is a complex phenomenon. Among the input data for a reservoir simulator the relative permeability associated

with every flowing phase is one of the most important data. Having the right relative permeability data for a reservoir would generate more accurate oil recovery predictions.

Compared to the extensive studies and published data available in the literature on relative permeability of light and heavy oils, there is scarcity of published experimental studies on relative permeability of bitumen in oil sand reservoirs. Considering bitumen recovery processes which are currently in-use or the potential ones, having realistic knowledge into the relative permeability behavior of flowing phases involved in a typical bitumen reservoir is a very important step toward the reservoir performance prediction and the efficiency of associated recovery process.

The objective of this research is to study and evaluate the relative permeability of existing fluids in an unconsolidated sand pack. This type of sand pack is meant to be a simplified version of a typical Alberta oil sand reservoir such as the Athabasca reservoir. The oil was selected to be a bitumen sample from the Athabasca reservoir as well, to make the lab scale core as similar to a typical oil sand reservoir as possible. Among the various recovery methods for a bitumen containing reservoir, our main interest in this study was to evaluate the relative permeability characteristics in operating conditions typical of a relatively cold zone which exist down-stream of an *in situ* combustion process. Even though this recovery method may be applicable in a typical oil sand reservoir as a secondary recovery method such as post SAGD process, getting a more clear insight toward the nature of flowing phases and their relative permeability was a major goal sought after, in this study.

The first experimental determination of relative permeability was reported in the early 1940s for light oil reservoirs. Measurements were performed either by steady-state co-injection method or unsteady-state technique. The later, has drawn more attention due to being faster and less

cumbersome. However each method has its own limitations and usually there are some simplifications in terms of experimental conditions such as using a small core plugs, sieved and reconstituted sand packs and refined oil samples instead of native reservoir cores. Traditionally relative permeability curves have been experimentally determined for two phase systems and the results were expanded for three phase by using mathematical models. The objective was to make the experimental setup as similar to a typical oil sand reservoir as possible; therefore the porous medium was intended to be real reservoir sand. Among the various saturation directions which exist during a typical gas injection process in two-phase or three-phase systems the ones which are more common during a typical combustion process, were selected to replicate in flood tests during the course of this study.

### 1.4 Organization of the thesis

Having Chapter one of this thesis devoted to background and objectives, in Chapter two some basic concepts and definitions as well as literature and previous studies are reviewed. Chapter two also includes the review of measurement methods of relative permeability and the factors which may affect it. At the end of Chapter two, the published literature on relative permeability of heavy oils and bitumen are summarized.

Chapter three includes the detailed description of the experimental setup which was designed and fabricated to conduct the core flood experiments. Detail description of various parts of the experimental setup as well as the characteristics of materials which were used in this study are explained. This chapter concludes with methods used to determine the required physical properties of the sand pack such as porosity and absolute permeability.

Chapter four of the thesis presents the first series of core flood experiments which include water/gas relative permeability. Steady-state and unsteady-state methods were used in these series of experiments and the details of each method are elaborated. Eventually the results from both methods are presented and compared. All water/gas experiments have been conducted at three different temperature and possible effects of temperature which ranges from room temperature up to 80$^{o}$C on relative permeability were investigated.

Oil/water experiments are presented in Chapter five. Both drainage and imbibition saturation change are explained and relative permeabilities which are determined from history match technique are presented along with the fluid production history. Water/oil experiments followed by gas injection into oil flooded core and associated relative permeability and fluid production of gas/liquid is determined by history match. In the last part of Chapter five the three-phase oil/water/gas flow and the resulting relative permeabilities are determined and presented.

The last chapter which is Chapter six, is assigned for Conclusions and Recommendations.

The units which are used in this thesis are a combination of SI units and Field units. Variables such as temperature, volume, flow rates, are reported in SI units but only the pressure is expressed in Field unit as pound per square inch (Psi). The reason is that in most of the oil laboratories this unit is used to monitor and measure the pressure and from the practical point of view it is more convenient to monitor the pressure in Field unit. However the equivalent value of pressure in SI unit is mentioned in a bracket right after the reported value in Psi. All of the reported pressure values are gauge pressures by default unless denoted as absolute pressure by Psia.

# CHAPTER 2: CONCEPTS AND LITERATURE REVIEW

## 2.1 Relative permeability concept

Mathematical description of fluid flow through a porous environment was first introduced by Henry Darcy in early 1850s by measuring the water flow rate through a sand pack filter. Darcy found out that the water flow rate q, through a vertical sand pack with cross-sectional area A and length L can be describe with the following correlation:

$$q = KA\frac{h_i - h_o}{L} \tag{2-1}$$

where $h_i$ and $h_o$ are the hydrostatic heads at the inlet and outlet of the sand pack and K is a constant. Even though Darcy's experiments were restricted to a sand pack which is fully saturated with water, later investigators found that Darcy's law is applicable to any fluid flow through a porous medium with some modifications. One of the modifications was that the constant K can be replaced by $k/\mu$ in which $\mu$ is the viscosity of the flowing fluid and k is a property of the porous material that is called permeability. By following a simple dimensional analysis, it can be shown that the permeability has the unit of length squared, and it was named Darcy to honor Henry Darcy. Physical meaning of Darcy unit may be easily described by considering a single-phase fluid with viscosity of 1 cP and flow rate of 1 $cm^3$ per second flowing through a porous material with cross section of 1 $cm^2$ under the pressure drop of 1 atm per

centimeter. In this case the porous material would have the permeability of 1 Darcy. The major requirement of this definition is that all of the pore space has to be saturated completely by a single flowing fluid. A more general form of Darcy's law for a single-phase, incompressible fluid under laminar flow would be:

$$v = -\frac{k\rho}{\mu}\frac{d\Phi}{dx} \tag{2-2}$$

where $\Phi = \frac{P}{\rho} + gz$ is the fluid potential.

In a typical oil reservoir, single phase flow barely occurs and obviously more modification will be needed to apply the Darcy's law into multi-phase flow. To obtain a more useful form of Darcy's law which has been widely accepted and used in reservoir engineering, it might be assumed that a typical rock has an effective permeability to each flowing fluid which includes oil, water and gas. The effective permeability of rock to any fluid with 100% saturation would be called the absolute permeability of that rock.

In reservoir engineering calculations, the ratio of effective permeability of each phase to a base value is used and it called relative permeability. This base value might be selected as either absolute permeability of rock or effective permeability to oil at residual water saturation. By this definition, relative permeability would be a dimensionless parameter and usually it is considered as a single-valued function of fluid saturation even though it depends on several other factors as it will be shown in a later section. In fact the relative permeability is a measure of the fractional loss of hydraulic conductivity for a given fluid due to the presence of other immiscible fluids in the porous medium. If the base value was selected as the absolute permeability of rock, for a system containing three immiscible phases, water, oil and gas, the new form of Darcy's law for each phase can be restated as:

$$v_o = \frac{kk_{ro}}{\mu_o}\left(\rho_o g \frac{dZ}{dS} - \frac{dP_o}{dS}\right) \tag{2-3a}$$

$$v_w = \frac{kk_{rw}}{\mu_w}\left(\rho_w g \frac{dZ}{dS} - \frac{dP_w}{dS}\right) \tag{2-3b}$$

$$v_g = \frac{kk_{rg}}{\mu_g}\left(\rho_g g \frac{dZ}{dS} - \frac{dP_g}{dS}\right) \tag{2-3c}$$

where the subscripts o, w and g, represent the oil, water and gas, respectively and s denotes the distance in direction of flow which is taken as positive. In this general form of Darcy's law $k_{ro}$ , $k_{rw}$ and $k_{rg}$ are the relative permeability of the three fluid phases at their respective saturations inside the rock and the direction of flow is taken as positive. Note that because of the interference of the phases present in multi-phase flow in porous medium, the total flow capacity of the porous environment will be reduced and that means the summary of effective relative permeability of flowing phases usually does not add up to unity:

$$\sum k_{ri} \leq 1 \tag{2-4}$$

There are several reasons for this interference. One factor is that the size of available flow passage in pore channels for each phase, shrinks due to the presence of other phases. Another reason is the blockage of some pore channels by immobile droplets of one of the present phases which restricts or completely prevents the flow of other phases. Also the capillary forces impede the flow by temporarily blocking the pore throats if the pressure gradient is lower than a certain amount.

## 2.2 Factors affecting relative permeability

The relative permeability concept was first postulated by Muskat and Meres who extended Darcy's law to two-phase systems (Honarpor 1986). In reservoir engineering terminology, the most common combinations of relative permeability for two-phase fluid are water-oil and liquid-gas. However gas-water relative permeabilities are used to describe the performance of gas reservoirs while gas-liquid are used for condensate reservoirs. Two-phase water-oil relative permeability is usually plotted versus water saturation. A general form is depicted in Figure 2.1. In this schematic graph, $S_{wc}$ denotes the irreducible water saturation which in most reservoirs is equivalent to connate water saturation. Water relative permeability reaches zero at $S_{wc}$ and this is the lowest saturation in which water is mobile. At this point only oil can flow even though the capacity of porous medium to oil flow is reduced because of the presence of the second immobile phase. In a similar manner $S_{orw}$ is the residual oil saturation which implies the minimum oil saturation could be encountered during a waterflood and oil phase reaches zero mobility at this saturation. In general as water saturation increases, water relative permeability increases while the oil relative permeability decreases.

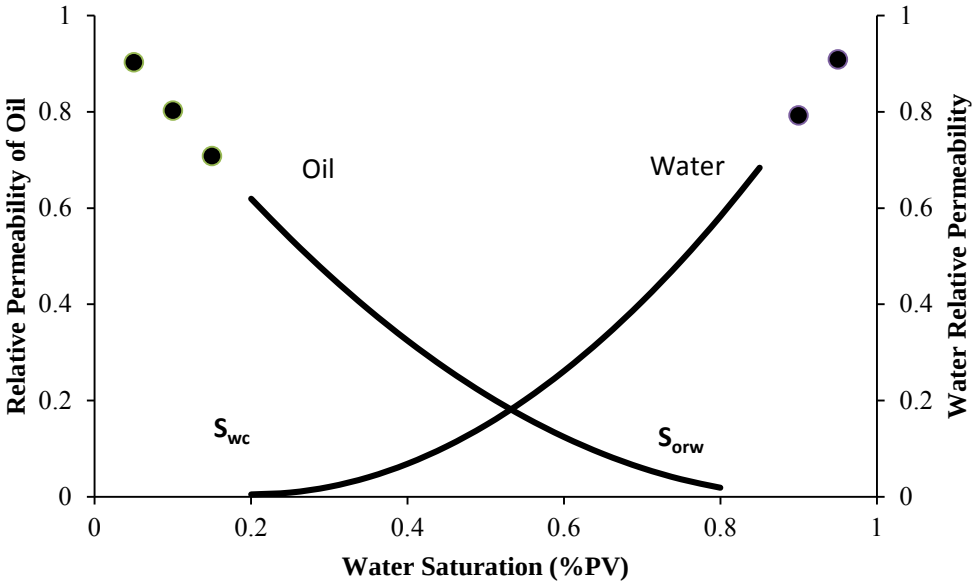


Figure 2.1 A typical two-phase relative permeability curve for oil-water

During the assessment of performance of an actual hydrocarbon reservoir, the left-side of irreducible water saturation and right side of the residual oil saturation is not encountered and has no significance. Based on this fact, there is an alternative definition for relative permeability which is currently used by many authors. According to this definition, the value of relative permeability of oil at irreducible water saturation is assumed to be unity therefore absolute permeability is defined as the effective permeability at irreducible water saturation. Based on this definition in an aquifer, relative permeability of water is greater than unity. By this alternate definition, relative permeabilities are normalized to the value at irreducible water saturation. (Honarpour 1986)

Several factors can affect the relative permeability in a porous environment. There has been extensive research by various authors on the factors which have an influence on relative

permeability such as wettability, fluid saturation, rock physical properties, saturation history or hysteresis, temperature, viscosity and interfacial tension even though the influence of some of these factor, especially the effect of temperature for instance, has been a matter of controversy as there is no unanimous agreement in published literature. However in this section a few of the factors whose influence on relative permeability is obvious, are reviewed with some details.

### 2.2.1 Effect of wettability

When a solid surface is in contact with two or more immiscible fluids, the relative attraction of each fluid on to the solid surface can be described by the concept of wettability. Wettability can be best described by the concept of a contact angle formed between a droplet of a fluid and a flat solid surface. By definition the contact angle is the angle formed between the tangent to a drop surface where it intersects with the solid in a horizontal direction. Conventionally the contact angle is measured through the liquid and its value ranges from zero to $180^o$. Zero contact angle represent complete wettability which means the liquid can spread completely on the solid surface while $180^o$ value for contact angle indicates that the liquid has no tendency to spread on the solid surface and it is totally a non-wetting fluid with respect to that solid surface. In general depending on whether the value of contact angle is lower or greater than $90^o$ the fluid is referred to as wetting or non-wetting respectively. In a typical hydrocarbon reservoir, in terms of wettability, a formation can be described as water-wet, intermediate or oil-wet. In a virgin reservoir, microscopic fluid distribution is determined by degree of rock preferential wettability. When the reservoir is strongly water-wet, the inside space of dead-end pores and small capillaries are filled with water and it covers the grain surface as well. In contrast, in a strongly

oil-wet formation, surface of grains is coated with oil while water resides in the center space of large pores as discontinuous drops. Therefore a strongly water-wet formation favors the movement of the non-wetting phase through pore space and this results in high effective permeability of the non-wetting phase at irreducible water saturation which is approximately equal to absolute permeability. In the opposite case in which the reservoir is strongly oil-wet, at irreducible water saturation, the presence of water droplets in large pores reduces the effective permeability to oil. The effect of wettability of reservoir rock on multiphase flow has been recognized in the petroleum industry for a long period of time. Preferential wettability of rock is known to have a large influence on the non-symmetrical shape of the relative permeability curves and therefore the relationship between saturation and relative permeability. For instance when the rock wettability for water declines, at a given saturation the relative permeability to oil declines as well, while the water relative permeability increases.

However there are contradictory results in the literature describing the effect of preferential wettability on relative permeability of oil and water. While there are findings that as rock gets less water wet, relative permeability becomes less favorable to oil production, some other reports showed that weakly water wet cores have lower residual oil saturations and more favorable oil relative permeabilities than strongly water-wet or oil-wet rocks. However this later behavior conceptually seems reasonable as in strongly water-wet cores, the capillary forces are strong and water is imbibed into smaller pores. The oil may be by-passed and trapped in larger pores and get surrounded by water which coats the surface and as a result, the oil will become immobile unless a very high pressure gradient exists across the pore channels to push it out. Under this condition a narrow saturation interval for two-phase flow would be encountered. But as the preferential wettability of rock changes from strong water wet into intermediate values, the capillary forces

become weaker and rapid trapping of oil in large pores should become less favorable. This makes the saturation interval for two-phase flow broader and leads to lower residual oil saturation. Based on the study published by McCaffery and Bennion (1974), relatively wide changes of wettability created a negligible effect on relative permeability, even though some other authors (Treiber 1972) reported that even a small variation in wettability produces considerable effects on relative permeability.

### 2.2.2 Effect of saturation history

It was mentioned earlier that relative permeability is often expressed as a function of saturation however such a functionality is not unique and it depends on the direction of saturation change. In other words, at a given saturation, the relative permeability of a porous environment to a given fluid, depends on whether that saturation has been reached by departing from lower or higher former saturation values. This behavior is sometimes referred to as saturation history effect or hysteresis. In a typical displacement process, when the wetting phase saturation is moving from lower to higher values, the resulting relative permeability curve is referred to as imbibition which implies an increase in wetting phase saturation. Injection of water during a water flood process is a good example of an imbibition process. In an opposite case when the saturation of the wetting phase has been reached by moving down from higher values, the relative permeability curve is called drainage relative permeability. Water-flooding an oil-wet reservoir and displacement of oil during the primary depletion of reservoir, are two examples of drainage process. The effect of hysteresis is more prominent for non-wetting phase relative permeability than relative permeability of wetting phase. A typical hysteresis effect on relative permeability for two-phase oil-water system is shown on Figure 2.2. For a strong water-wet rock, water drainage and

imbibition relative permeabilities are essentially equal, however for the non-wetting phase, the relative permeability of drainage is higher than the relative permeability for imbibition. On a microscopic scale, the cause of hysteresis is believed to be related to pore size distribution. During water imbibition when water invades the oil-filled pores of different sizes, and pushes the oil out, oil rejection continues as long as there are still continuous escape paths available for oil. But during a drainage process these continuous escape paths re-establish at higher oil saturation which results in higher relative permeability to drainage process.

### 2.2.3 Effect of temperature

Investigating the effect of temperature on relative permeability, has received considerable attention since the mid-50s and despite the extensive published studies, there is no unanimous agreement among different authors as they reported contradictory results. Some of the studies which found relative permeability independent of temperature, have suggested that most of the reported temperature effects can be attributed to artifacts of the unsteady–state technique. Maini and Okazawa (1987) used an unsteady-state method to measure the relative permeability of heavy oil and water systems over a temperatures range starting from room temperature to 200 degree Celsius and reported that the relative permeability varies with temperature. However in another study by Polikar et al. (1990) the relative permeabilities of water and Athabasca bitumen at temperatures ranging from 100 to 250 degree Celsius were measured and the conclusion was that temperature has little or no effect on relative permeability.

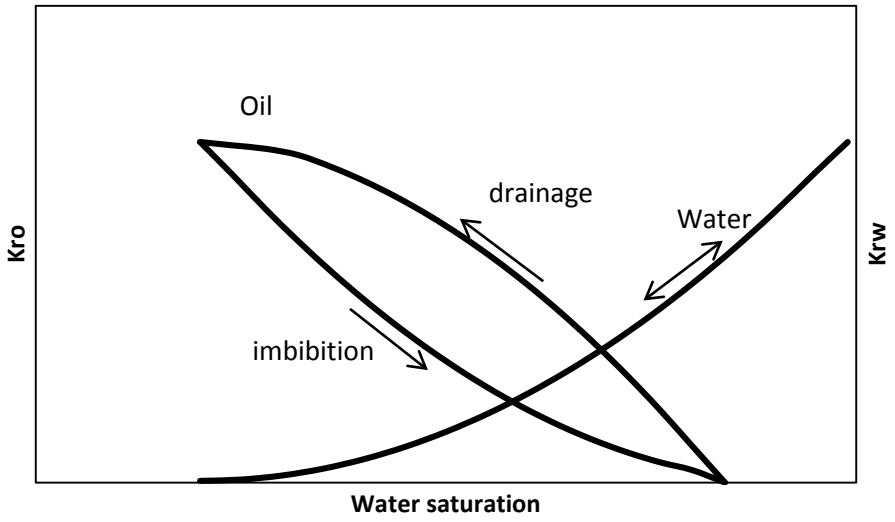


Figure 2.2 Hysteresis effect on a typical two-phase oil-water system for a strong water-wet reservoir

## 2.3 Measurement of relative permeability

Various methods have been developed to determine the experimental values of relative permeability for two-phase and three-phase systems. Two commonly used categories are steady-state methods and unsteady-state methods. Two other categories which were used in literature (Honarpour 1986) are capillary pressure methods and centrifuge methods. In all of these methods, either a consolidated or unconsolidated core sample might be used as representative of the real reservoir. The steady-state method involves simultaneous injection of a fixed ratio of fluids through the test sample until reaching a steady pressure drop and uniform saturation across the core. In the unsteady-state methods, also called displacement methods, fluids are injected one by one in a certain sequence with one or two fluids being displaced by the injecting fluid depending on the sequence under investigation. Capillary pressure methods were developed mostly for drainage relative permeability calculations and include the injection of a non-wetting

phase such as gas to displace a wetting phase such as water or oil. A typical capillary pressure method generates the capillary pressure curve of a core sample which is required to calculate the relative permeability of the core through certain equations. Several equations are available in the literature. (Honarpour 1986)

In the centrifuge technique, the core sample is initially saturated uniformly with two phases and then put under the centrifuge force. The produced liquids from the core sample are collected in transparent tubes which are connected to the core holder and overall production is monitored throughout the test (Honarpour 1986). Main advantage of centrifuge methods is that they are faster than the regular steady-state methods and they are not subjected to unfavorable viscous fingering effects. However in general, centrifuge methods have not been widely used.

In the current study, both steady-state and unsteady-state techniques were used to measure the relative permeability therefore more detailed review of these two methods are presented in following section.

### 2.3.1 Steady state methods

In steady-state methods a fixed ratio of fluids is injected through the test sample to obtain a uniform pressure drop and saturation across the core sample. These methods offer flexibility in controlling the saturation and several injection ratios might be employed to cover the whole saturation range. Several techniques were proposed and employed in the literature to obtain uniform saturation across the core sample. A major difficulty in designing the steady state methods is how to deal with so called capillary end effects at the outlet face of the core sample.

One of the best methods which has been widely used, is the so called Penn-State method proposed by Morse et al. in 1947 and later modified by several other investigators. The core

sample consists of three segments: front, middle and end segment. Middle segment is the main sample on which the relative permeabilities are measured. The front segment provides complete mixing of flowing phases before they enter the middle segment and performs a uniform distribution while the end segment reduces the capillary end effect at the outlet face of the middle segment. Experiment starts with saturating all three samples with one phase, for instance water, and flowing under a certain constant pressure drop. Then the second phase injection such as gas starts while slightly reducing the flow rate of the water and trying to maintain the initial pressure drop. After maintaining the equilibrium condition, the flow rates of two phases and pressure drop are recorded. Saturation of the primary sample needs to be measured to complete the data required to determine the relative permeability. However there are some difficulties associated with measuring the saturation across the middle segment. Having the primary sample removed out of the core holder and measuring its weight was the first method used. Other alternative methods to determine the water saturation without removing the primary sample from the core holder is measuring the electric resistivity of the primary sample. Some other *in situ* methods to determine the core saturation are electric capacitance, nuclear magnetic resonance, X-ray absorption and gamma-ray absorption. By using this approach end points and few middle point relative permeabilities can be determined however it is a time consuming approach to determine a complete range of relative permeability curves.

### 2.3.2 Unsteady-state methods

In view of the time-consuming nature of steady state methods, unsteady state methods which involve displacing one or two phases by a third injected phase, are faster and easier to run. Unsteady methods are also considered to be more representative of how the displacement

process occurs during a typical oil recovery in terms of rapid saturation change at non-equilibrium state. However these methods are more difficult to interpret and more complicated to analyze mathematically. Generally the theory developed by Buckley and Leverett (1942) and later extended by Welge (1952) are widely accepted and used to determine the relative permeability of flowing phases by using the raw data extracted from an unsteady-state experiment. The basic mathematical analysis in this approach, is a combination of Darcy's law with a definition of capillary pressure developed by Leverett (1941) to obtain the following correlation for fractional flow of water at the outlet face of the core:

$$f_{w2} = \frac{1+\frac{K_0}{q_t \mu_0}\left(\frac{\partial P_c}{\partial x} - g\Delta\rho \, sin\theta\right)}{1+\frac{k_o}{k_w}.\frac{\mu_w}{\mu_o}} \tag{2-5}$$

where $q_t$ is the superficial velocity of total outlet flow out of the core, $\Delta\rho$ is the density difference between displacing and displaced fluids, and $\theta$ is the angle of core central axis with the horizontal direction. For negligible capillary pressure and a horizontal core, a simplified version of this equation, first derived by Welge (1852), is

$$S_{w.avg} - S_{w2} = f_{o2} Q_w \tag{2-6}$$

where $S_{w.avg}$ is the average water saturation and $Q_w$ is the cumulative water injected in pore volumes and subscript 2 denotes the outlet face of the core. In equation 2-6, $S_{w.avg}$ and $Q_w$ can be determined through experimental injection data by a simple mass balance and then by plotting

$Q_w$ versus $S_{w.avg}$ , the slope would be the fractional flow of oil at the outlet face of the core $f_{o2}$ which is defined as

$$f_{o2} = \frac{q_o}{q_o + q_w} \tag{2-7}$$

This equation can be combined with Darcy's law to get a new equation to calculate the ratio of relative permeability of oil and water:

$$f_{o2} = \frac{1}{1 + \frac{\mu_o / k_{ro}}{\mu_w / k_{rw}}} \tag{2-8}$$

By calculating the $f_{o2}$ from Equation 2-6 and having the viscosities of the oil and water at operating conditions, the ratio of relative permeabilities of oil and water ${k_{ro}}/{k_{rw}}$ can be determined from Equation 2-8. For any other two-phase system such as gas-oil or gas-water, a similar expression can be derived simply by replacing the corresponding subscribes in equations 2-5 to 2-8. However only the ratio of the two relative permeabilities can be determined by using the Welge approach and in most cases there is a high interest toward calculating the individual relative permeability of each flowing phase. One extension of the Welge approach which was developed by Johnson et al. (1959), made it possible to determine the individual relative permeability of each phase. Their proposed method which is known as JBN method, has drawn intensive attention and is used by many researcher. By introducing the relative injectivity of core sample designated by $I_r$, they came up with the following correlation to estimate the relative permeability of the displacing and displaced phase. In the case of water displacing oil, the $k_{ro}$ and $k_{rw}$ can be determined from the following equations:

$$k_{ro} = \frac{f_{o2}}{d\left(\frac{1}{Q_w I_r}\right)/d\left(\frac{1}{Q_w}\right)} \tag{2-9}$$

$$k_{rw} = \frac{f_{w2}}{f_{o2}} \frac{\mu_w}{\mu_o} k_{ro} \tag{2-10}$$

According to the JBN method, the relative injectivity $I_r$ describes the manner in which the intake capacity varies with cumulative injection. From a physical point of view, relative injectivity can be considered as the ratio of intake capacity of the core sample at any instance during the injection process to the intake capacity of the system at the starting moment of the injection at which only oil is flowing through the system. Therefore the $I_r$ can be determined through the following equation

$$I_r = \frac{(u/_{\Delta P})\ at\ any\ stage\ of\ flood}{(u/_{\Delta P})\ at\ start\ of\ flood} \tag{2-11}$$

where $u$ is the average velocity of approach toward the inlet of the sand face. For a water flood it will be equal to the injection flow rate of water divided by the cross sectional area of the core sample.

There are two conditions which have to be satisfied for the JBN method to be applicable for any core flood experiment (Johnson et al., 1959). First the flow velocity has to be high enough to reach a stabilized displacement and second, the flow velocity remains constant at all cross sections of the core. In stabilized displacement the pressure drop across the core is high compared to the capillary pressure difference between two flowing phases. When the pressure drop across the core is high the pore volume with dominant capillary pressure will be restricted into a very small portion of the total pore volume. Having a constant velocity at all cross sectional area of the core requires having immiscible and incompressible flowing fluids and

when one of the phases is gas, to be as close as possible to incompressible assumption, the operating pressure must be sufficiently high compared to the pressure drop across the core.

After introduction of the JBN method several other techniques have been developed by different investigators to calculate individual two-phase and three-phase relative permeability from displacement data. The first technique to calculate the three phase relative permeability from displacement data was proposed by Sarem in 1966. This method was basically an extension of JBN method to three phase systems. Similar to the JBN method, the effect of capillary forces on saturation distribution across the core was neglected in Sarem's method and the capillary end effect was not taken into account as well. Another major assumption to calculate the three-phase relative permeabilities was that the relative permeability of each phase is a function of its own saturation only and does not depend on saturation of other phases.

In a similar approach Donaldson and Dean (1966) proposed a technique to calculate the three-phase relative permeabilities from displacement data which did not include two major simplifying assumptions of Sarem's method. They were neglecting the capillary effects and dependence of relative permeability of each phase on its own saturation.

Sarem's major assumption that relative permeability of each phase depends only on its own saturation, was criticized by Saraf and Fatt (1967) who used the magnetic resonance technique to monitor liquid saturations in unsteady-state displacement experiments. Based on their report, only the relative permeability of water was a function of its own saturation and was independent of the saturation of oil and gas. However oil relative permeability was reported to be a function of both oil and water while gas relative permeability was found to be a function of the total liquid saturation inside the core.

It was reported in a later study by Saraf et al. (1982) that relative permeability of porous medium to oil was dependent on saturation of all present phases. Effect of saturation direction and hysteresis were also investigated in this study and while no hysteresis effect was reported on relative permeability of water, relative permeability of gas was found to be strongly dependent on the direction of saturation.

Sigmund and McCaffery (1979) developed a technique to determine the two-phase relative permeabilities of heterogeneous reservoirs by an unsteady state method. They analyzed the pressure drop and recovery response obtained from the unsteady state method by a nonlinear least square technique. By making a step change in the inlet flow rate to the core, a saturation wave propagates through the core and arrives at the outlet end of the core. Transient pressure behavior and the displaced fluid recovery response were recorded during this transient process. This transient process which can be described in terms of the Buckley-Leverett incompressible two-phase flow equation was simplified by using finite-difference approximation. The observed pressure and recovery response was then analized to obtain relative permeabilities by fitting the approximated form of the Buckley-Leverett equation using a nonlinear least-square method. Relative permeability curves for water and oil were assumed to be correlated as two unknown parameters, $\varepsilon_w$ and $\varepsilon_{nw}$. These parameters reflect the shape of wetting and nonwetting relative permeability relations which are defined by the following correlations:

$$k_{rw} = k_{rw}^{o}\left(\frac{(s_e)^{\varepsilon_w} + As_e}{1+A}\right) \tag{2-12}$$

$$k_{rnw} = k_{rnw}^{o}\left(\frac{(1-s_e)^{\varepsilon_{nw}} + B(1-s_e)}{1+B}\right) \tag{2-13}$$

where normalized saturation $s_e$ is defined as:

$$s_e = \frac{s_w - (s_w)_{min}}{(s_w)_{max} - (s_w)_{min}} \quad (2\text{-}14)$$

$k_{rw}^o$ and $k_{rnw}^o$ are the end point values of relative permeability curves and A and B are constants with value of 0.01 and were used for computational purposes to linearized the relative permeability curves as they approach zero. $(s_w)_{min}$ and $(s_w)_{max}$ are the irreducible and maximum water saturations. The authors (Sigmund and McCaffery ,1979) reported a significant capillary effect on recovery and pressure response in some examined cases and concluded that the capillary forces are most likely to have significant effects on low-rate displacements in the drainage direction.

## 2.4 Review of published data on relative permeability of heavy oils and bitumen

Any experimental method to determine the relative permeability of a system which involves heavy oil or bitumen is more difficult and more time consuming than the same method when employed on a light oil system. Therefore there are very few published experimental data on heavy oil systems compared with the extensive published data for light oils in the literature. In this section the published data on heavy oils and bitumen systems with more focus on oil-sands and heavy oil deposits in Alberta are reviewed.

Primary experimental measurement of relative permeability of heavy oils have been conducted by the Alberta Research Council on Athabasca bitumen and by the Petroleum Recovery Institute on Lloydminster heavy oil. Later on, more studies were conducted on various Alberta deposits by other investigators which will be reviewed in the current section.

Waxman et al. (1980) studied the flow of Peace River tar through Peace river cores at elevated temperature. For some of the studied core samples, the relative permeabilities were determined by using the steady-state method. This study continued later by Closmann et al. (1985) with the aim of measuring the relative permeability of tar-water on Peace River preserved cores at elevated temperatures. They employed the steady-state method to determine the relative permeability and used electrical resistance of each core sample to measure the water saturation. Three types of tar were used in their experiment which included unaltered tar, thermally altered tar and deasphalted tar. They reported a dependency of relative permeabilities on the previous thermal history of the tar. They also found that the relative permeability of unaltered tar is shifted toward the region of low water saturation, while that for thermally altered tar is closer to the oil permeability curve for water-wet unconsolidated sands, reported by Leverett (1939). However oil permeability for deasphalted tar lies at an intermediate saturation between those of thermally altered and unaltered tar.

Maini and Batycky (1985) conducted unsteady state tests on preserved core plugs over a temperature range from room temperature to 272$^{o}$C, to measure the relative permeabilities of oil and water. They used both horizontally and vertically drilled core plugs to determine the effect of flow direction on relative permeability and on their temperature dependence. Unsteady-state method was employed to carry out the displacement tests and by recording the pressure drop and production data, relative permeabilities were determined through a history match by using a technique which was developed by Sigmund and McCaffery (1979).

Their results showed that both end point saturations and end point relative permeabilities were affected by temperature. Although the dependence of residual oil saturation on temperature was less clear they found that water saturation increased with increasing temperature. However the

residual oil saturation was found to be decreasing up to a certain temperature, beyond which it starts increasing. End point effective permeability to water appeared to be independent of temperature while the endpoint effective permeability to oil decreased with increasing temperature. In terms of the influence of direction of coring, they found that the effective permeability of oil is one or two orders of magnitude lower in vertically drilled plugs compared with horizontally drilled plugs. However in both directions, endpoint water relative permeability of water was reported to be similar.

Greaser and Shore (1980) evaluated the steam flood performance at the Kern River field in California which is a heavy oil reservoir with viscosity of 4000 cp at reservoir condition. They reported values for endpoint relative permeabilities at two temperatures but did not mention the source of these data and the method used to determine them. In a later study by Leung (1983), end point relative permeability data for Athabasca bitumen were determined through history matching the performance of a steam-stimulation well and the results were compared with Kern River field study by Greaser and Shore (1980) however complete relative permeability curves were not obtained in this study.

In a study published by Settari and Raisbeck (1981) two-phase relative permeability data for oil and water was used to model hydraulic fracturing during the cyclic steam stimulation in an oil sand reservoir. They emphasize the effect of three-phase relative permeability during the early stages of production but their model was not capable of simulating the three-phase flow. Their data was derived from analyzing the production history of a field pilot.

Dietrich (1986) developed a numerical model for cyclic steam stimulation of Canadian and German tar sands through hydraulically induced fractures. For relative permeability, he used

power law expressions for drainage and imbibition processes and took into account the hysteresis effects.

Maini and Sayegh (1983) conducted an experimental study on Lloydminster heavy oil reservoir to evaluate the so called $CO_2$ huff-n-puff process. As a part of their experimental work, they performed core floods to determine the relative permeability of oil/water and gas/water at reservoir conditions. As porous medium, they used an unconsolidated core which was prepared from a fresh core sample drilled from the Lloydminster reservoir. The oil and brine samples were also collected from the same formation. The oil sample was cleaned by centrifugation to separate water and fine clays. They used the displacement method to run the core flood tests and used a history match technique to determine the two-phase relative permeabilities. These authors derived an analytical relation between effective gas permeability and gas saturation and another one between effective oil permeability and gas saturation at residual water saturation.

Bennion et al. (1985) measured the relative permeabilities of water and oil for a preserved core from a Sparky Sand in the Lloydminster area. They compared their results with those reported for an extracted and mineral-oil-saturated core from the same formation. They ran a series of water floods and oil floods at three different temperatures and measured endpoint permeabilities of water and oil. The relative permeabilities were calculated by history match using a two-phase numerical simulator and a non-linear least square regression procedure. Hysteresis was reported on both oil and water relative permeabilities. Both sets of relative permeabilities were used to evaluate the performance of a single cycle steam stimulation process. They found that the simulation which used the relative permeabilities measured from preserved core, was able to provide a closer match to field water production than the simulation using the extracted core relative permeabilities. Endpoint saturation and relative permeabilities were reported by Adam

(1982) for three different Lloydminster fields during his water flood performance study on the Lloydminster area.

A comprehensive study on low and high temperature waterflood and steamflood test which were conducted over 15 year period was published by Bennion et al. (2006). They analyzed a total of 43 different studies on samples taken from the heavy oil producing regions in western Saskatchewan and central and eastern Alberta sedimentary basin. All tested samples were preserved core and over 90% of them were sourced from the McMurray sandstone formation. They used actual reservoir bitumen with gravities ranging from 7.5 to 12 API with viscosity ranging from 1,000,000 mPa.s to 8000 mPa.s . On 41 out of 43 tests, the unsteady state method was used to determine relative permeability for water-oil and for the remaining two tests, they used the steady state method. In unsteady state tests, relative permeabilities were determined by using a history match technique. They provided correlations to estimate low and high temperature water-oil relative permeabilities. In these correlations, relative permeability of oil and water was expressed as a function of normalized water saturation in the form of power function. Low temperature interval covers the range from 60 to 100 degree Celsius while the high temperature interval applies for temperatures of 150 to 275 degree Celsius. In addition to relative permeability of oil and water, they also provided other correlations to calculate residual oil saturation and endpoint permeability to brine as a function of waterflood temperature. They observed considerable variation in measured relative permeabilities of oil and water for different samples they examined and concluded that this scatter pattern is due to variations in reservoir quality and lithology. However they pointed out that the developed correlations should be used for preliminary evaluation purposes only and are not an accurate replacement for actual laboratory data measurements for a specific reservoir samples.

Bennion et al. (1993), conducted two series of steady-state tests to measure water-oil relative permeabilities on unconsolidated cores at elevated temperatures. They used composite core stacks of actual preserved reservoir core material, mounted in a Penn-State type core holder to eliminate the capillary end effects. The core holder also included a customized lead sleeve and arrangement to prevent fine clay production. By observing low endpoint water permeability and higher irreducible water saturation, they concluded that the cores were still water wet at an elevated temperature of 200 $^{0}$C. Substantial hysteresis was reported on non-wetting phase (oil) in both tests while the hysteresis was much less obvious on water relative permeability. Relative permeability values of each individual phase was greater when its saturation was increasing than when decreasing. Formation of stable emulsions was reported by the authors with up to 27% (by mass) of water emulsification in the oil. Measured relative permeability data showed some degree of experimental scatter and they used a power law formulation to regress the relative permeability of either water or oil, as a function of normalized water saturation. Even though this single-parameter power-law function may not be the best fit, as the authors pointed out, it can be useful for preliminary simulation work with reasonable accuracy.

Tang and Firoozabadi (1999) studied the gas and liquid relative permeabilities of heavy oil during cold production. They conducted two series of solution-gas drive tests, with mineral oil and heavy crude oil with viscosities of around 30,000 cp (at 24$^{o}$C) and 10,000 cp (at 35$^{o}$C) respectively. As porous media, they used clean Ottawa sand which was placed in a clear acrylic tube as the core holder. Methane was used as the gas phase and it was mixed with both oil samples to create live-oil fluids to be used as the oil phase in actual experiments. Experiments started with injecting the core with live oil and letting it reach a stable pressure and temperature, and eventually start depleting the core while measuring the produced gas and liquid. Having

measured the production and pressure drop data, they developed a mathematical method to calculate the relative permeability of gas and liquid. In this method they assumed one-dimensional pseudo-steady-state flow of gas and oil with uniform saturation. They observed very low gas relative permeability especially for gas saturations under 10%. They concluded that the main mechanism for relatively high recovery efficiency from heavy oil reservoirs under solution-gas drive is low gas mobility.

Polikar et al. (1991) carried out an extensive experimental study on water-oil relative permeabilities for Athabasca oil sands at elevated temperatures aiming at the possible effect of temperature on relative permeability. Experiments were run over temperatures ranging from 100$^{o}$C to 250$^{o}$C and both steady-state and unsteady-state methods were employed. They observed that oil relative permeability curve was convex and concluded that temperature has little or no effect on relative permeability of water-oil systems. They also found that there was little difference between the results from steady and unsteady state methods.

# CHAPTER 3: EXPERIMENTAL SETUP AND PROCEDURES

This chapter starts with a detailed review of the experimental setup and the hierarchy of design steps which were made to improve the performance of the experimental apparatus. Then the materials used in all experiments and the methods for preparing them will be discussed. As well, some preliminary calibration and measurements which were required before the major tests will be explained in details.

## 3.1 Experimental apparatus details

The experimental setup is a customized core-flood apparatus which was designed and fabricated to perform sequential injection of oil, gas and water at constant temperature and a specified pressure. The porous media was an unconsolidated core consisting of real reservoir sand whose details are given later in this chapter. Figure 3.1 shows a schematic of the experimental apparatus. Core holder, sample cylinders and a back pressure regulator are sitting inside an air bath which is depicted by the dashed line in Figure 3.1. Injection and overburden pumps, pressure monitoring system as well as liquid and gas collection system are located outside the air bath at room temperature. Details of each part of the apparatus are given next.

### 3.1.1 Description of sand pack and core holder

An aluminum sleeve with diameter of 1.5 inch (38 mm) and around 2 feet (60 cm) length was used to build the sand pack. On both ends of the aluminum sleeve, two aluminum heads were installed to operate as a cap and fluid distributor. Two heads were made of aluminum as well and each of them had two holes, one for a pressure line and one for fluid flow line. To prevent fine

sand particles from moving out of the sand pack and getting into the production lines, a piece of steel screen was installed on the inner face of both heads by using a custom designed steel ring which keeps the edges of screen in touch with the inner face of each head to prevent sand bypass. The inner face of both heads was grooved as concentric circles with center-crossing lines to get an evenly distributed flow into the sand face. Figure 3.2 presents a close up of the final design of the head.

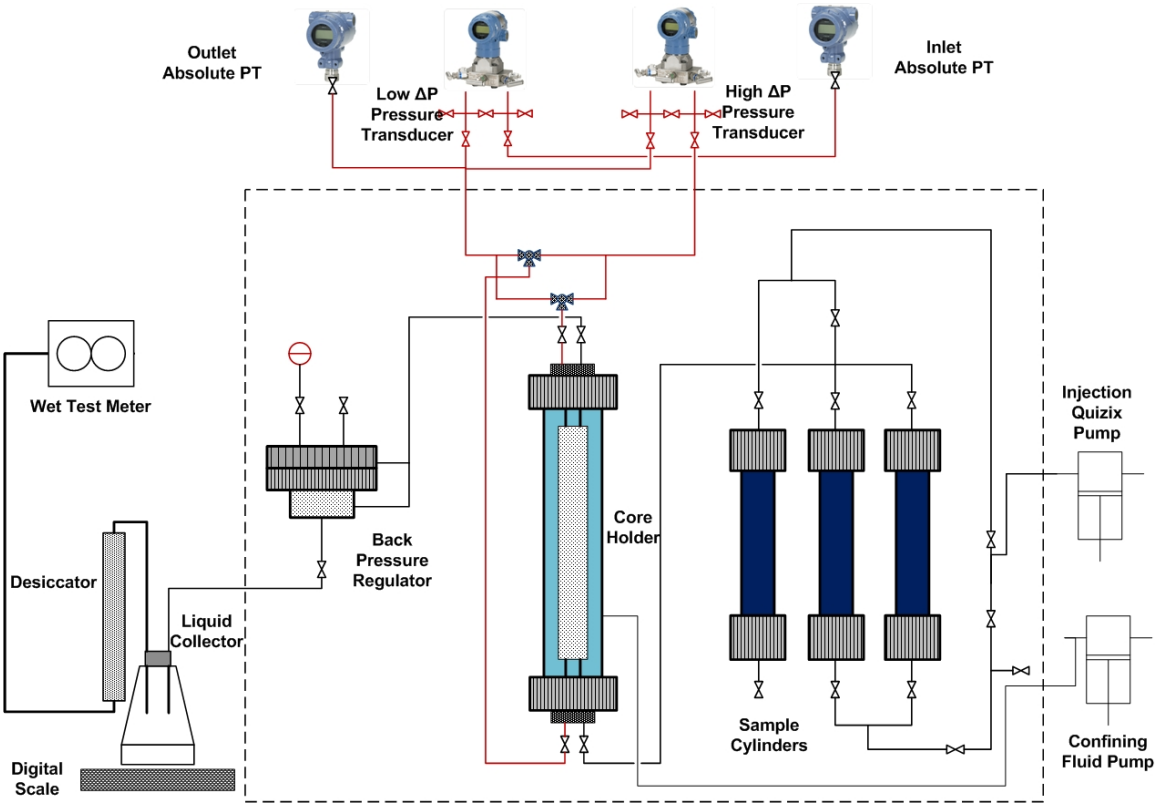


Figure 3.1 Schematic of experimental core-flood apparatus

A homogeneous batch of Athabasca sand was collected after screening some part of a large batch of real sand. The main objective was to transfer the sand sample into the aluminum sleeve in such a way that the resulting sand pack be as homogeneous as possible. One of the heads were secured and welded on the sleeve and empty sleeve was mounted in vertical direction with open end pointing upside. An air-driven vibrator was attached into the outer surface of the aluminum sleeve using a pair of plastic cuffs. A continuous stream of sand was directed from a funnel into the sleeve while the vibrator was left running. After the required amount of sand was transferred into the sleeve the second head was secured and installed and sand pack was turned upside down and vibration continued for the same period of time in order to improve the homogeneity of the sand pack.

Having the aluminum sleeve packed with reservoir sand, both heads were secured and welded into the sleeve and required pressure and flow lines installed by using the proper fittings. The aluminum sleeve is sitting inside an outer cylinder made from steel which can hold pressures up to 4000 psi (27.58 MPa). After installing the aluminum core holder, the outer cylinder was filled with water and pressurized using a manual Ruska pump to apply the required confining pressure to the sand pack. The core holder sits inside an air bath whose temperature can be set and controlled through the data acquisition system. There are four fans installed inside the oven to create air circulation and reduce the temperature gradient. Every fan pushes the air through a duct and an electric strip finned heater is installed at the end of the duct to supply the required heat.

Figure 3.2 Inner-face view of sand pack head showing the installed screen and distribution channels

#### 3.1.1.1 Capillary end effects

The so-called capillary end effects can make significant impact in a typical core-flood experiment. The end effects take place at the outlet face of a core during a simultaneous flow of two or three phases because of the discontinuity in capillary pressure which exists when flowing phases are about to leave the core and enter the non-porous space with no capillary pressure. The discontinuity in capillary pressure makes it more difficult for wetting phase than non-wetting phase to leave the outlet face of the core. Therefore a buildup of the wetting phase occurs at the outlet of the core which can influence the end point saturation values and end point permeabilities. In calculating the relative permeabilities from core-flood data, theoretically it is possible to include the effect of the capillary pressure however in most cases the required capillary pressure versus saturation data are not available for the rock-fluid systems which is under investigation and this type of data are very difficult to determine.

Capillary end effects can be neglected under certain operating conditions (Maini and Okazawa, 1987) therefore it is necessary to set an appropriate criteria and run the core flood experiment

under the required operating condition. A scaling coefficient defined by Bentsen (1978) can be used to determine a critical value above which the capillary end effects can be neglected. This scaling coefficient is defined as $LV\mu_w$ in which L is the length of the core (cm) , V is the Darcy velocity (cm/min) and $\mu_w$ is the viscosity of displacing fluid (cp). In a core flood experiment where $LV\mu_w > 1$ (with units in cm.cm/min.cp) it is reported that the capillary end effects will be fairly small and they can be neglected (Kyte and Rapoport, 1958). In a given displacement process, the injection flow rates must be high enough in order to maintain this criteria. However in other side, having a high flow rates in heavy oil systems might result in viscous fingering and unstable front. That means in many heavy oil systems it is almost impossible to have a stable flow (Maini and Okazawa, 1987).

During the course of this study, the above mentioned criteria to prevent the capillary end effects were taken into account in setting the injection flow rates in order to hold the condition $LV\mu_w > 1$ to be true. Therefore the capillary effects were neglected in all of the conducted experiments in this study.

### 3.1.2 Injection system

A Quizix pump was used to inject the required fluid into the sand pack. The Quizix pump was a QX6000 series and it is capable of injecting flow rates from 0.001 $cm^3$/min to 50 $cm^3$/min at injection pressures up to 6000 psi (41.36 MPa). This model consists of two barrels which can be operated individually or as a pair to provide a continuous flow. This pump is controlled by connecting it into a computer through a USB port and it can be operated through software named “Pump Works” which is supplied by the manufacturer. There are over 10 predefined operating modes which can be loaded based on the required injection mode. The two most frequently used

modes are constant flow rate and constant pressure. Working fluid which was used by the Quizix pump in this study was distilled water which in turn can be used as a medium to inject the required injection fluid into the sand pack by using a simple piston-cylinder. By making the proper arrangement in controlling software, all injection data such as injection pressure, cumulative injection volume, real time and date, can be logged and recorded as a text or spreadsheet file.

### 3.2.3 Pressure measurement and monitoring system

In core flood experiments the absolute pressure at the inlet and outlet of the core as well as the pressure drop across the core needs to be measured and monitored. In the current apparatus, very accurate Rosemount pressure transducers were used. There were two absolute pressure transducers each of which was connected to the inlet and outlet face of the sand pack. Also two differential pressure transducers were installed to measure the pressure drop across the core. One of the differential pressure transducers was selected for very low range pressure differential and the other one was assigned for higher differential pressure range and they were referred to as "Low ΔP" and "High ΔP" respectively. Low ΔP transducer can measure the pressures as low as 0.01 inch of water (2.49 Pa) up to maximum pressure of 200 inches of water (49.8 kPa), while the High ΔP transducer can measure the pressure values ranging from 0.01 psi (68.95 Pa) up to 4000 psi (27.58 MPa). Using these two transducers together, the apparatus was capable of measuring very low pressure drops which might occur during a gas flood as well as very high pressure drops which might be encountered during an oil flood.

### 3.2.4 Sample storage system

To store the injection fluids and to be able to inject them into the sand pack at the required temperature and pressure four sample cylinders were used. These cylinders were made of stainless steel and they were a simple piston-cylinder system which can be used to transfer the working fluid by a service fluid. The service fluid was distilled water which was connected directly into the injection Quizix pump and filled one side of the piston while the working fluid such as oil, was sitting on the other side. Every piston was equipped with two sets of durable Viton O-rings which are suitable for high temperature. Both heads on each cylinder were sealed by one Viton O-ring as well. Maximum storage volume of each cylinder was around 480 $cm^3$ and they were rated for pressures up to 4000 psi (27.58 MPa).

### 3.2.5 Liquid and gas collecting system

To study the relative permeability of flowing phases the cumulative and incremental quantity of each phase during the core flood experiments needed to be determined. A dome-type back pressure regulator was installed on the production line right after the sand pack to maintain the required pressure and release the required amount of fluid to keep the pressure below the set point value. Downstream of the back pressure valve, there was a separator which collected the produced liquid and released gas into a desiccator. This liquid separator was mounted on a digital scale which measured the instantaneous mass of produced liquid. Any entrained liquid or vapour would be absorbed by highly dry and adsorbent solid particles which are packed inside the desiccator. Dry gas was passed through a wet-test-meter and its volume was measured by the number of revolutions which were made on the wet-test-meter. Number of revolutions of the wet-test-meter was translated into an electric signal by using a rotary encoder which was

attached into the central axel of wet-test-meter. This signal was collected by the data acquisition system and was translated into produced gas volume.

### 3.2.6 Data acquisition system

Relative permeability determination depends on the availability of all pressure and flow data during the core flood experiment. That means that pressure drop across the core along with injection and production flow rates need to be recorded at every reasonable time step to keep track of the saturation change inside the sand pack. In the current apparatus, the data acquisition system was coded in Lab View environment and it was able to record two pressure drops ("Low $\Delta P$" and "High $\Delta P$"), inlet and outlet pressure of sand pack, overburden pressure, temperature of air bath at 6 different points, volume of produced gas and weight of the produced liquid and real date and time. By using a digital gauge, barometric pressure was also recorded. Time step for recording the data and temperature set-point for each thermocouple can be set through an appropriate menu. All recorded data are stored as a text file which later on can be imported into spreadsheet to do the required analysis.

## 3.2 Materials

### 3.2.1 Porous medium

In this study cleaned unconsolidated Athabasca sand was used as the porous media to conduct the relative permeability measurements. Batches of real Athabasca sand were sieved and the fraction which was finer than 130 mesh was selected for making the sand pack. After packing the core holder with sand by a procedure which was described earlier in current chapter, a couple of water floods were conducted on the core to measure the porosity and absolute permeability of

sand pack. Despite installing a fine mesh at each inner face of the core holder heads, there were signs of very fine clay inside the production lines. To avoid the by-passing of fine clay, the sand batch, were sieved and any clay less than 250 mesh was removed and the core holder was packed with clay-free sand.

### 3.2.2 Bitumen

For the oil phase, a solvent-extracted bitumen sample from a reservoir in Alberta was used. The extraction process was conducted in the ISCRG chemical analysis facility by a procedure which is briefly reviewed here. The first step was removing the water content of bitumen samples received from the field. This is done using a Dean-Stark distillation on the entire sample. In this method, for each batch around 500 $cm^3$ of bitumen was diluted with toluene with a ratio of 1 to 1 and the diluted bitumen was set to boil inside a 1000 $cm^3$ flask. The evolving vapor was directed into a water-cooled condenser and finally collected inside a so-called Dean-Stark trap in which water collected at the bottom and toluene on top. Water volume was read directly from the scale which lines up with water meniscus. To remove any core particles or sand grains, the residual oil was filtered using the Whatman paper filter number 4, which can remove all particles larger than 25 μm. As a last step, bitumen samples were transferred into glass flasks with known weight and put under house vacuum while their weight are recorded regularly until they reached a constant weight.

### 3.2.3 Water and gas

In this study distilled water was used as the water phase in all core flood experiments. For the sake of simplicity nitrogen was selected as the gas phase because of very low solubility in oil and water.

## 3.3 Dead volume of the sand pack

In assembling any sand pack for core flood experiments, in addition to real pore volume of sand pack, there is going to be some extra volume associated with injection/production and pressure lines which is called dead volume. Dead volume itself consists of two different types which are static and dynamic dead volume. Static dead volume consists of pressure lines in which there is no fluid flow while the dynamic volume includes the injection and production lines right before and after the sand faces. In designing the core holder, there has to be maximum effort devoted to minimize the dead volume and after assembling the core, the dead volume must be measured and recorded as it will be required for later mass balance and modelling purposes. Figure 3.3 shows a schematic view of the aluminum sleeve and the heads on each end as well as the pressure and injection lines. The dead volume include the volume of four pieces of $^{1}/_{8}$ inch lines and the four empty holes inside the heads which stretch from sand face until the NPT unions. Individual value of each sub-volume were measured by a porosimeter using helium injection as described in porosity measurement procedure and total dead volume calculated as 8.3 $cm^3$. It should be mentioned that half of this dead volume which includes the pressure monitoring lines is static dead volume and the other half is dynamic dead volume.

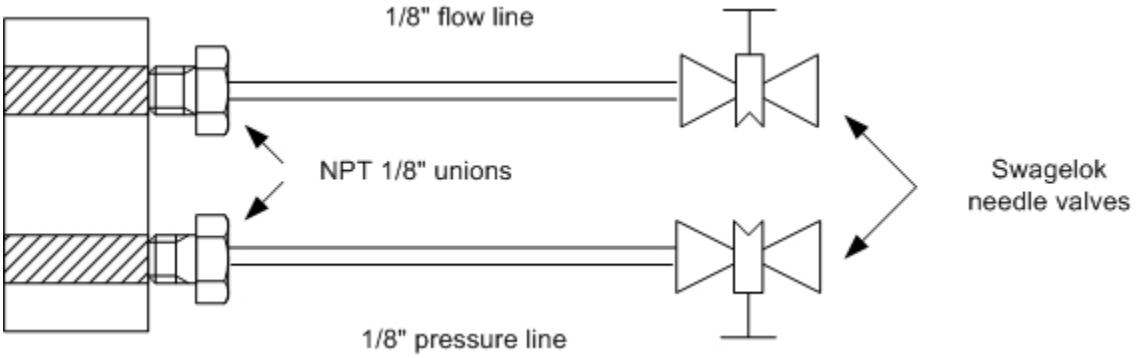


Figure 3.3 Schematic indicating the head of aluminum sleeve and dead volume

### 3.4 Porosity measurement

One of the important characteristics of any porous medium is its pore volume and its porosity which is required directly or indirectly in designing and operating the core flood experiments as well as measuring the relative permeabilities. After the unconsolidated core was packed, its pore volume and its porosity was measured through the two following methods:

#### 3.4.1 Helium injection

The pore volume of the sand pack first was measured by using an automated porosimeter model AP-608 manufactured by Coretest System Incorporation. This apparatus which was originally designed to measure the porosity and permeability of consolidated core plugs can also be used to measure confined volumes such as volume of a transfer vessel or sample cylinder. Volume measurement is started by injecting a required amount of helium gas till the pressure of the unknown volume reaches around 200 psi (1.38 MPa). Provided that no leak is present in the system, the pressure is dropped by sending a part of the initial injected gas into a secondary storage vessel with known volume. After reading a stable condition the final pressure was

recorded and by assuming an isothermal condition, the unknown volume is measured by using Boyle's law:

$$P_1V_1 = P_2V_2 \qquad (3\text{-}1)$$

Having the sand-pack mounted inside the water jacket, three out of the four inlet/outlet lines were blocked and the sand pack was connected to the porosimeter. A confining pressure of nearly 200 psi was applied right before the start of helium injection step of the porosimeter operation and the pore volume of sand pack was measured. This measurement process was repeated until the readings were within 0.5% variation. The average value of the best three readings was selected as the pore volume which was 212.7 $cm^3$.

### 3.4.2 Water injection

In addition to measuring the pore volume by helium injection, water injection was also used as an alternative way to estimate the pore volume. The pore volume which is measured by helium injection, is expected to be slightly higher than the measured pore volume by water injection. To prepare the sand pack for water injection, three out of four valves right before the sand face were closed and the fourth valve was connected to a vacuum pump to evacuate any gas out of the sand pack. After having the sand pack under vacuum for over half an hour, the last valve was closed and sand pack was isolated from the vacuum pump and water was pushed through the injection line up to the entrance of fourth valve. At this point, the pump volume was reset and then the valve opened to inject water into the sand pack until the pressure was 200 psi (1.38 MPa). The volume of injected water is equal to the pore volume of sand pack plus the total dead volume. Having the dead volume measurement, the pore volume of sand pack was estimated to be around 209.9 $cm^3$. To calculate the porosity the bulk volume of sand pack needs to be calculated. The

exact dimensions of the cylindrical aluminum core holder were measured by a digital caliper and the bulk volume of the empty spaces between the two heads which is filled with sand only, was estimated to be 554.1 $cm^3$. Based on this calculation, the porosity of the sand pack by water injection was 37.88% while helium injection test resulted in a value of 38.37% for sand pack porosity.

### 3.5 Absolute permeability of the sand pack

Having the sand pack mounted inside the water jacket and testing all of the pressure and injection lines for any leaks, the sand pack was ready for the core flood tests. The first test which was the simplest and yet very important one, was measuring the absolute permeability of the sand pack. Absolute permeability can be determined by flowing a single-phase fluid at a certain flow rate, through the sand pack. By measuring the pressure drop across the core and knowing the viscosity of the fluid, Darcy's law was used to determine the absolute permeability of the sand pack. Absolute permeability tests were conducted at room temperature and a net confining pressure of 500 psi (3.45 MPa) by water injection. Five different flow rates of water starting from 1 $cm^3$/min to 5 $cm^3$/min were applied and the steady state pressure drops across the core were measured as indicated in Table 3.1. Water was injected from the bottom of the sand pack upward and after injecting about two pore volumes of water, the back pressure was set at 500 psi (3.45 MPa) and for every flow rate, the pressure drop across the core was monitored to determine the development of a stable condition.

Table 3.1 Absolute permeability measurement for sand pack

| Injection rate ($cm^3$/min) | Pressure drop ($inH_2O$) | Pressure drop (atm) | Absolute permeability (Darcy) |
|---|---|---|---|
| 1 | 3.55 | 0.00872 | 10.03 |
| 2 | 6.72 | 0.01651 | 10.59 |
| 3 | 9.87 | 0.02425 | 10.82 |
| 4 | 13.07 | 0.03211 | 10.89 |
| 5 | 16.25 | 0.03993 | 10.95 |

# CHAPTER 4: TWO-PHASE WATER-GAS EXPERIMENTS

## 4.1 Outlook of water-gas experiments

As outlined in Chapter two, there have been quite a few previous studies on relative permeability of heavy oils and bitumen mixtures with water and gas. These studies mostly focused on either water-oil or gas-oil relative permeability. But there is scarcity of published data on water-gas mixtures especially in unconsolidated porous media. A good understanding of the water-gas relative permeability characteristic is very important in designing any recovery method involving gas injection into reservoirs with high water saturation in which there would be a high chance for water being displaced with gas. The objective of water-gas experiments was to study the relative permeability behavior of water-gas mixtures in a typical oil sand reservoir and investigate some existing insights on having a high relative permeability of gas in water-gas mixtures. In this chapter the experimental procedure and results in two-phase water-gas mixtures were described. Both steady state and unsteady state methods were used to determine the relative permeabilities of water-gas systems. To study the possible effect of temperature, three sets of experiments were conducted at three different temperature: room temperature, 40 and 80$^{o}$C. The physical properties of water and nitrogen such as viscosity and density which are required to calculate the relative permeabilities from either steady-state or unsteady-state methods are summarized in Table 4.1. These data were collected from NIST data base at pressure of 500psi (3.45 MPa) and three temperatures at which the water/gas experiments were conducted.

Table 4.1 Viscosity and density of water and nitrogen at pressure of 500psi (3.45 MPa) and three different temperatures

| Temperature | | 23ºC | 40ºC | 80ºC |
|---|---|---|---|---|
| Water | Density (g/cm$^3$) | 0.99905 | 0.99368 | 0.97328 |
| | Viscosity(mPa.s) | 0.93117 | 0.65325 | 0.35523 |
| Nitrogen | Density (g/cm$^3$) | 0.039403 | 0.037107 | 0.032684 |
| | Viscosity(mPa.s) | 0.018300 | 0.019041 | 0.020733 |

## 4.2 Description of experimental and analysis methods

### 4.2.1 Steady-state method

Relative permeabilities in water-gas systems were first measured by the steady-state method. Sample cylinders were charged with water and the air bath temperature was set to the desired temperature and left overnight to reach a stable temperature. As a preliminary step, the sand pack was fully saturated with water and pressurized to 500 psi (3.45 MPa). To keep the production at a constant pressure, back pressure regulator was pressurized to 500 psi (3.45 MPa) using nitrogen. A confining pressure of 1000 psi (6.89 MPa) is applied using a manual Ruska pump so that sand pack was put under a net pressure of 500 psi (3.45 MPa). Before the start of injection, the data acquisition system was activated and set to record all required data. For the steady state method, water and gas were co-injected by two independent lines into the inlet of the sand pack. The experiment started with two initial values for water and gas flow rate. As the injection

continued, the saturation of water and gas changed along the sand pack and the pressure drop started to decrease due to increasing gas saturation compared to zero gas saturation at fully water-saturated core at the beginning of co-injection process. Reaching a plateau in pressure drop is an indication of constant saturation and it signals the beginning of the steady state condition at the current injection flow rate. Knowing the values for injection rates and pressure drop as well as the viscosity of water and nitrogen at the test temperature, the relative permeability of the sand pack to each of the flowing fluids at current saturation was calculated. This generates only a single point on a relative permeability curve and to determine more points, the saturation needed to be changed by either increasing the gas flow rate or decreasing the water flow rate.

To determine the value of saturation for both water and gas at each state, a simple mass balance was used. Assuming Δt indicates the time it takes to reach the pressure drop plateau from the initial homogeneous water saturation $S_w^1$ to a secondary steady value of $S_w^2$ at a water injection rate of $q_w$ , and $m_{w,prd}$ is the mass of produced water during Δt, the mass balance equation would be :

$$[(S_w^1 - S_w^2)V_P + V_d]\rho_w^{RC} + \Delta t.q_w.\rho_w^{RC} = m_{w.prd} \qquad (4\text{-}1)$$

where $V_P$ is the pore volume of sand pack $V_d$ is the dynamic dead volume and $\rho_w^{RC}$ is the density of water at reservoir condition. The first term in the left hand side of the mass balance equation is the net water produced due to saturation change inside the sand pack while the second term indicates the water injected by the pump during Δt injection period. Starting from any known initial saturation, the final saturation was determined and having the relative permeability of each phase calculated, a single point was obtained on the relative permeability versus saturation curve. A benefit of employing the steady state method is the ability to determine any desired data point in any saturation between irreducible water saturation $S_{wir}$ and irreducible oil saturation $S_{oir}$

even though it might take a few injection flow rate adjustment which in turn is quite time consuming.

### 4.2.2 Unsteady state method

To run the unsteady state method, the sand pack had to be returned into a fully water saturated state as the initial condition. After running a series of steady state determinations, there is going to be a gas saturation inside the sand pack which needs to be totally removed. By applying adequate vacuum on the cell for about an hour and then flooding the cell with over four pores volumes of water, the sand pack was returned into a fully water-saturated state. By pressurizing the cell to 500 psi (3.45 MPa) and applying a confining pressure of 1000 psi (6.89 MPa), the first unsteady state test was started after reaching the uniform temperature. All unsteady state tests were run only in the drainage saturation direction which means water is displaced by gas.

### 4.2.3 Processing the raw data

Raw data were collected by the data acquisition system as described earlier on Chapter 3. As well, the injection fluid data by Quizix pump can be recorded independently by the software which was supplied by its manufacturer. Among the recorded data, injection flow rate, pressure drop across the core and time are the most important parameters which were used directly to determine the relative permeabilities. Other data mostly provided a tool to monitor the process and to determine some important moments such as breakthrough of injected phase.

The number of pore volumes injected was determined from cumulative injection and pore volume of sand pack but there had to be some corrections applied to the amount of cumulative injection measured by the injection pump. The fact is that the injection pump operates at room

temperature and the reported cumulative volume is measured at room temperature as well. Water enters the sample cylinder bottom to push the piston and the injection fluid toward the sand pack. For test temperatures above room temperature, the sample cylinder temperature is higher than the pump temperature, hence there is volume expansion for water as a result of thermal expansion. Therefore the real cumulative injection volume is higher than the value which is measured by the pump and this correction must be applied to the recorded raw injection data.

The other correction was applied to breakthrough time which is the time from start of injection to the first appearance of the injected fluid either as gas bubbles or water/oil slugs at the exit transparent line just upstream of the liquid collector. The reason is that the real breakthrough happens right after the core outlet face and it takes a few seconds for exiting fluid to travel from the core outlet face toward the back pressure regulator and then to the liquid collector. Therefore the dynamic volume after core outlet was measured and it was required in correcting the breakthrough time. This time lag also influenced the produced fluid mass which was recorded continuously by a digital scale at any specific time during the flood. Corrections were required to assign the produced amount of liquid to the right corresponding time at which the produced liquid reached the core outlet face.

Recorded pressure drop data across the core might fluctuate in some cases. This happens when the injected fluid is lighter than the fluid which initially saturates the core. The source of this fluctuation is the operation of the back pressure regulator which intermittently opens and closes to keep the core pressure at the given set point. This type of behavior is normal for dome-type back pressure regulators as the gas inside the dome space is compressed and lets the circular disc lift up to release a small amount of fluid out of the core to maintain the constant pressure. For calculation purposes an average value for pressure was used at each period.

### 4.2.4 Determination of water/gas relative permeabilities by unsteady-state method

After processing the raw data from the unsteady state method, relative permeabilities of the water/gas system were determined by using the so-called JBN method. This method was first developed by Johnson, Bossler and Naumann (Johnson et al., 1959 ) and it was briefly reviewed in Chapter 2. For the two phase water-gas system, this method requires the following two derivatives be determined directly from the injection data:

$$\frac{d\left(\frac{1}{Q_w I_r}\right)}{d\left(\frac{1}{Q_w}\right)} = \frac{f_{w2}}{k_{rw}} \tag{4-2}$$

$$(f_w)_2 = \frac{dS_{avg}}{dQ_g} \tag{4-3}$$

Where $Q_w$ and $Q_g$ are the number of pore volumes of injected water and gas respectively, $(f_w)_2$ is the fraction of water saturation at the outlet face of the core and $S_{avg}$ is the average water saturation inside the sand pack at any instance during the flooding process. $I_r$ represents the relative injectivity of the sand pack as explained in Chapter 2. These two derivatives may follow irregular patterns when they are calculated directly from cumulative injection data and this could result in unsmooth and non-monotonic relative permeability determinations. In the current study these two derivatives were calculated by using a graphical method which includes fitting a curve which gives a reasonable regression constant while having a simple mathematical formula. In the case of first derivative, (Equation 4-2) a plot of $\frac{1}{Q_w I_r}$ versus $\frac{1}{Q_w}$ resulted in a straight line with constant slope in water-gas experiments. For the derivative in Equation (4-3), a polynomial or

logarithmic equation gave a good fit of the plotted average water saturation $S_{avg}$ versus number of pore volumes of injected gas $Q_g$. When the regressed function is determined, its derivative can be easily found at any point. Details of such a calculation are described for one of the water/gas systems in the next section.

### 4.2.5 Detailed calculation for a particular water/gas experiment

The above mentioned procedures for processing the raw data to determine the relative permeabilities from either steady state or unsteady state methods is presented for a water/gas drainage experiment at 40°C with more details. Only preliminary calculations are shown and the final relative permeabilities are presented under results and discussion.

The steady state method starts with co-injection of water and gas into a fully water saturated sand pack. Variation of pressure gradient across the core is shown in Figure 4.1.

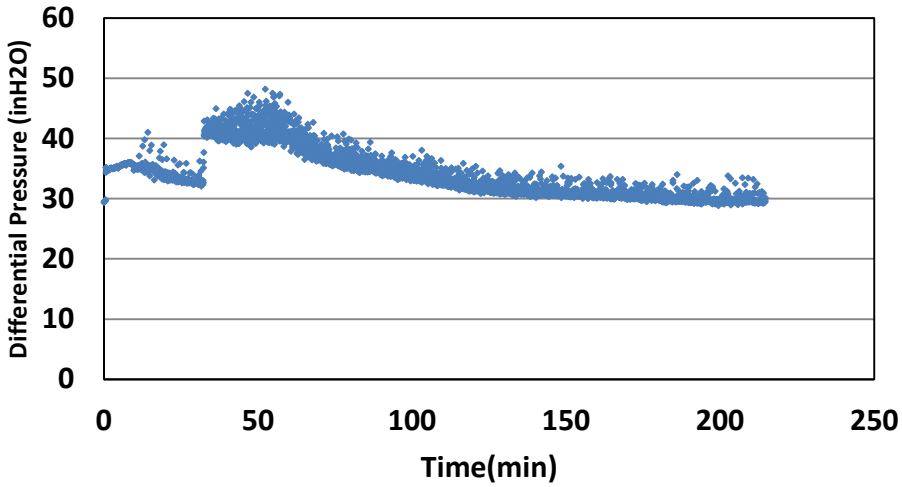


Figure 4.1-Variation of differential pressure in steady-state experiment for water/gas at 40°C

The differential pressure eventually stabilized at around 30 inches of water (7.47 kPa) in this case. Figure 4.2 shows how water saturation changes with injection time. Average water saturation was calculated by a simple mass balance on water similar to Equation 4-1 with initial water saturation of 1 which corresponds to a fully water-saturated core at the beginning of gas injection. For this particular case, the gas injection was started a few seconds ahead of the water injection while the injection time was set to be the water injection start time. Therefore water saturation started from an initial value which was lower than unity. At the earlier times of injection, as gas entered into the fully water saturated core, water saturation kept declining till it reached a minimum value and after that it started to rise again and eventually it stabilizes at around 0.88 which gave the steady state saturation corresponding to current flow rates of both water and gas.

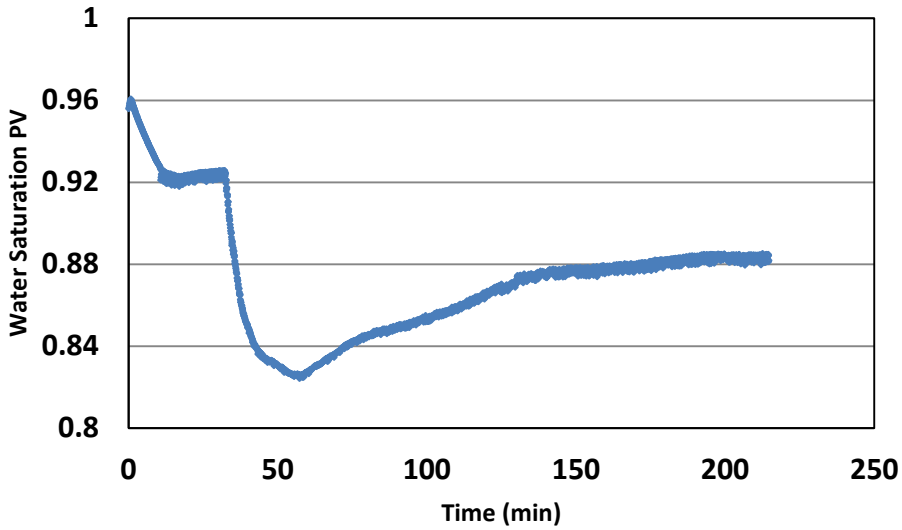


Figure 4.2 Average water saturation in steady-state experiment for water/gas at 40°C

The unsteady state method for the same temperature started with injecting gas into a fully water saturated sand pack which is a primary drainage process. As the gas front moved along the core, water saturation declined as indicated in Figure 4.3. This decline continued until the water saturation reached the residual water saturation. As stated in the JBN method, the slope of the average gas saturation versus number of injected pore volumes needed to be calculated at any saturation during the flood. This plot is indicated in Figure 4.4 for the unsteady state test at room temperature. Starting from a fully water saturated core, the gas breakthrough happened after about 0.76 pore volume of gas was injected into the core. To be able to calculate the required slope, an equation such as a polynomial or a ratio function was fitted to the appropriate portion of the plot and by having the mathematical equation of the fitted function, its slope was easily determined by differentiation. One more slope which has to be calculated was the slope of a plot of $\frac{1}{Q_w I_r}$ versus $\frac{1}{Q_w}$ as stated in Equation 4-2. For a gas flood at room temperature this plot appeared to be a straight line and its slope was easily determined by regressing a straight line through the data points. Figure 4.4 shows this plot for a displacement test at room temperature.

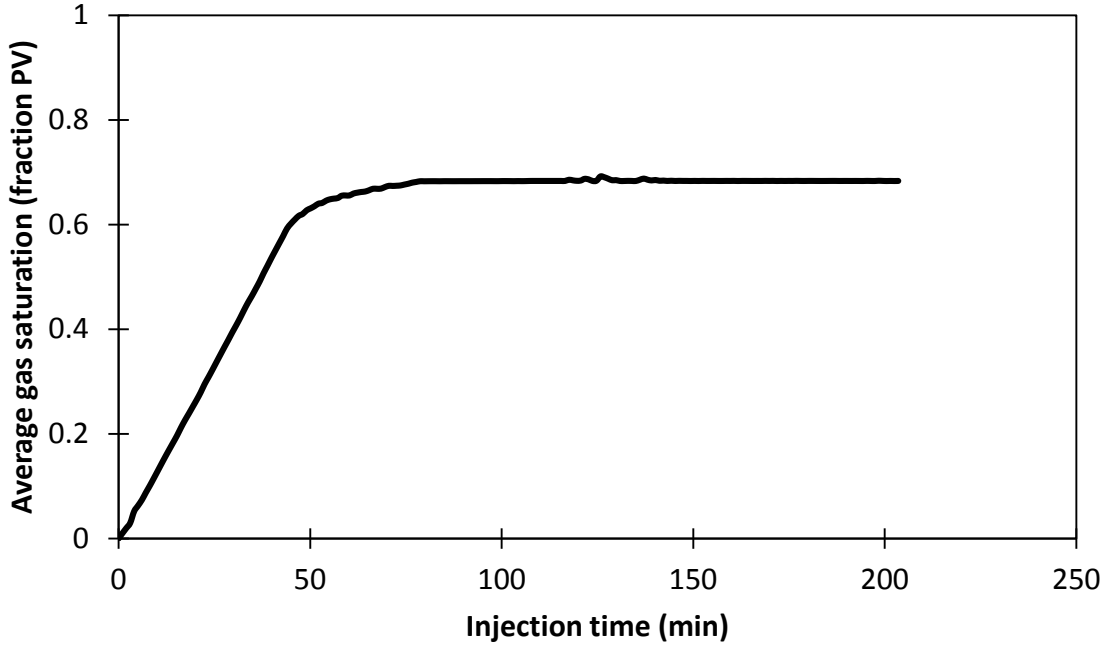


Figure 4.3 Average gas saturation inside the core at unsteady state experiment for water/gas at 23ºC

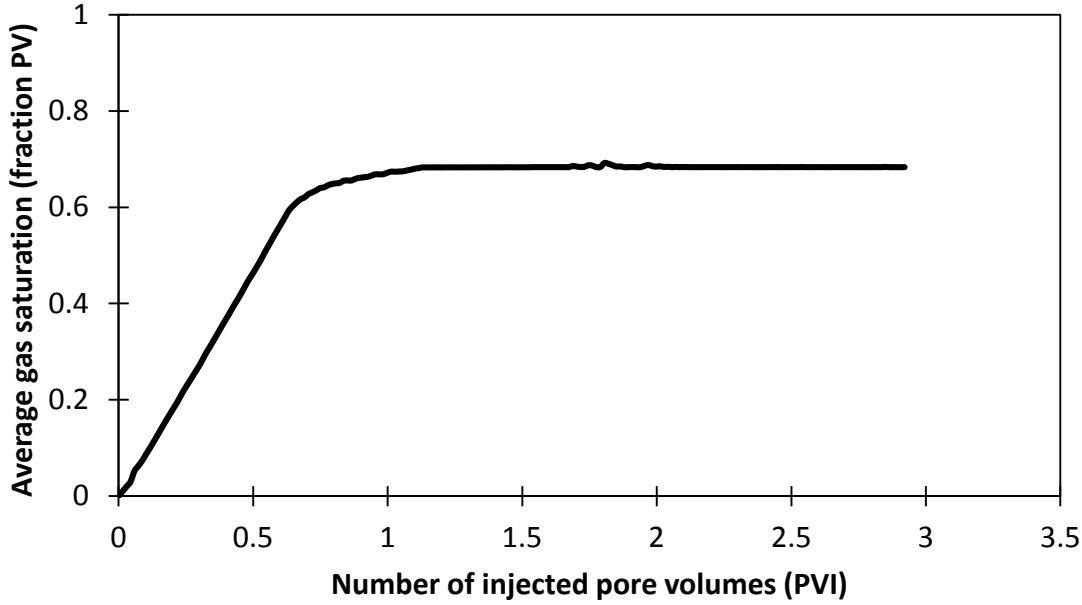


Figure 4.4 Average gas saturation versus number of pore volumes of gas injected at unsteady state experiment for water/gas at 23ºC

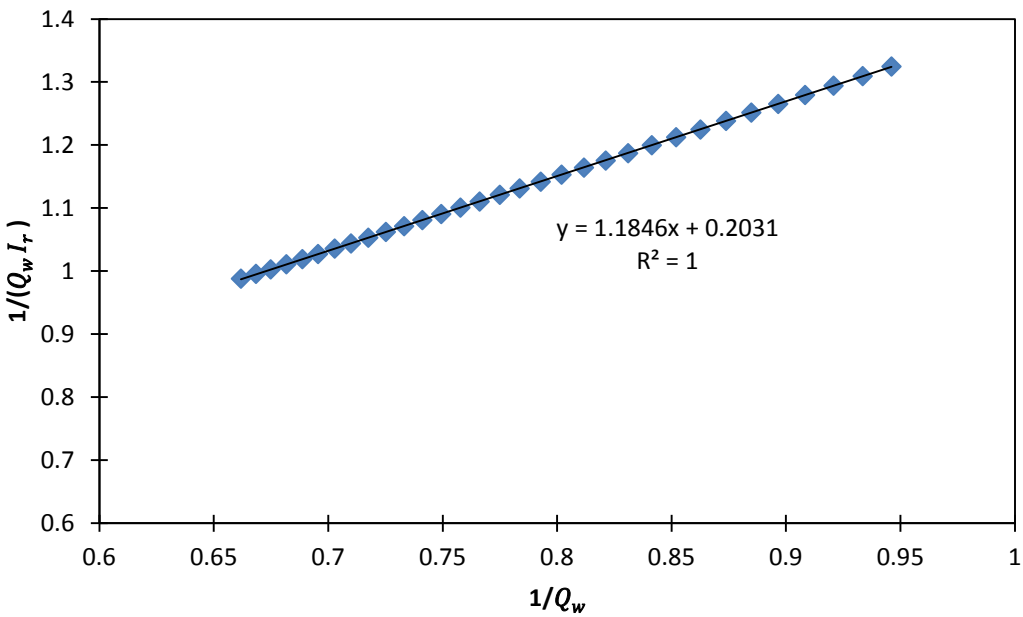


Figure 4.5 A plot of $\frac{1}{Q_w I_r}$ vs $\frac{1}{Q_w}$ for a gas-water displacement at room temperature. Slope and regression constant are shown by fitting a straight line.

### 4.3 Results and discussion

Relative permeabilities for the water-gas system in drainage process as determined by using both the steady-state and unsteady state methods are shown in Figures 4.6 to 4.11. The figures are presented starting from the results for room temperature, then 40ºC and then 80ºC. In order to compare the results, for every temperature the results from the unsteady-state method were shown first and then the results for both methods were presented in a single graph. In all of these graphs, water relative permeability was shown on primary vertical axis while the gas relative permeability was shown on the secondary vertical axis. Relative permeabilities from the unsteady state method, are shown as a continuous line and the steady-state relative permeabilities are depicted as individual data points.

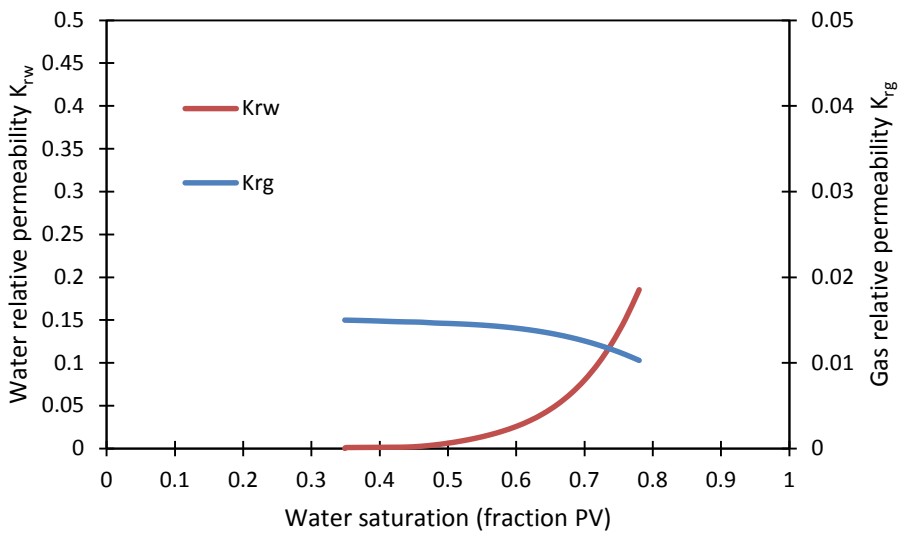


Figure 4.6 Drainage relative permeability of water-gas at room temperature from unsteady-state method

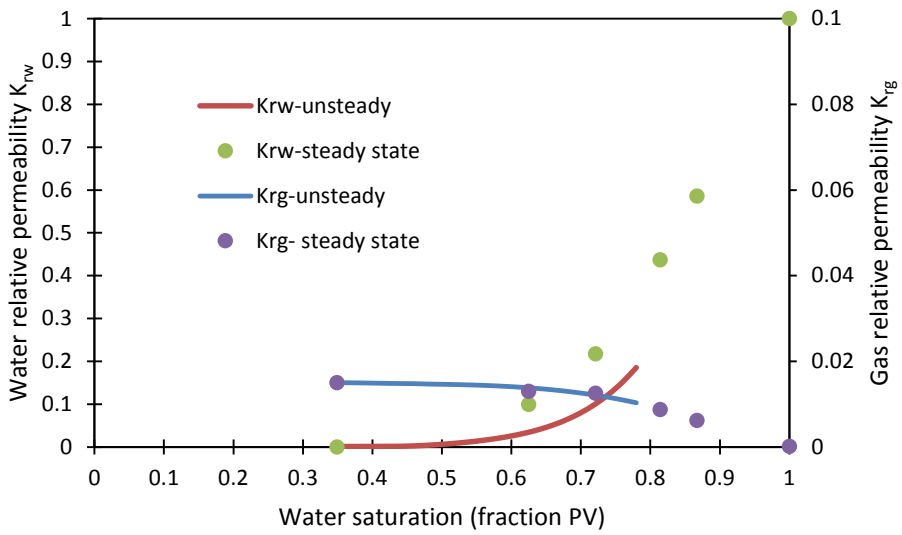


Figure 4.7 Drainage relative permeability of water-gas at room temperature by steady-state and unsteady-state method

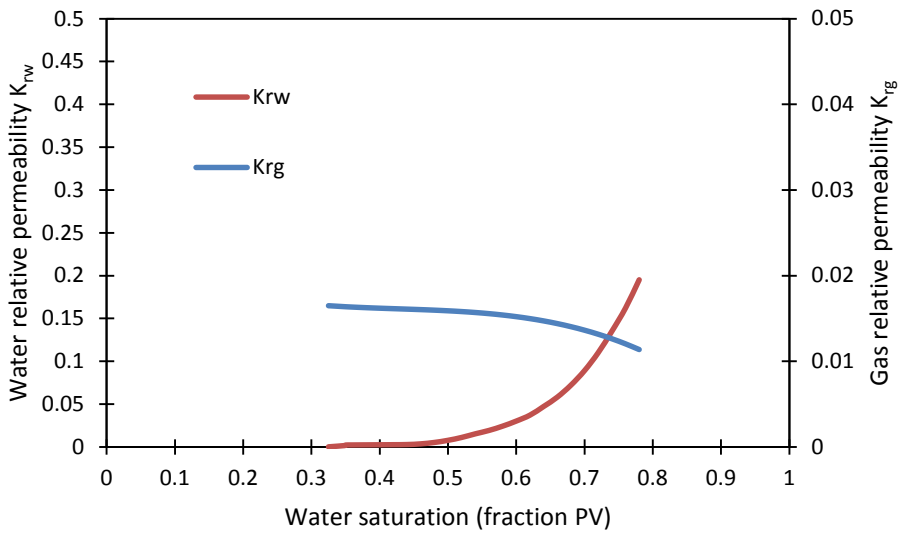


Figure 4.8 Drainage relative permeability of water-gas at 40°C from unsteady-state method

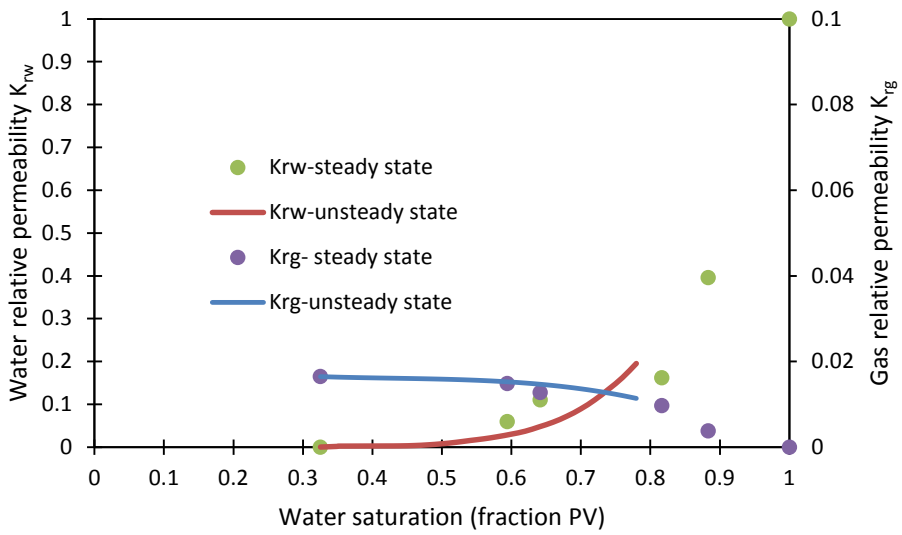


Figure 4.9 Drainage relative permeability of water-gas at 40°C by steady-state and unsteady-state method

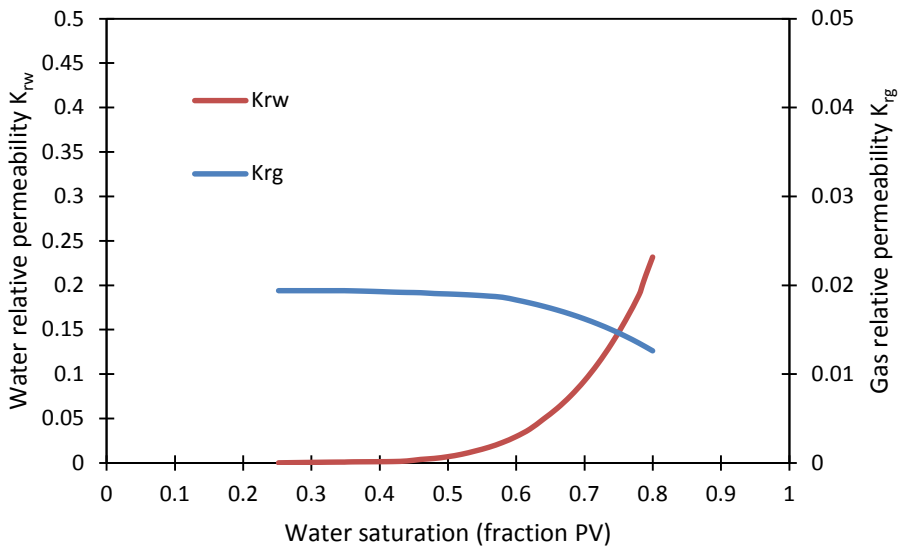


Figure 4.10 Drainage relative permeability of water-gas at 80°C from unsteady-state method

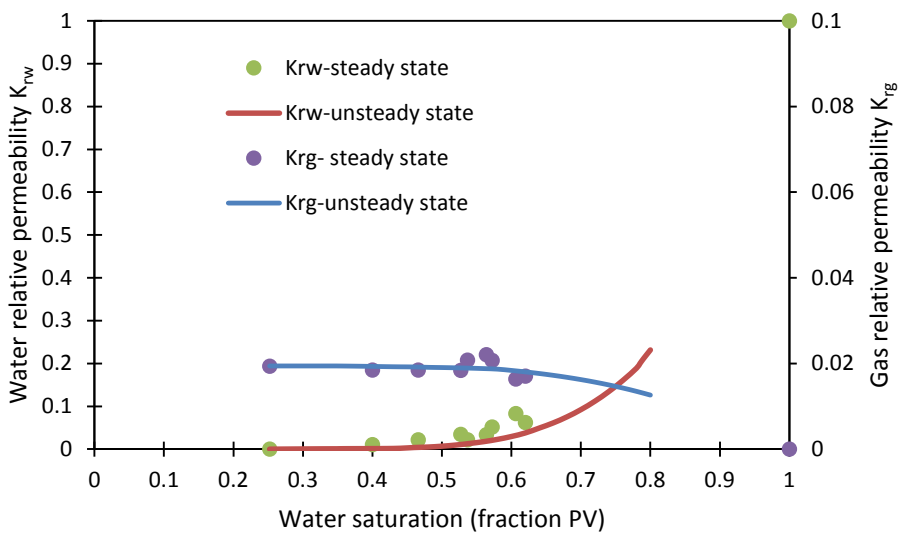


Figure 4.11 Drainage relative permeability of water-gas at 80°C by steady-state and unsteady-state method

Overall, the gas relative permeability values even around the highest gas saturation were very low compared to the water relative permeability values around high water saturation zone. Despite some scatter in steady-state data, unsteady state results were in relatively good agreement with the ones from the steady state method for both water and gas. Among the three investigated temperatures, the deviation between the steady state and unsteady state methods is more prominent for water relative permeability at room temperature as shown in Figure 4.7. This might be caused by uncertainties in determining the relative injectivity parameter, $I_r$, which is required in JBN method as explained earlier on Chapter 2. (Equation 2-11)

In terms of temperature effect on relative permeabilities of water/gas system, the end point saturations were changed by increasing the temperature. Table 4.2 shows the end point saturations at the three examined temperatures. Residual water saturation declined at higher temperatures in drainage process where gas displaced the water from a fully water-saturated core. In the same manner residual gas saturation decreased by increasing the temperature from room condition to 80$^{o}$C for the imbibition process in which gas was displaced by the water when a water-flood process was conducted on gas-swept core.

Table 4.2 End point saturations for drainage/imbibition processes in water/gas systems at different temperatures

| Temperature | Residual water saturation (drainage process) | Residual gas saturation (imbibition process) |
|---|---|---|
| Room temperature | 0.349 | 0.273 |
| 40$^{o}$C | 0.325 | 0.257 |
| 80$^{o}$C | 0.252 | 0.184 |

End point relative permeabilities also were affected by temperature. As is indicated in Table 4.3 end point water and gas relative permeabilities increased with temperature.

Table 4.3 End point relative permeabilities for drainage/imbibition processes in water/gas systems at different temperatures

| Temperature($^oC$) | Relative permeability of gas at residual water saturation (drainage process) | Relative permeability of water at residual gas saturation (imbibition process) |
|---|---|---|
| Room temperature | 0.0150 | 0.198 |
| 40 | 0.0165 | 0.235 |
| 80 | 0.0194 | 0.295 |

Despite the increase of end point saturation and end point relative permeability, water permeability was not influenced by temperature significantly even though the gas relative permeability was shifted to higher values by increasing the temperature. Temperature effect on relative permeability is summarized in Figure 4.12.

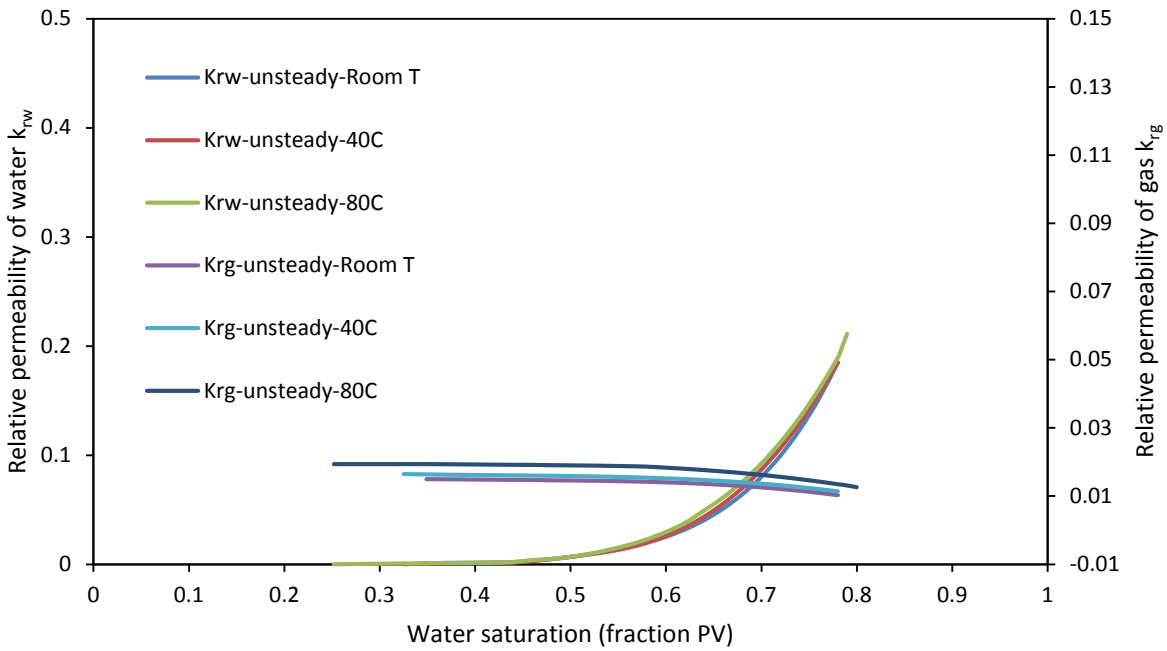


Figure 4.12 Effect of temperature on relative permeabilities of water/gas

The observed shift in gas relative permeability at different temperatures raises the question that whether or not the increase in relative permeability is due to temperature or just a result of uncertainty in measured variables. In order to investigate the shift, an error analysis was conducted to check whether or not the differences are within the experimental error limit. General form of Darcy's law was selected to do error analysis. The variables which involve are injection flow rate, fluid viscosity, cross sectional area of core, pressure drop and length of the sand pack. Any uncertainty which exist during the measurement of these variables, has an impact on the calculated effective permeability of the flowing fluid. By taking a differential from both sides of the Darcy's law and after doing some arrangement, the following equation will be resulted:

$$\left|\frac{dk_e}{k_e}\right| = \left|\frac{d\mu}{\mu}\right| + \left|\frac{dq}{q}\right| + \left|\frac{dA}{A}\right| + \left|\frac{dL}{L}\right| + \left|\frac{d(\Delta P)}{\Delta P}\right| \qquad (4\text{-}4)$$

note that the brackets designate the absolute amount of the inside variables. Typical values of these variables along with the associated uncertainty are listed at Table 4.4.

Table 4.4 Typical values and uncertainties of variables that appear in Darcy's equation to calculate the effective permeability of gas at 500 psi (3.45 MPa)

| Variable | Viscosity (cp) | Flow rate ($cm^3$/min) | Cross sectional area ($cm^2$) | Length of sand pack (cm) | Pressure drop (in $H_2O$) |
|---|---|---|---|---|---|
| Typical value | 0.02075 | 3.000 | 9.97 | 55.57 | 40.00 |
| Uncertainty | 2% | 0.0001 | 0.01 | 0.01 | 0.01 |

Using the typical values of each variable along with the corresponding uncertainty in Equation 4.4, the uncertainty of calculated relative permeability of gas is 2.3%. In order to check whether or not the observed difference between the gas relative permeabilities at three temperatures are meaningful the difference between the values of endpoint gas relative permeabilities were compared with the calculated uncertainty. Based on the values which are listed in Table 4.3, end point gas relative permeability at 40$^o$C (0.0165) is about 10% higher than its value at room temperature (0.015) and at 80$^o$C the gas relative permeability (0.0194) is over 10% higher than its value at 40$^o$C and over 20% higher than its value at room temperature.

# CHAPTER FIVE: OIL/WATER/GAS EXPERIMENTS

## 5.1 Introduction

This chapter includes the experiments which were conducted to study and determine the relative permeabilities in two-phase and three-phase oil/water/gas systems. For these mixtures the relative permeabilities were determined through a history match technique by using a reservoir simulator. The displacement experiments were isothermal floods at 80$^{o}$C carried out at typical oil sand reservoir pressure. This chapter begins with introducing the details of building the fluid model in the reservoir simulator which includes the physical properties used to define the pseudo components. Physical model of the core and number of grid blocks used will be explained next. Processing the raw experimental data in the way they can be entered into the simulator and building the so-called field history files will also be explained. Two-phase oil/water experiments will be the first series of experiments which were explained and the resulting relative permeabilities for drainage and imbibition processes are presented. The next series of experiments start with gas injection into an oil flooded core at residual water saturation to simulate and study the relative permeability behavior for gas injection into a fresh reservoir. Next three-phase flow of oil/water/gas was conducted by injecting a slug of oil into the gas flooded core followed by a slug of water. This three-phase flow simulates the saturation reversal which occurs during combustion when the oil bank re-saturates the gas-flooded zone. All of the core flood experiments which were conducted during the course of this study with water, oil, and gas were given a number and summarized in Table 5.1 for a convenient reference.

Table 5.1 Summary of the two-phase and three-phase water/oil/gas floods

| Experiment number | Description |
|---|---|
| 1 | Primary drainage: Injection of oil into fully water saturated core |
| 2 | Imbibition: Water injection into the oil-flooded core at residual water saturation |
| 3 | Secondary drainage: Oil injection into the water-flooded core at residual oil saturation |
| 4 | Gas injection into the oil-flooded core at residual water saturation |
| 5 | Injection of a slug of oil followed by a slug of water into gas-flooded core finally followed by gas injection until no liquid production |

## 5.2 Description of simulation of core flood process

Details of simulation work were described in this section. This includes the details of building the fluid model inside the simulator, building the physical model of the core, defining the grid blocks and defining the field history files out of experimental data.

### 5.2.1 Fluid model description

The first step in simulating a core flood process by using a reservoir simulator is to build the fluid model and this means specifying the pure materials such as water and nitrogen and defining the oil as a combination of pseudo components. In this study the reservoir simulation package by Computer Modelling Group CMG$^{TM}$ was used as the simulator. To define the pseudo components of the oil, the oil package of Virtual Material Group simulator (VMGSim$^{TM}$) was used as the author found the VMGSim oil package was more convenient and straight forward for dividing the oil into pseudo components.

As stated in Chapter three, the oil sample used in this study was a solvent-extracted bitumen sample from a reservoir in Alberta. In order to define the pseudo components a characterization method was used. Simulated distillation was used to analyze the oil sample and to determine the true boiling point (TBP) curve. Simulated distillation which is based on gas chromatography (GC) is a technique that has been used to analyze the oil with a comparable accuracy to actual distillation and it can identify hydrocarbon components as heavy as $C_{80}$ (Curvers et al. 1989) in a matter of hours with a small fluid sample. For the oil sample which was used in the current study the resulting TBP data are presented in Table 5.2. By using the oil package of VMGSim$^{TM}$ the oil was cut into five pseudo component as stated in Table 5.3. These five pseudo components were introduced into the CMG WINPROP to build the fluid model to be used in CMG STARS. To complete the fluid model in WINPROP , there has to be some extra physical and thermodynamic data for oil. The most useful data is a set of saturation pressure versus temperature however because of the lack of such data for the oil used in this study, a set of isothermal density-pressure data were obtained and used to complete the fluid model.

Table 5.2 SimDist result for extracted oil sample

| Recovered Mass % | Boiling point C | Recovered Mass % | Boiling point C | Recovered Mass % | Boiling point C | Recovered Mass % | Boiling point C |
|---|---|---|---|---|---|---|---|
| IBP | 223.8 | 22 | 398.0 | 43 | 493.7 | 64 | 598.6 |
| 1 | 238.3 | 23 | 403.4 | 44 | 498.1 | 65 | 603.7 |
| 2 | 256.1 | 24 | 408.8 | 45 | 502.6 | 66 | 608.9 |
| 3 | 268.4 | 25 | 414.0 | 46 | 507.1 | 67 | 614.0 |
| 4 | 279.2 | 26 | 418.9 | 47 | 511.8 | 68 | 619.1 |
| 5 | 288.7 | 27 | 423.7 | 48 | 516.4 | 69 | 624.3 |
| 6 | 296.7 | 28 | 428.2 | 49 | 521.3 | 70 | 629.6 |
| 7 | 304.1 | 29 | 432.9 | 50 | 526.2 | 71 | 634.9 |
| 8 | 311.1 | 30 | 437.3 | 51 | 531.1 | 72 | 640.2 |
| 9 | 317.8 | 31 | 441.8 | 52 | 536.1 | 73 | 645.7 |
| 10 | 324.7 | 32 | 446.2 | 53 | 541.2 | 74 | 651.1 |
| 11 | 331.2 | 33 | 450.7 | 54 | 546.4 | 75 | 656.8 |
| 12 | 337.8 | 34 | 455.2 | 55 | 551.8 | 76 | 662.4 |
| 13 | 344.3 | 35 | 459.7 | 56 | 557.1 | 77 | 668.4 |
| 14 | 350.3 | 36 | 464.1 | 57 | 562.2 | 78 | 674.7 |
| 15 | 356.3 | 37 | 468.3 | 58 | 567.4 | 79 | 681.2 |
| 16 | 362.3 | 38 | 472.4 | 59 | 572.7 | 80 | 688.0 |
| 17 | 368.3 | 39 | 476.6 | 60 | 577.9 | 81 | 694.6 |
| 18 | 374.3 | 40 | 480.7 | 61 | 583.1 | 82 | 701.1 |
| 19 | 380.3 | 41 | 484.9 | 62 | 588.2 | 83 | 707.8 |
| 20 | 386.3 | 42 | 489.2 | 63 | 593.4 | 84 | 715.3 |
| 21 | 392.3 | 43 | 493.7 | 64 | 598.6 | 85 | 724.3 |

Table 5.3 Properties of pseudo components used to characterize the oil

| | **Hypo 1** | **Hypo 2** | **Hypo 3** | **Hypo 4** | **Hypo 5** |
|---|---|---|---|---|---|
| Molecular Weight | 379.63 | 652.61 | 950.25 | 1313.95 | 1360.21 |
| Normal Boiling Point (°C) | 345.86 | 530.37 | 703.15 | 951.96 | 1130.36 |
| Liquid Density @298K (kg/m$^3$) | 926.06 | 1006.82 | 1072.53 | 1162.36 | 1217.24 |
| Acentric Factor | 0.673 | 1.033 | 1.300 | 1.275 | 1.181 |

Density of oil was measured by a Anton Paar densitometer at 80°C from atmospheric pressure up to 3000 psi (20.64 MPa) and the values were used as a set of constant composition expansion (CCE) data in WINPROP. Density measurements are plotted against the corresponding pressure in Figure 5.1. Viscosity of oil was measured by a Cambridge Viscometer at different temperatures at a pressure of 500 psi (3.45 MPa). The results are listed in Table 5.4.

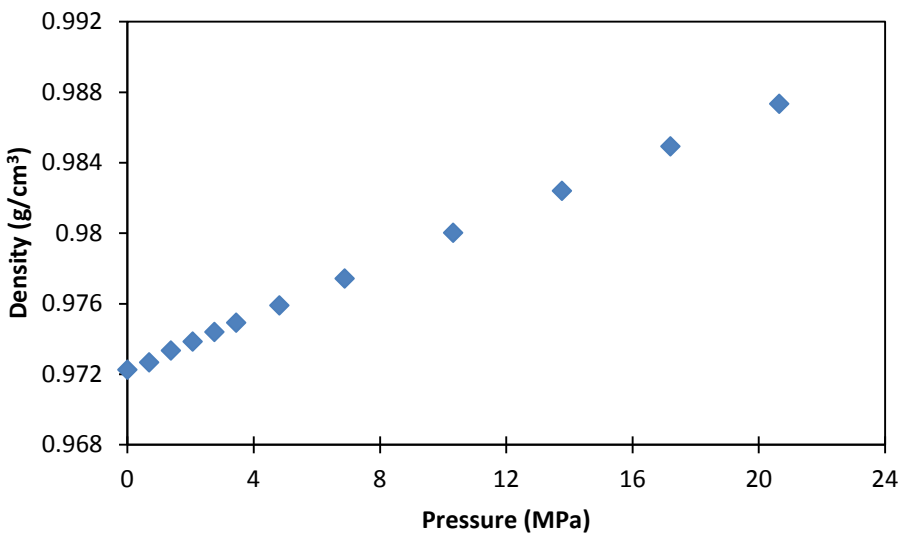


Figure 5.1 Density-pressure data of oil measured at 80°C

Table 5.4 Viscosity of oil at 500 psi (3.45 MPa) and different temperatures

| Temperature ($^oC$) | Viscosity (cp) |
|---|---|
| 25 | 294,500 |
| 40 | 38,700 |
| 55 | 7,400 |
| 80 | 1,400 |

### 5.2.2 Simulation model definition

As stated earlier in Chapter three, the assembled sand pack was a cylindrical shaped core with known dimension which was mounted inside an annulus and confining pressure was applied by using water. The simulation model was built by using CMG Builder. The flow inside the sand pack was assumed a 1-dimensional linear flow and in order to account for cylindrical flow passage inside the sand pack, the cylindrical grid was used with 56 longitudinal divisions with 1 centimeter width. Schematic of the model is shown in Figure 5.2 in which the color of each grid block refers to its distance from the top face.

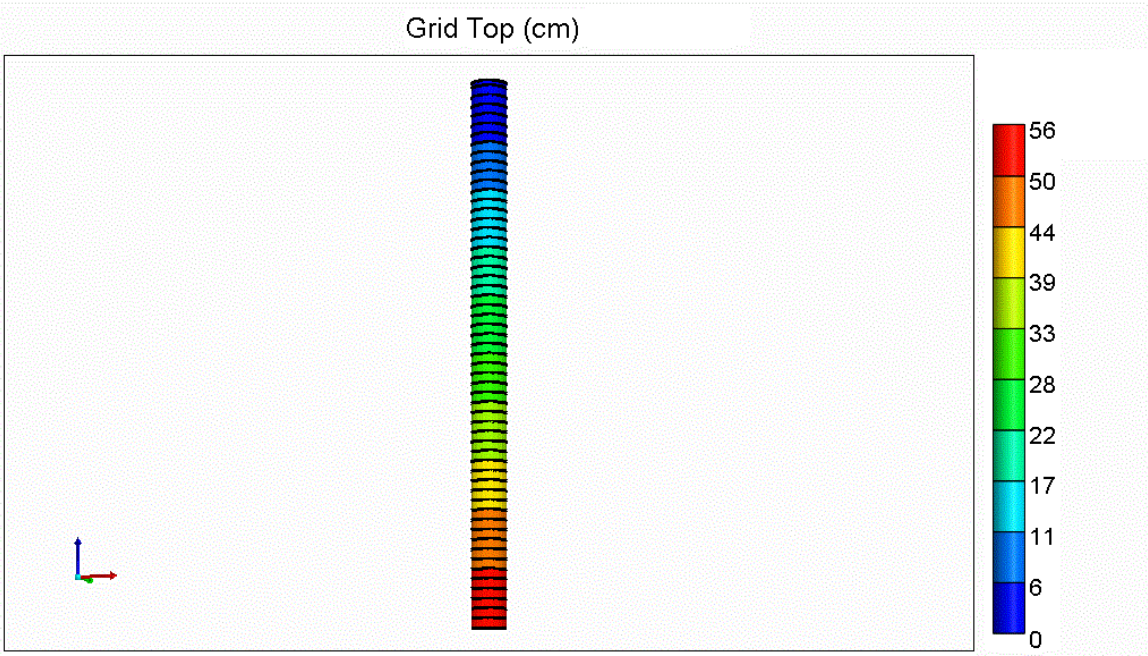


Figure 5.2 Physical model of sand pack simulated as a cylinder with 56 grid blocks

Two wells were defined at each end of the sand pack. The first one was at block #1 and the second one was at block #56. During the flood operation, one of the wells acted as injector and the other one acted as producer.

### 5.2.3 Preparing the field history files

All injection and production data as well as pressure drop which were recorded during the core flood experiments by using the data acquisition system needed to be entered into the simulator in order to replicate the flood process. The input data has to be in a specific format so called "field history format" and their time sequence and units also must be expressed in acceptable units based on the simulator procedure. The most commonly used field history files in CMG reservoir

simulator package are injection flow rate, production volume and pressure of injection and production wells.

### 5.3 Two phase oil/water experiments

In this section the experimental method and results for two phase oil/water experiments were presented. Three sets of oil/water displacements were conducted in this study which includes two drainage and one imbibition process.

#### 5.3.1 Primary drainage process

The first two-phase oil/water displacement was a drainage process. Core was evacuated of any gas by pulling a vacuum and then fully saturated with water. Oil was charged into the sample cylinders inside the air bath. The air bath temperature was set at 80$^{o}$C and it was left running overnight to develop a stable temperature throughout the system. As a preparation step to actual displacement test, water saturated core was pressurized to 500 psi (3.45 MPa) while 1000 psi (6.89 MPa) overburden pressure was applied using confining water. Data acquisition system was activated and all settings were checked to be ready to start the oil injection into the core. As a last step before injection, oil was pushed up to the core bottom entry right before the last inlet valve and it was pressurized slightly higher than the core initial pressure. The bottom entry valve was opened to start the oil injection process. Pressure drop across the core got higher as more oil was injected into the core as is indicated in Figure 5.3. Oil break through happened after injection of about 0.89 pore volumes of oil and another jump of differential pressure was observed which is related to an increase of pressure at the production side due to oil entering into the back pressure regulator.

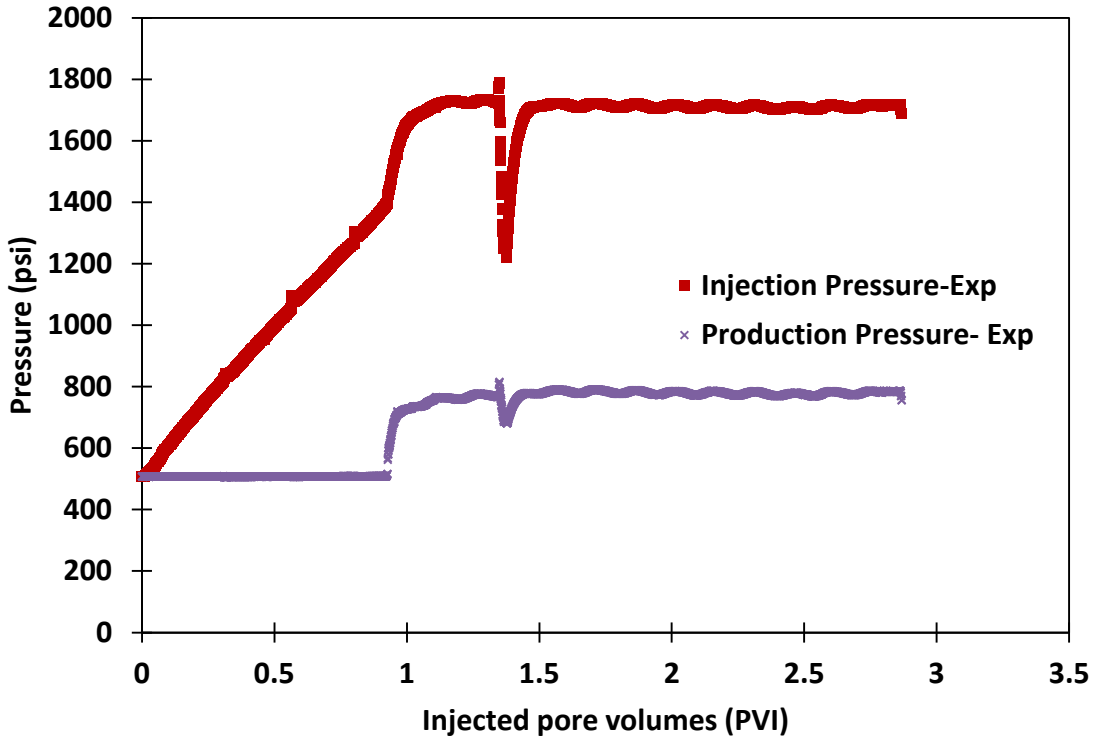


Figure 5.3 Injection and production pressure during oil injection in primary drainage process at 80ºC

Pressure drop remained almost constant after oil leaves the back pressure regulator until the end of the injection process. Due to injection pump interruption during the oil injection there was a sharp drop in both injection and production pressures around 1.5 pore volume injected.

#### 5.3.1.1 Collecting and analyzing the produced fluids

On the production side, the amount of produced oil and water was measured either continuously or at specified produced fluid volume intervals depending on having a full visual separation of oil and water. Due to formation of emulsion between the oil sample used in this study and water, there was no clear two-phase boundary in the liquid separator and therefore to measure the

amount of produced water and oil, discrete samples with volume of about 30 $cm^3$ were taken and analyzed individually to determine the water content. For primary drainage the water content of each sample were determined by Karl-Fischer coulometric titration method.

#### 5.3.1.2 Results and discussion

Residual water saturation is one of the parameters which needs to be determined after the drainage process. As stated by Maini and Okazawa, 1987, in heavy oil systems it is difficult to precisely determine the residual saturations of either oil or water and usually the extrapolation of recovery data to infinite throughput is necessary to estimate the residual saturations. Unlike for light oils the viscosity ratio of oil and water is high in heavy oil system and therefore the extrapolated residual saturations are usually lower than the measured value. Maini and Okazawa stated that for a typical heavy oil system, with oil/water viscosity ratio of 10 or less, 90% of ultimate recovery can be reached after 5 pore volumes throughput. But over 35 pore volumes throughput is required for viscosity ratio of 100 to get 90% of ultimate recovery. The throughput can be over a thousand pore volumes for higher viscosity ratios and that makes it experimentally impractical. Therefore one has to rely on an extrapolation method to get an estimation of the residual fluids saturation. Even though such an extrapolation may not be reliable it has been demonstrated that the water relative permeability is almost insensitive to the endpoint water saturation and in a history match technique the extrapolated value for water saturation will result in water relative permeability which is the extension of true relative permeability curve into higher water saturations. On the other hand oil relative permeability is more sensitive to the selected end point water saturation.

In the primary drainage flood for the current study around three pore volumes of oil were injected into the fully water-saturated core and after analyzing the collected samples the end point water saturation was calculated as 7.9%. To check the value of end point water saturation at infinite throughput, water recovery versus inverse of injection time was depicted as shown in Figure 5.4. Through extrapolation the value of endpoint water saturation was calculated as 2.4%. This value was used in the history match technique to determine the relative permeability in primary drainage process.

As mentioned earlier for conducting the history match, the STARS© simulator from CMG was used. The whole idea was to select a parametric form for relative permeabilities and by manipulating the parameters one can determine the relative permeability which would result in the best possible fit for produced fluids and pressure drop.

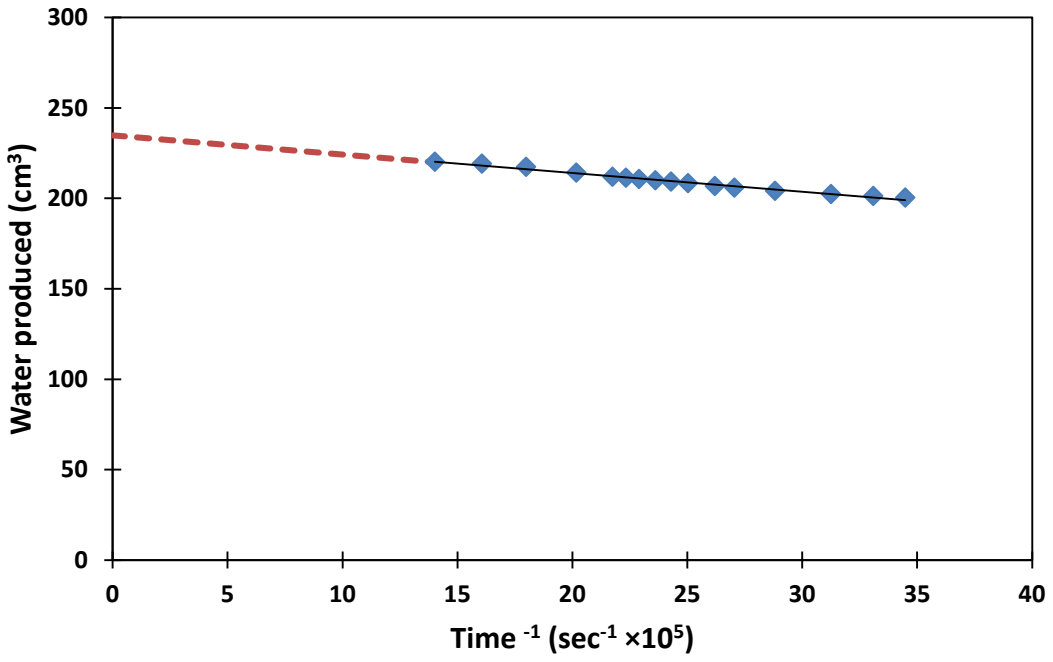


Figure 5.4 Extrapolation of produced water amount to infinite time

In STARS© there are built-in correlations for relative permeability calculations which in fact are Corey's equations. For oil/water systems the correlations for relative permeabilities are

$$k_{row} = k_{rowc}\left(\frac{1-S_w-S_{orw}}{1-S_{wr}-S_{orw}}\right)^{A_{ow}} \quad (5\text{-}1)$$

$$k_{rw} = k_{rwro}\left(\frac{S_w-S_{wr}}{1-S_{wr}-S_{orw}}\right)^{A_w} \quad (5\text{-}2)$$

By extracting the available endpoint saturations and relative permeabilities from experimental data the unknown parameters in these correlations are determined through minimizing the difference between experimental and simulated values of production and differential pressure data.

For all of the water/oil displacement experiments in this study no reasonable match was found based on the built-in correlations in STARS©. To find the proper shape of the relative permeabilities which could generate the experimental production and pressure drop data, other proposed models for heavy oils were examined. Starting from primary drainage oil/water process, the model proposed by Sigmund and McCaffery (1979) was found to generate the best possible match. This model which was reviewed in Chapter two, each water and oil relative permeability has two unknown parameters. Using the typical values for heavy oils which were reported by Maini and Batycky 1985, an initial shape for the relative permeability curves for water and oil which generates close match was determined. This initial shape was manually adjusted to get the closest match to experimental production and pressure data. The resulting relative permeabilities are shown in Figure 5.5. The final shape of relative permeability curves then fitted into Sigmund and McCaffery (1979) model by using a non-linear regression method to determine the exact values of two unknown parameters. Even though the quality of fit was

very good for water relative permeability curve, however the oil relative permeability which was predicted using Sigmund and McCaffery model shows some deviation. Through a minor modification on the governing equation of oil relative permeability, the quality of fit improves significantly. Table 5.5 summarized the unknown parameters $\varepsilon_w$ and $\varepsilon_{nw}$ and other constant values which appear in Sigmund- McCaffery model as well as the exponent for modified oil relative permeability correlation. Having all of the parameters and constant values, Equations 2-12 and 2-13 were used to get the governing mathematical equations of water and oil relative permeabilities from Sigmund- McCaffery model which are listed in Table 5.6.

Table 5.5 Parameters and constant values of Sigmund- McCaffery model for primary drainage at 80ºC

| **Parameter/ Constant** | **Calculated value** |
|---|---|
| Exponent parameter of water relative permeability $\varepsilon_w$ | 3.544 |
| Exponent parameter of oil relative permeability $\varepsilon_o$ (original model) | 0.616 |
| Exponent parameter of oil relative permeability $\varepsilon_o$ (modified model) | 1.609 |
| End point water relative permeability $k_{rw}^o$ | 0.008 |
| End point oil relative permeability $k_{ro}^o$ | 0.869 |
| Maximum water saturation $(s_w)_{max}$ | 1.00 |
| Minimum water saturation $(s_w)_{min}$ | 0.02 |
| Constants A and B | 0.01 |

Table 5.6 Mathematical equations of water and oil relative permeabilities from Sigmund-McCaffery model for primary drainage process

| | |
|---|---|
| Relative permeability of water | $k_{rw} = 0.008\left(\frac{(s_e)^{3.544} + 0.01s_e}{1.01}\right)$ |
| Relative permeability of oil from original model | $k_{row} = 0.869\left(\frac{(1-s_e)^{0.616} + 0.01(1-s_e)}{1.01}\right)$ |
| Relative permeability of oil from modified version | $k_{row} = 0.869\left(\frac{1-{s_e}^{1.609} + 0.01(1-s_e)}{1.01}\right)$ |
| Normalized saturation | $s_e = \frac{s_w - 0.02}{1 - 0.02}$ |

Figure 5.5 shows the relative permeabilities for oil and water. Dashed lines are the adjusted relative permeabilities determined from history match and the continuous lines are the fit from Sigmund/MacCaffery model.

The resulting relative permeabilities show that the water relative permeability is about two orders of magnitude lower than the relative permeability of oil.

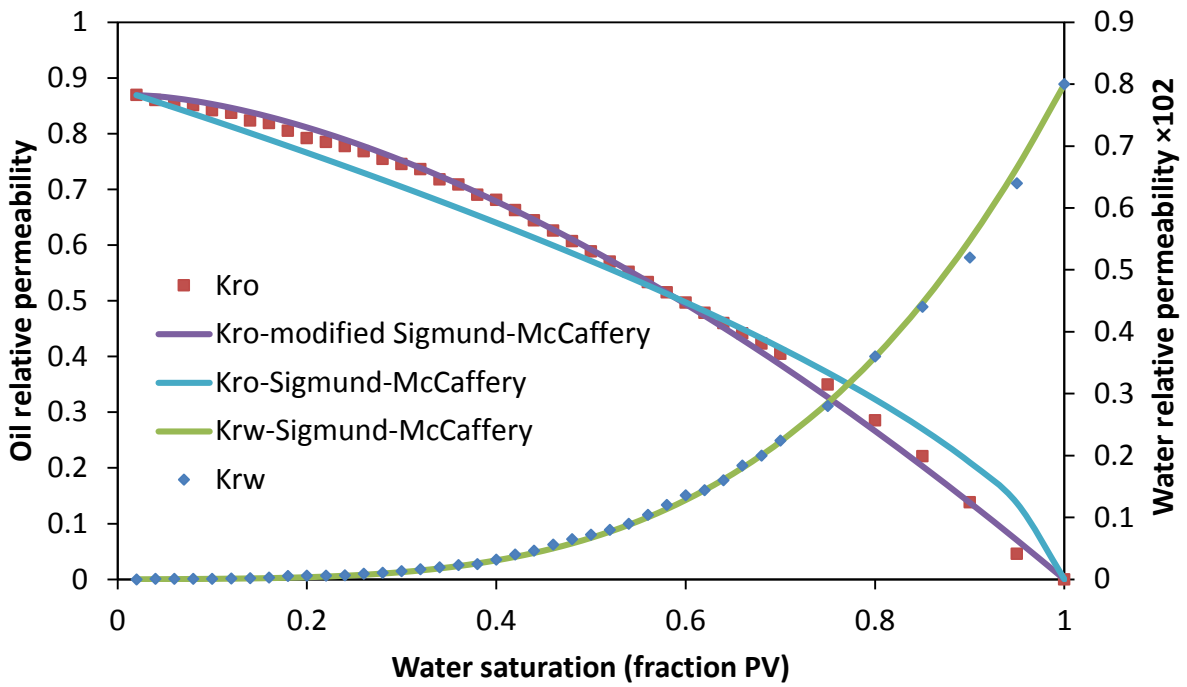


Figure 5.5 Relative permeability of oil/water in primary drainage

By using this set of relative permeability curves the history match results for production and pressure drop are presented in Figure 5.6 and Figure 5.7 respectively. Volumes of injected and produced fluids which were depicted in Figure 5.6 were converted to standard conditions. The corresponding temperature and pressure at standard conditions was assumed to be 25$^{o}$C and 1 atmosphere respectively. Note that in running the simulation, the injection flow rate and production pressure were treated as input parameters into the simulator and by adjusting the relative permeability of oil and water, the injection pressure and produced water and oil were matched.

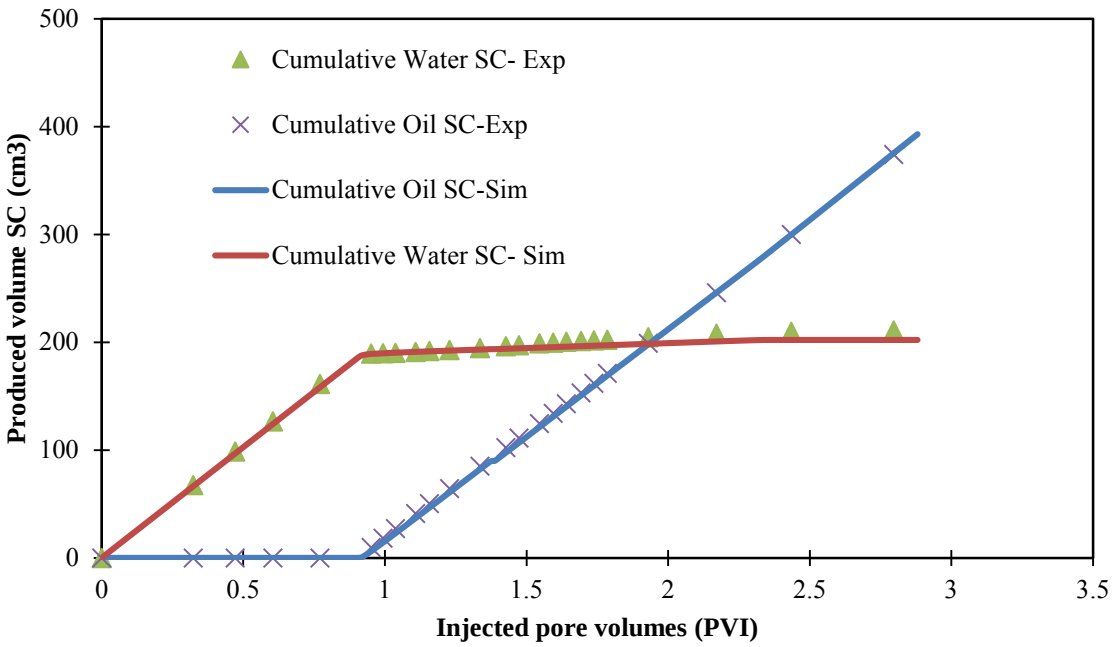


Figure 5.6 History match of water and oil production for primary drainage

Based on the results from Figure 5.6 , history match results for produced oil and water are in very good agreement with experimental data.

For the pressure drop results in Figure 5.7, there is some deviation right after the oil break through and the injection interruption point which happened after 1.4 pore volume injected. Beyond these two regions, the match is close to experimental pressure drop.

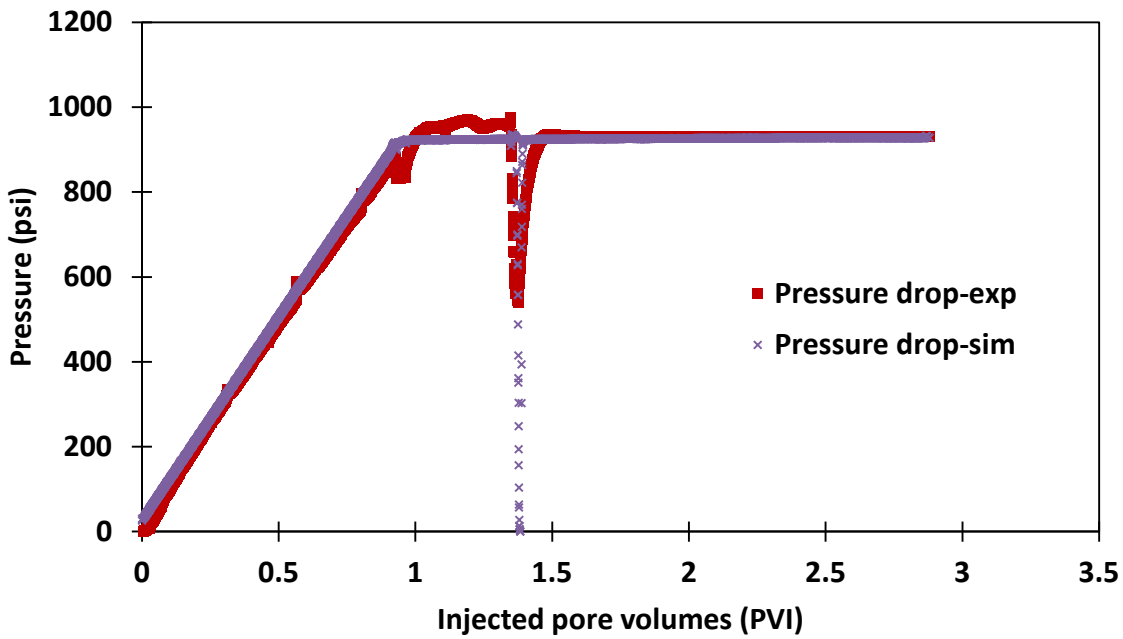


Figure 5.7 History match of pressure drop for primary drainage process

### 5.3.2 Imbibition process

After running a drainage process which includes injection of oil into the water saturated core, the reverse process was conducted. In the imbibition process, the non-wetting phase (oil phase) was displaced by the wetting phase (water phase). The intention of doing the reverse process was to study the relative permeability behavior against the direction of saturation change and determine any possible hysteresis.

To prepare the core for the imbibition process, the temperature of the air bath was set at 80ºC and the whole system was left under temperature control over night to reach a stable temperature. Initial pressure of core was 500 psi (3.45 MPa) with a confining pressure of 1000 psi (6.89 MPa) which corresponds to a net pressure of 500 psi (3.45 MPa). By starting the water injection,

produced fluids were collected as discrete samples of about 30 $cm^3$. Water flow rate during the imbibition process was kept constant at around 1.5 pore volume per hour. For imbibition process the analysis of produced samples were done by using the Dean-Stark distillation method. The details of this method were explained at Chapter 2.

#### 5.3.2.1 Results and discussion

Relative permeability of water and oil were determined by history match. Similar to the drainage process injection flow rates and production pressure were assumed as input parameters and the injection pressure and produced amount of water and oil were matched by adjusting the relative permeability. Figure 5.8 shows the resulting relative permeabilities of water and oil.

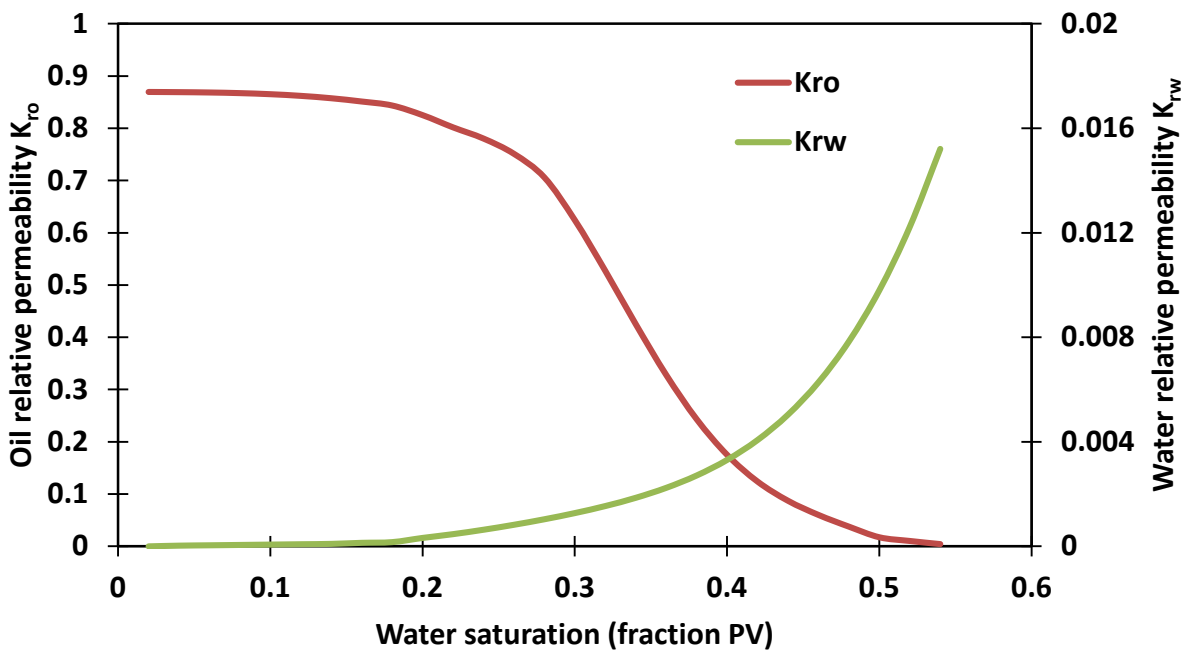


Figure 5.8 Relative permeability of oil/water in imbibition process

The shape of the water relative permeability curve is very similar to the one measured in the drainage process however the shape of the oil relative permeability turns out to be totally different than its counterpart in the drainage process. It follows a very low slope at high oil saturation and starts gaining a steep slope at lower oil saturation and then passes through an inflection point around $S_w$=0.35 in which the slope restarts to decline. This behavior produces an unusual shape for oil relative permeability which implies a high degree of hysteresis effect.

History match results for produced water and oil are presented in Figure 5.9. For both water and oil production, the agreement between experimental and simulated values are obvious.

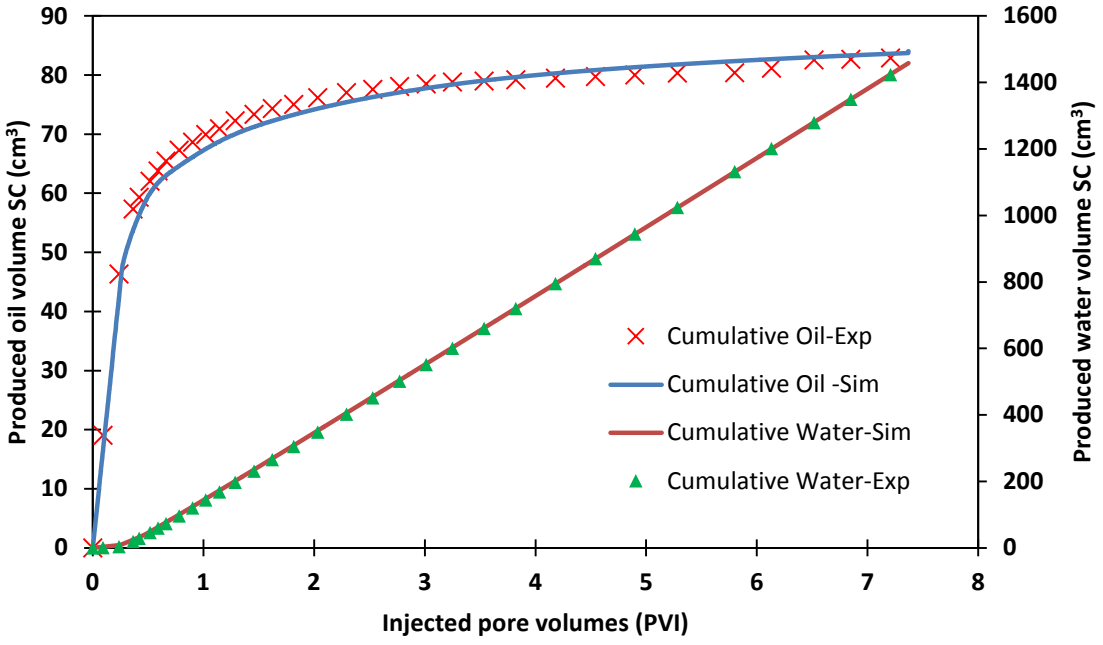


Figure 5.9 History match of water and oil production for imbibition process

History match results for differential pressure are shown in Figure 5.10. The scatter values for the experimental differential pressure are the result of back pressure operation when it tries to maintain a constant pressure at the outlet of the core. This behavior is a characteristic of liquid filled system in which a very small change in volume can make a significant impact on the pressure. Simulated pressure drops exceed the experimental values at the start of the injection. Note that the experiment starts from a static condition and at the beginning of the injection the compressibility of the fluids inside the transfer vessels and sand pack comes to play. Also there was some instability in confining pressure at the start of the test which led to a sudden change in core net pressure. As stated before the confining pressure can be adjusted by using a manual Ruska pump and at the start of the injection it was not at the value to apply the net pressure as planned. But in the simulator the pressure was assumed constant during this period. After the start point, the quality of match improves and the simulated values are close to the experimental ones.

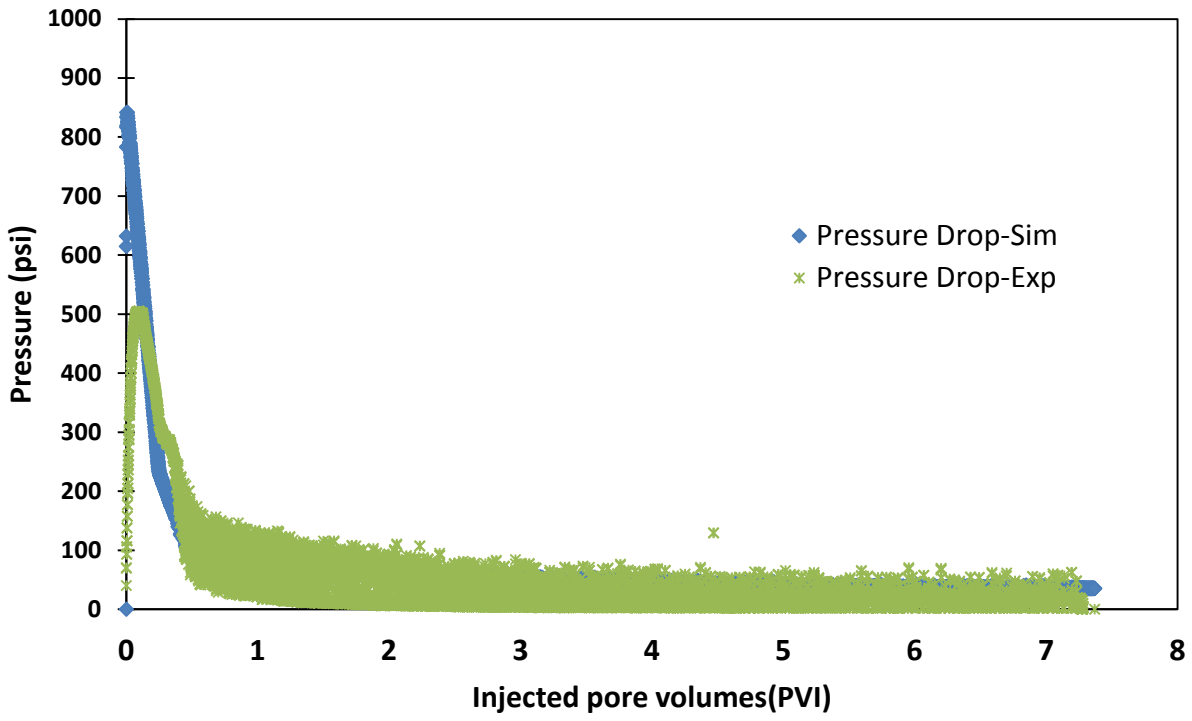


Figure 5.10 History match of pressure drop for imbibition process

### 5.3.3 Secondary drainage process

After running the primary drainage and imbibition on the core, the idea of running a secondary drainage to get a better understanding of relative permeability was deemed to be useful. The required preparations were made to run a second oil flood on the core which was at residual oil saturation. The resulting relative permeabilities for oil and water are shown in Figure 5.11. By following the same method explained in the primary drainage, the relative permeabilities were derived by manual adjustment through the simulator and then fitting into the Sigmund-McCaffery model. Parameters of the original and modified version of the model and the resulting

equations for relative permeability of water and oil are summarized in Table 5.7 and 5.8, respectively.

Table 5.7 Parameters and constant values of Sigmund- McCaffery model for secondary drainage

| **Parameter/ Constant** | **Calculated value** |
|---|---|
| Exponent parameter of water relative permeability $\varepsilon_w$ | 4.254 |
| Exponent parameter of oil relative permeability $\varepsilon_o$ (original model) | 0.394 |
| Exponent parameter of oil relative permeability $\varepsilon_o$ (modified model) | 2.994 |
| End point water relative permeability $k_{rw}^o$ | 0.0012 |
| End point oil relative permeability $k_{ro}^o$ | 0.869 |
| Maximum water saturation $(s_w)_{max}$ | 0.55 |
| Minimum water saturation $(s_w)_{min}$ | 0.02 |

Table 5.8 Mathematical equations of water and oil relative permeabilities from original and modified Sigmund- McCaffery model for secondary drainage process

| | |
|---|---|
| Relative permeability of water | $k_{rw} = 0.0012\left(\frac{(s_e)^{4.254} + 0.01s_e}{1.01}\right)$ |
| Relative permeability of oil from original model | $k_{rnw} = 0.869\left(\frac{(1-s_e)^{0.394} + 0.01(1-s_e)}{1.01}\right)$ |
| Relative permeability of oil from modified model | $k_{rnw} = 0.869\left(\frac{1-{s_e}^{2.994} + 0.01(1-s_e)}{1.01}\right)$ |
| Normalized saturation | $s_e = \frac{s_w - 0.02}{0.55 - 0.02}$ |

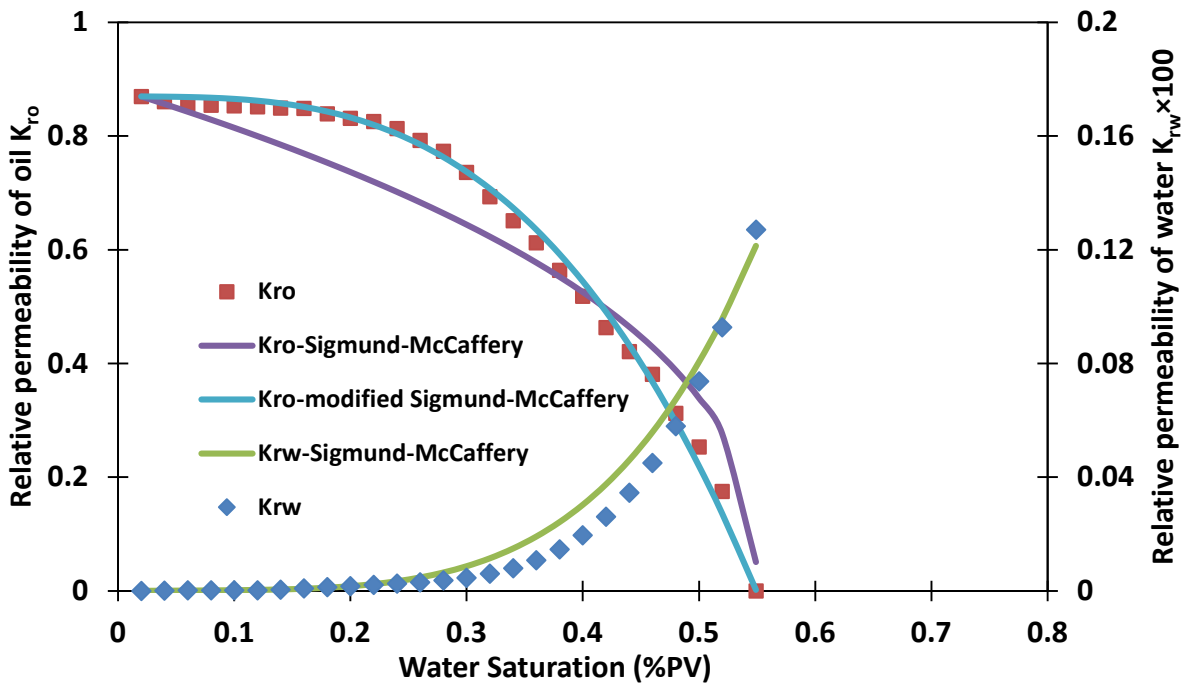


Figure 5.11 Relative permeability of oil/water in secondary drainage process

Figure 5.12 shows the history match results for produced oil and water. As is expected there is a sharp rise in produced water volume at the beginning of the flood and then it follows a mild increase afterword. Note that in secondary drainage nearly six pore volume of oil was injected into the core which is almost double that injected during the primary drainage however the trend of cumulative water production still indicates no sign of plateau. This type of behavior complies with the fact that for a heavy oil it might take over a few dozen injected pore volumes to reach residual saturation as discussed earlier under the primary drainage.

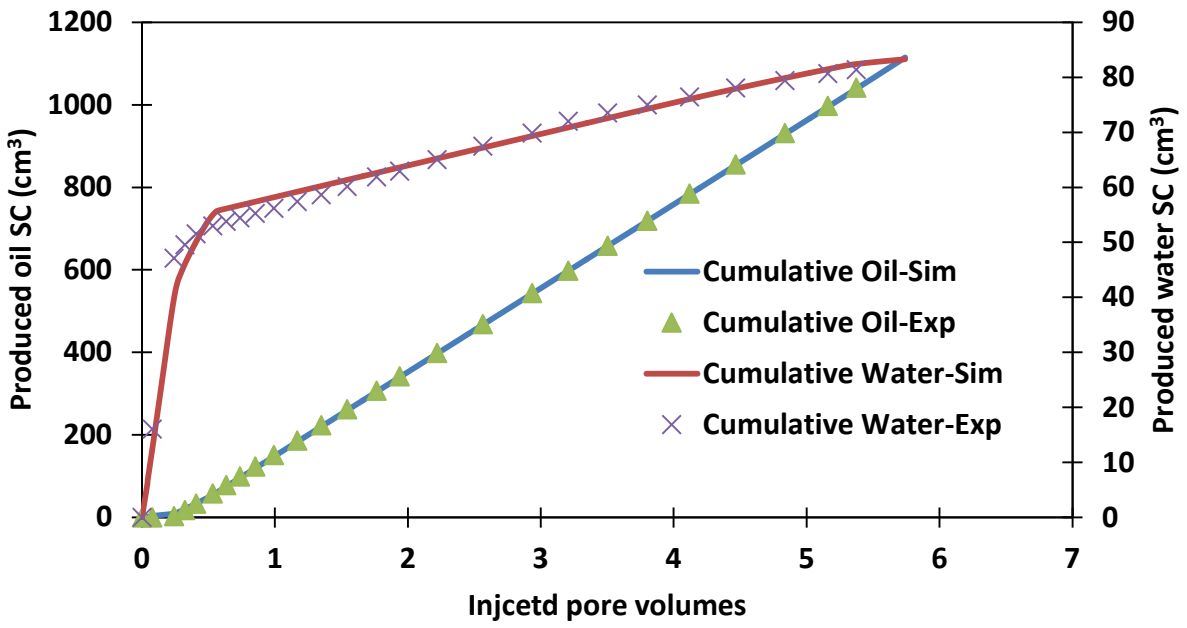


Figure 5.12 History match results for produced oil and water in secondary drainage

As in the previous two oil/water displacements, the injection flow rate and production pressure were treated as simulation input for the secondary drainage process and therefore injection pressure and fluid production were matched by adjusting the shape of the relative permeability curves. Figure 5.13 shows the input production pressure along with experimental and simulated production pressure.

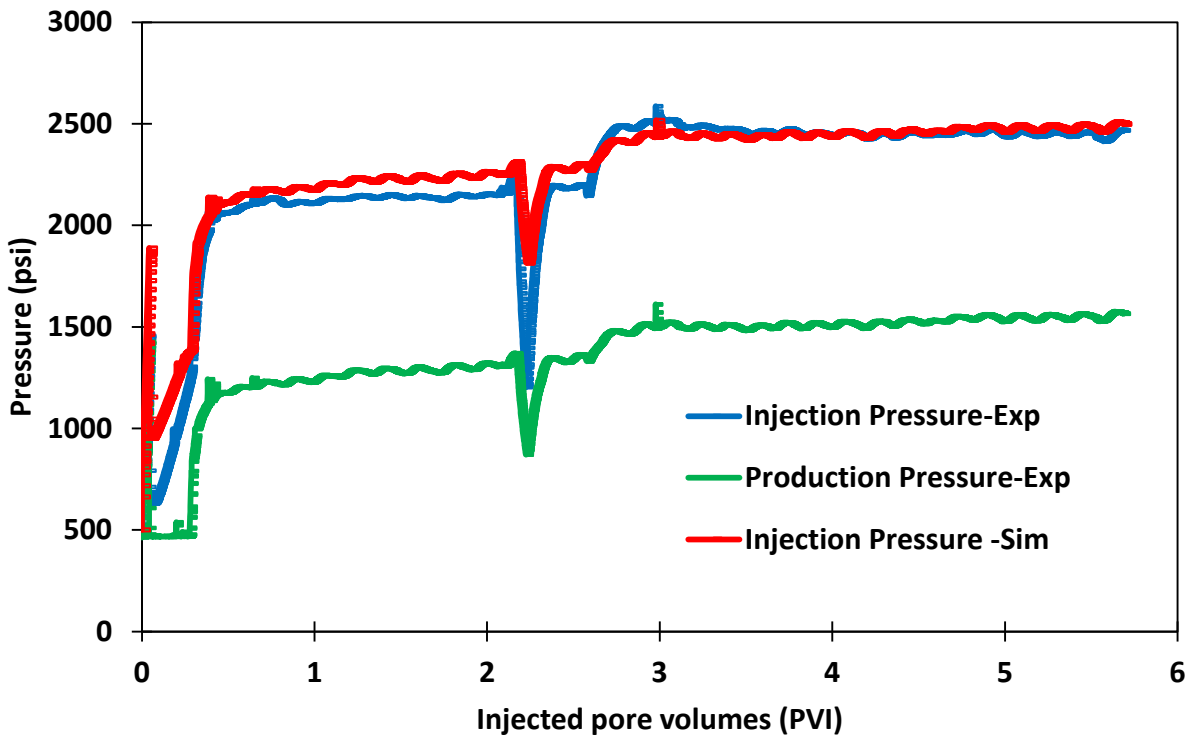


Figure 5.13 Injection and production pressure at secondary drainage

Secondary drainage started with a water-flooded core with an oil saturation value which was very close to residual oil saturation. Therefore at the beginning of the oil flood the produced fluid was primarily water which flowed through the back pressure regulator at nearly constant pressure of 500 psi (3.45 MPa) which was the set point on the gas-filled dome of the back pressure regulator. During this period the injection pressure followed nearly a constant increasing slope which is the result of moving the oil bank inside the core and this caused a higher pressure difference across the core. But as soon as the breakthrough of the oil bank happened and oil made its way into the production line and eventually back pressure regulator, production pressure experienced a hike and to supply a constant flow rate, the injection pressure

supplied by the pump started a sharp increase as well. After the oil bank passed the back pressure regulator the production pressure followed a slight slope and around 2.3 injected pore volumes an interruption in pump operation happened due to the over limit injection pressure which was set before the start of flood. This pump interruption caused a sharp drop in the outlet and inlet pressure of the core as it appears as a V shape region on Figure 5.13. After resuming the pump operation, both pressures rebound until the production pressure faces an increase around 2.5 pore volume injection point. This sharp increase is more likely due to partially blockage of one of the valves on the production line or malfunctioning of the back pressure regulator.

### 5.3.4 Concluding remarks on two-phase oil/water experiments

In this section the hysteresis effects which were seen on drainage and imbibition process are highlighted and discussed in more details. Comparison of the calculated relative permeabilities and end point saturation values with available literature data are also presented.

### 5.3.1 Hysteresis effects

A review at the oil relative permeabilities for imbibition and drainage processes which were illustrated on Figures 5.8 and 5.11 indicate a hysteresis on oil relative permeability. To provide a closer view, both relative permeabilities are shown together in Figure 5.14. The arrows indicate the direction of water saturation change for drainage and imbibition process.

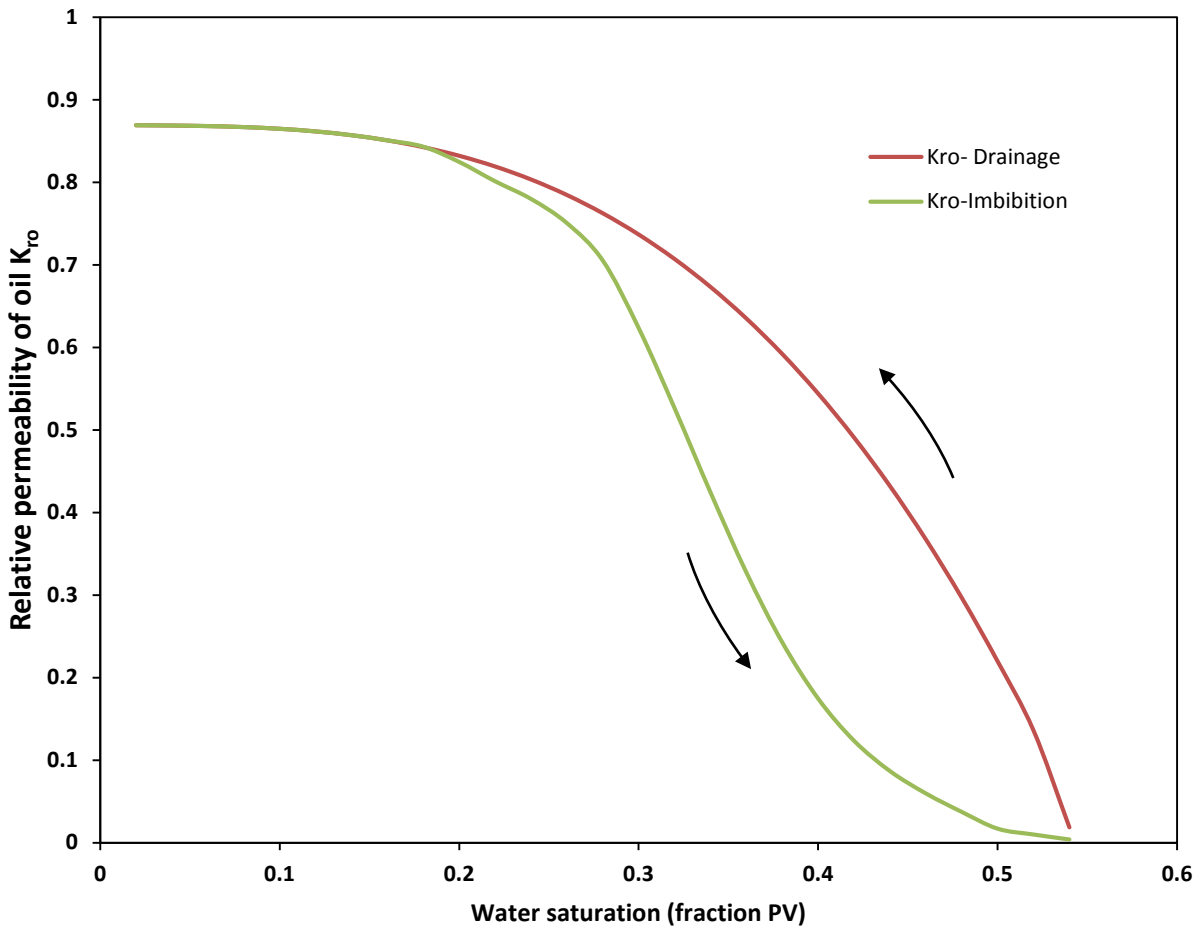


Figure 5.14 Hysteresis of oil relative permeability in drainage and imbibition process

During the imbibition process, water was injected into the core at nearly residual water saturation and the oil relative permeability followed the same path as the drainage process from residual water saturation of $S_w = 0.02$ to around $S_w = 0.20$ where it started to deviate towards lower values than the drainage oil relative permeability.

This deviation got larger with increasing water saturation and the maximum deviation occurred around $S_w = 0.4$ where a slope change happened and the imbibition relative permeability curve

turned back towards the drainage curve and eventually acquired zero value at residual oil saturation of $S_{orw} = 0.46$.

However the hysteresis was not limited to the non-wetting phase and it was found to exist for the wetting phase as well. Figure 5.15 shows the calculated water relative permeability curves for primary and secondary drainage as well as the imbibition process. During the drainage process when water was displaced by the oil, the relative permeability of water acquired much lower values compared with the corresponding oil relative permeabilities as was discussed in previous sections. Lower water relative permeabilities were seen during the imbibition process as well however they showed an increase compared with the drainage relative permeabilities as the water saturation rose during the imbibition process. This behavior appeared as a hysteresis in water relative permeability as illustrated in Figure 5.15. The arrows indicate the direction of change for water saturation during the imbibition and drainage process.

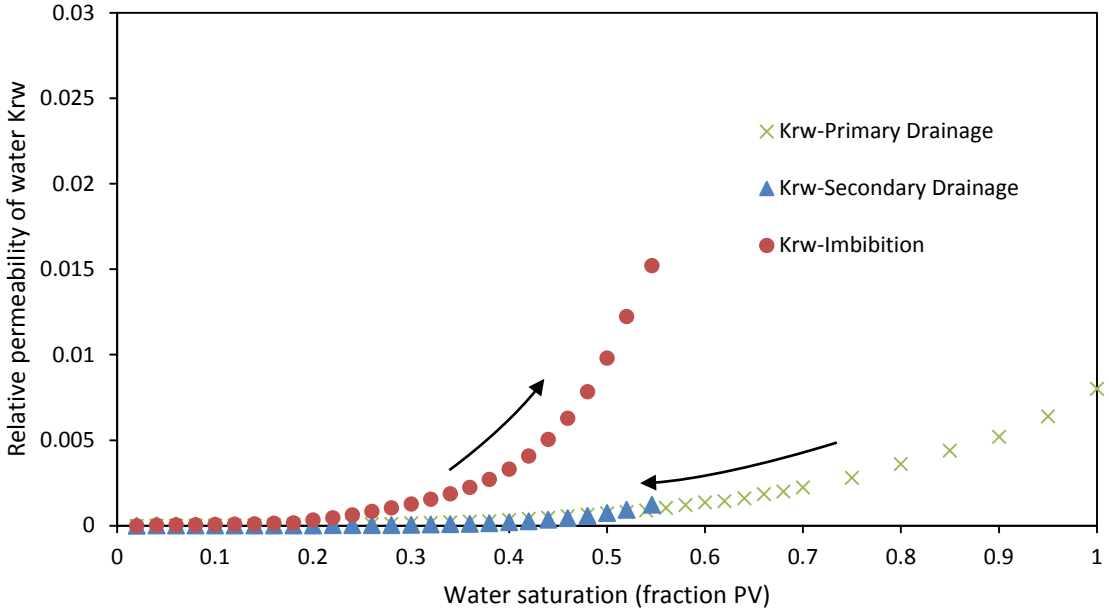


Figure 5.15 Hysteresis on water relative permeability for drainage and imbibition process

### 5.3.2 Comparison with literature

In this section the calculated relative permeabilities of oil and water and the endpoint saturations are compared with some of the available literature data. In Chapter 2, some of the published studies on relative permeability characteristics of western Canadian bitumen producing formations were reviewed. These studies generated two-phase water/oil relative permeabilities and the end point saturations for the bitumen and water systems at different temperatures. The majority of the reviewed studies (Bennion 2006, Polikar 1990, Frizzel 1990) investigated the imbibition relative permeability of the oil/water system in which the oil phase saturation was

declining. Drainage relative permeabilities were reported by Bennion et al. (1993) for water/bitumen system.

In a study which was published in 2006, Bennion et al. developed a series of correlations to calculate the imbibition relative permeability of bitumen/water at low and high temperatures. The developed correlations for the low temperature range of $60^{o}C < T < 100^{o}C$ to calculate the oil and water relative permeabilities are:

$$k_{rw} = 0.021(1 - S_N)^5 \tag{5-3}$$

$$k_{ro} = (S_N)^{2.2} \tag{5-4}$$

where $S_N$ is the normalized water saturation function defined as:

$$S_N = {(0.6 - S_w)}/{(0.45)} \tag{5-5}$$

it can be seen that water saturation has to be within the range of $0.15 < S_w < 0.60$. Calculated relative permeabilities using the above mentioned correlations are plotted along with the corresponding imbibition relative permeabilities from the current study as illustrated in Figure 5.16. While the shape of both water relative permeabilities follow a similar concave pattern the pattern of the oil relative permeabilities are different. Water relative permeability predicted by Bennion et al. is slightly lower than the corresponding value from the current study and oil relative permeabilities are close at water saturations larger than 40%. At lower water saturations they deviate and follow a different pattern.

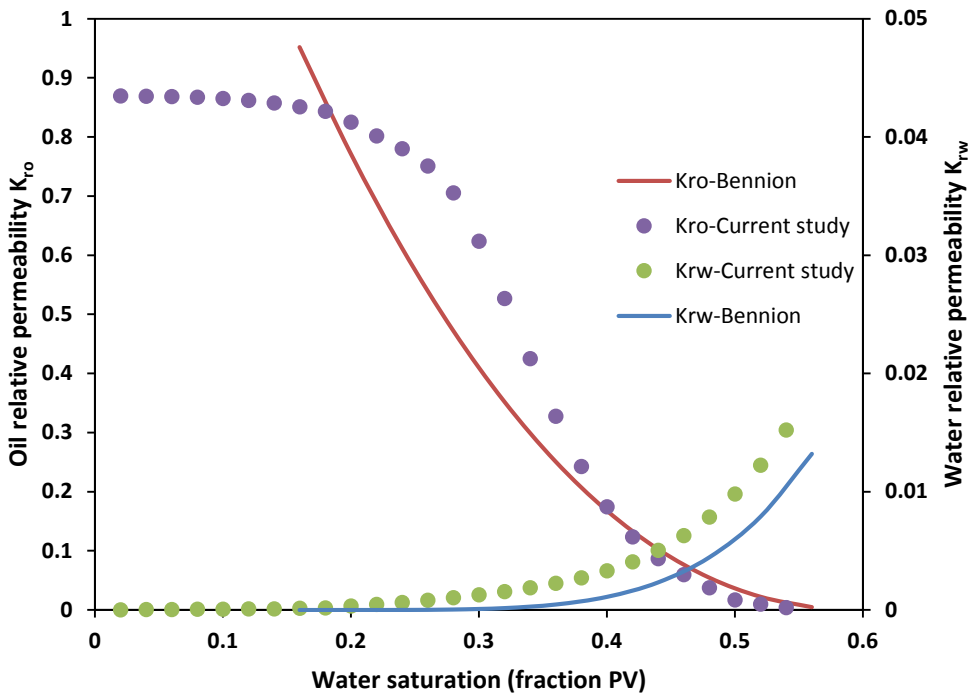


Figure 5.16 Comparison of imbibition relative permeabilities with Bennion's correlations

Polikar et al. (1990) published water/bitumen relative permeabilities at elevated temperatures which range from 100°C to 250°C using unsteady-state and steady-state methods. Steady-state experiments were conducted at two temperatures, 125°C and 175°C and the results were fitted by a power-law function using all the data points. The correlations are as follows:

$$k_{rw} = 2.025(S_w - 0.068)^{3.58} \tag{5-6}$$

$$k_{ro} = 0.752 - 2.282(S_w - 0.068)^{1.55} \tag{5-7}$$

The calculated relative permeabilities from these two correlations are plotted in Figure 5.17. Unsteady-state relative permeabilities at 125°C which were calculated by using the JBN method by Polikar et al. (1990) are also plotted in Figure 5.17 in order to compare both series of data with the results from the current study.

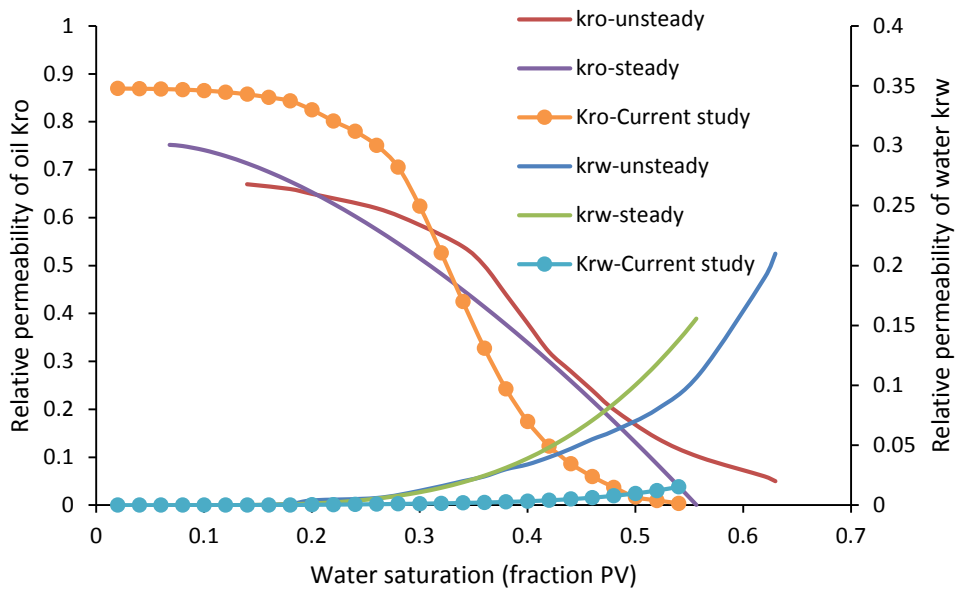


Figure 5.17 Comparison of the water/bitumen relative permeabilities reported by Polikar et al. (1990) with current study

The reported results by Polikar et al. show deviation between the unsteady-state and steady-state methods near the end point saturations. Compared to the current study, the reported water relative permeabilities were significantly higher. Oil relative permeabilities were of the same order of magnitude and $k_{ro}$ from the current study is higher at higher oil saturations. It can be

seen however that the shape of the oil relative permeability curve from the current study is similar to the calculated curve from unsteady-state method by Polikar. Residual water saturation in current study, $S_{orw}$ = 0.455 is very close to the reported value of $S_{orw}$ = 0.444 in Polikar's steady-state experiments.

In the study by Bennion et al. (1993), imbibition and drainage relative permeability of water/bitumen were calculated by a steady-state method at 200°C. The authors reported hysteresis on both oil and water relative permeability curves during the drainage and imbibition process. They concluded that the individual phase relative permeability was higher when its saturation was increasing than when it were decreasing. This complies with the results from the current study.

### 5.4 Gas/liquid displacement

During any recovery process which involves injecting a gas into a natural reservoir, such as *in situ* combustion, injected gas displaces some of the reservoir fluids into the production well. In case of *in situ* combustion, flue gas which is being produced from burning a fraction of the oil in the combustion front, displaces some reservoir fluid into the cold part of the reservoir. To study the relative permeability behavior in this type of displacement, an experiment was designed and conducted on the sand pack. During the last displacement test, the core was flooded with oil and the final state of the core was close to residual water saturation which resembles a natural reservoir. To simulate the gas flow into the fresh part of the reservoir, nitrogen was injected into the oil-flooded core to displace the fluids into the production side of the core. To have a more stable front during the gas flood, gas injection was conducted from the top of the core towards

the bottom and produced fluid was collected from the bottom. This means that the injection well was switched into production well and vice versa. The same changes were done on the pressure lines as well and in order to do that, two special three-way valves were installed in a loop which can switch the low/high pressure side of the differential pressure transducers into the proper entry point at inlet and outlet of the core.

### 5.4.1 Practical difficulties

Injecting a gas into a liquid filled core is usually associated with practical difficulties. Most of these difficulties stem from high compressibility of gas which makes the gas injection a challenging process. In core flood experiments it is crucial to have the cumulative quantity and flow rates of injected and produced fluids as accurate as possible. For liquids measuring the injected and produced amounts usually is simple especially when accurate pumps are employed. A similar method can be applied to gases by using a mass flow meter. However in the current study there was no access to a mass flow meter for gas injection, hence the cylinder-piston system was used to conduct the gas injection. Sample cylinders were filled up with nitrogen and water was used to push the gas into the core. Compressibility of gas makes it difficult to control the injected amount of gas at a desired value. For instance to maintain the gas flow rate of 5 $cm^3$/min at the injection pressure, by using a piston-cylinder, the flow rate of water can be set at the same number but after a certain injection period, the cumulative injected volume of water measured by the pump, may or may not be equivalent to the cumulative injected amount of gas. The reason is that a fraction of the piston movement caused the gas to be compressed rather than pushing the equivalent volume out of the cylinder. This uncertainty is more severe at low injection pressures and it can be reduced as the injection pressure increases.

One method to check the accuracy of the measured gas volume by the pump is to compare the produced gas volume measured by the wet test meter with the cumulative injected value by the pump. By doing a simple mass balance the amount of gas inside the core can be calculated by having the amount of produced volume of liquids. Adding this value to the wet test meter reading which is converted to the injection pressure condition, results in the total injected gas.

The gas flood experiment started with pressurizing the core up to a pressure slightly below the back pressure regulator set point pressure. Stored gas inside the sample cylinders was pressurized to the same pressure as the core while the last valve on the injection line was kept close. To start the gas injection the pump was activated and the last valve cracked open to let the gas and core communicate. As the pump kept running the injection pressure increased until the core pressure was about to exceed the set point pressure of the back pressure regulator. The moment at which the first drop of liquid passed through the back pressure regulator, was assumed as the onset of gas injection into the core. Figure 5.18 shows the variation of injection pressure during the gas flood. The pattern which was followed by the injection pressure was mostly affected by changes in the injection flow rate as well as changes which were dictated by the production end and back pressure regulator. As discussed earlier, operation of the back pressure regulator creates fluctuation on the production side even when the fluids are in a liquid state, the fluctuations can be considerable. For any displacement process which involves gas, this fluctuation is more severe because of the gas compressibility. For gas/liquid mixtures at the production end of the core, observed pressure instabilities were more severe. This behavior is shown in Figures 5.18 and 5.19 during the gas injection experiment.

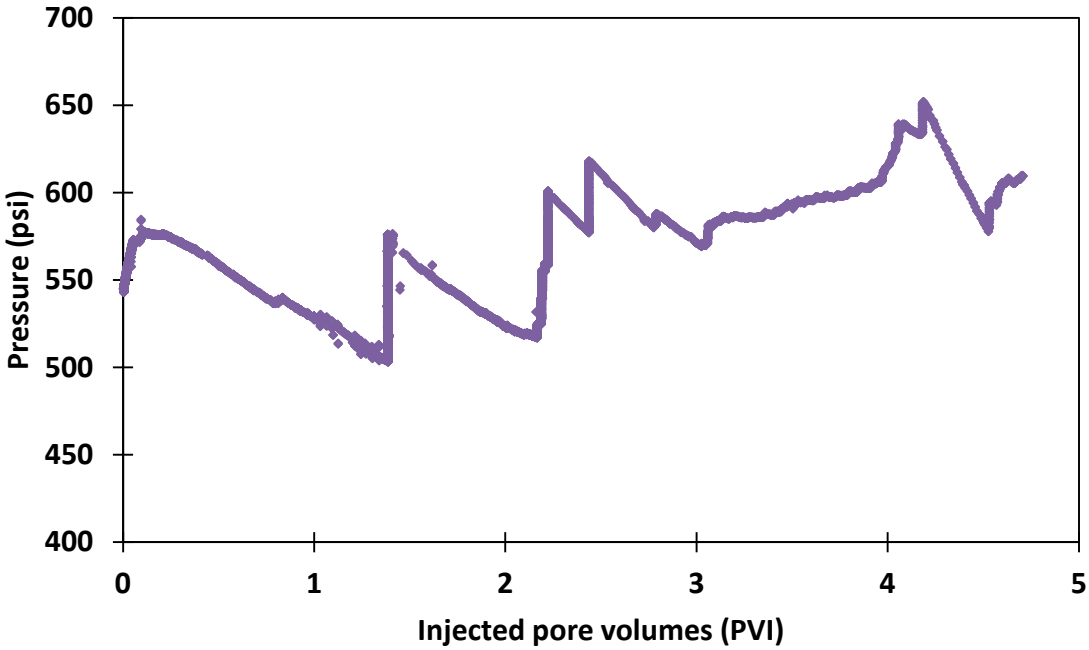


Figure 5.18 Variation of injection pressure during liquid displacement by gas injection

As gas moved along the core from top to bottom, the liquid was pushed out of the bottom and moved through the back pressure regulator. The production pressure started rising and so did the injection pressure. When gas breakthrough happened after 0.15 pore volume injection, production pressure declined which is followed by a decline in the injection pressure. Around 1.4 injected pore volumes, the production suddenly stopped and after evaluating the system, a malfunction was suspected on the production line most likely in the back pressure regulator. Due to this malfunction, injection pressure started to rise as a result of the pressure build up in the production line. Injection was stopped and the back pressure regulator was removed and flushed and reinstalled and gas injection was resumed. By resuming gas flow through the system, the production pressure started to decline up to 2.2 pore volume and gas injection flow rate was increased at this point from 0.5 PV/h to 1 PV/h. As a result, pressure started to first build up

followed by a decline as a result of the decrease in production pressure. Two more increased injection rates of 1.5 and 2.5 PV/h were applied to assess the effect of higher injection rates on liquid production and pressure profiles.

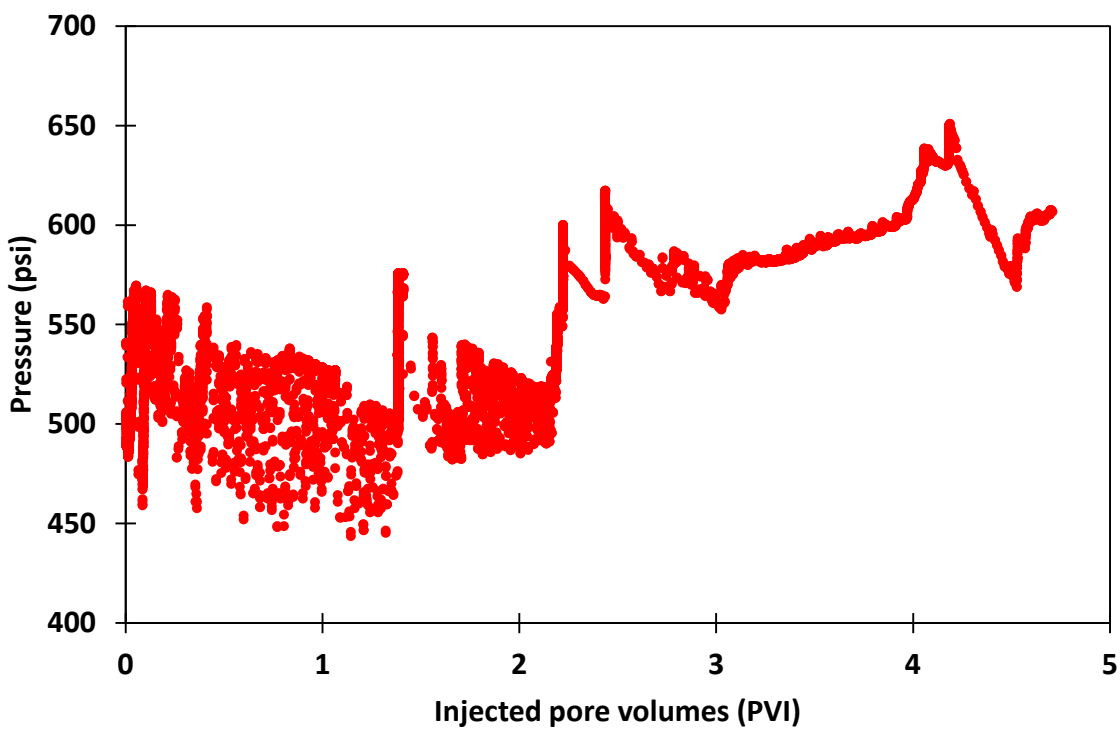


Figure 5.19 Variation of production pressure during liquid displacement by gas injection

### 5.4.2 Results and discussion

To conduct the history match on the gas injection process, injection and production pressures were assumed as two input variables and liquid and gas production were matched by adjusting the relative permeabilities of the gas and liquid. Figure 5.20 shows the resulting relative permeability curves for the gas/liquid. The gas relative permeability is about two orders of magnitude lower than the liquid relative permeability.

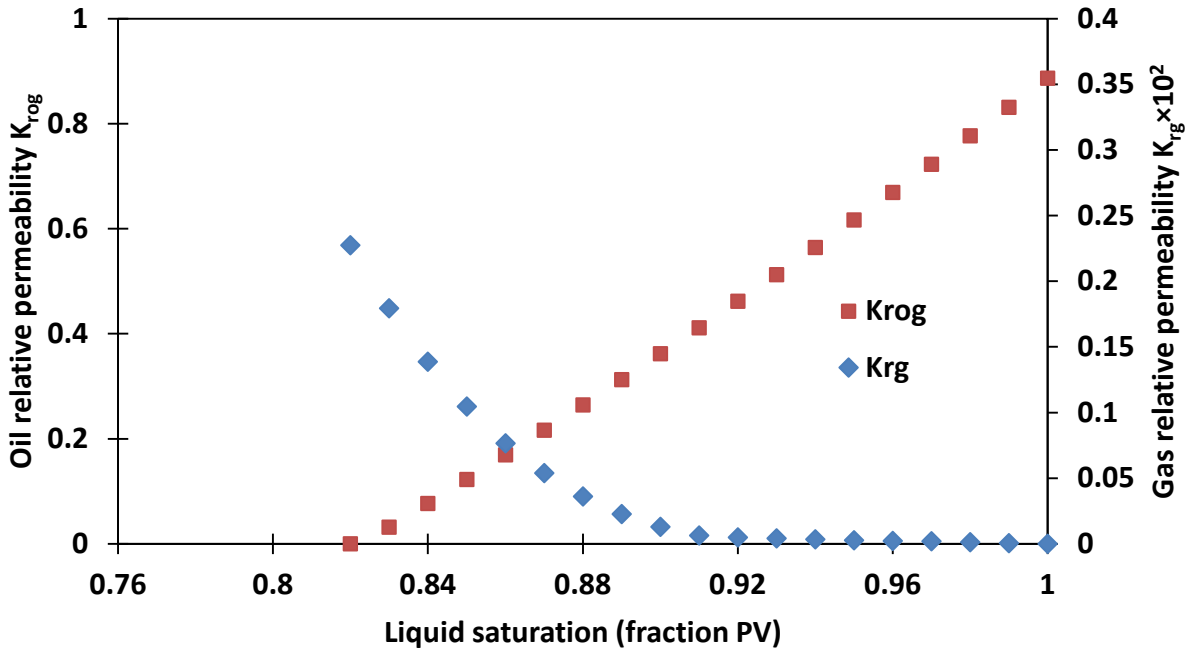


Figure 5.20 Relative permeability of gas/liquid in liquid displacement by gas injection at 80ºC

History match results for produced volumes of gas and liquid are shown in Figure 5.21. At the beginning of gas injection, liquid production follows a sharp increase until the gas breakthrough point and this rise continues up to 0.4 injected pore volumes. This early high liquid production rate is a result of the high liquid relative permeability at the higher liquid saturations which exists throughout the core during the early stages of the gas flood. However as soon as the liquid saturations drop into lower values as the gas saturation increases, liquid permeability approaches zero and liquid becomes less and less mobile. Overall the match for liquid production is very close.

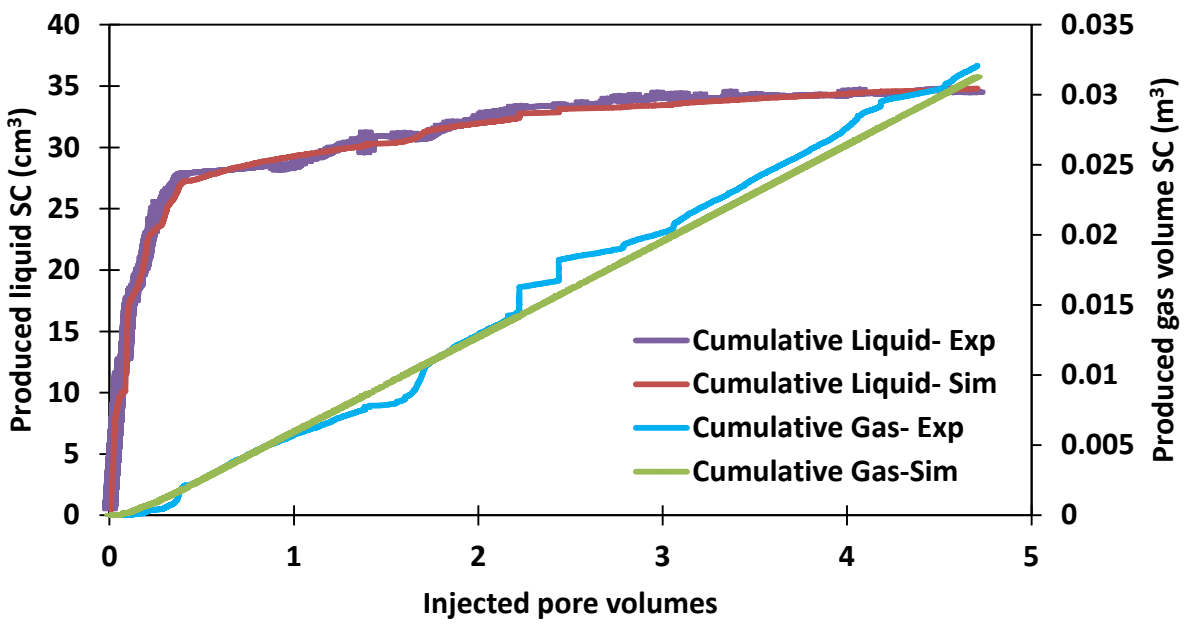


Figure 5.21 History match results for produced liquid and gas in gas flood experiment

Matched results for the gas production are also very close at early stages of the flood up to around 2.2 injected pore volumes. There is a bump around 1.6 PVI which is more likely due to a pressure fluctuations dictated into the simulator. Produced gas volume is overestimated by the simulator after 2.2 PVI.

### 5.5 Three-phase water/oil/gas experiment

During gas injection into a reservoir, there are several displacement modes as discussed earlier. One of the displacement modes happens when the oil bank moves into the region which is already swept by flue gas. During this phenomenon, saturation reversal happens and liquid saturation starts to rise. This behavior was simulated in this study by designing a displacement test which follows the same saturation hysteresis that exists during saturation reversal.

This experiment was conducted after the previous gas flood test while the core was swept by gas and it was sitting at residual liquid saturation. Therefore the initial state of the sand pack corresponds to the condition which existed at the beginning of saturation reversal. To simulate the oil bank which was being followed by a water bank, a slug of oil which was about 0.3 pore volumes was first injected and followed by a slug of water equal to 0.3 pore volumes. Gas injection was started after injecting the water slug and it was continued until there was no liquid production.

To calculate the three-phase relative permeabilities there are three built-in methods available in CMG STARS which are Stone's first and second methods and the linear interpolation method. All of these methods (Stone, 1970 and 1973) combine two-phase water/oil and gas/liquid relative permeabilities to calculate the three-phase relative permeability of oil.

Stone's methods are probability models and they were developed based on the assumption that the three-phase water/gas/oil flow can be bounded by two-phase water/oil flow at one boundary and oil/gas flow at the other (Honarpour, 1986). In most of the probability models, it is assumed that the gas relative permeability is a function of gas saturation only and in the same manner the water relative permeability depends only on water saturation. In a water-wet system the gas phase behaves as the non-wetting phase and the oil phase acts as the phase with intermediate wettability. Three-phase relative permeability to oil in a water/oil/gas system will therefore be bounded by two extreme boundaries which include relative permeability to oil in a water/oil system at low gas saturations and relative permeability to oil in a gas/oil system at low water saturations. These two terminal relative permeabilities were combined in Stone's models to obtain a three-phase result by using the channel flow theory in porous media and simple probability models. Several modifications were proposed on Stone's methods in order to comply the predicted results with available experimental data (Honarpour, 1986).

CMG STARS uses a modified version of both Stone's methods as outlined in the STARS manual (2012). In order to apply the Stone's first method on a three-phase system, the gas connate saturation cannot acquire a value other than zero. In other word, connate gas saturation $S_{gc} > 0$ is not allowed in two-phase gas/liquid data in the Stone's first method as outlined in the STARS manual.

Regarding the Stone's second model, CMG STARS uses a modified version which was proposed by Aziz and Settari (1979). Details of this method with involving equations are summarized in Appendix A. Linear interpolation is the third available method to calculate the three-phase oil relative permeability in CMG STARS. According to this method, the middle phase relative permeability is calculated from a linear interpolation scheme proposed by Baker. (1988).

In this current study, two-phase relative permeability of water/oil and gas/liquid which were determined in early experiments, were used to calculate the three-phase oil relative permeability by using both of the Stone's methods and Baker linear interpolation method. Calculated three-phase relative permeabilities of oil from each method were plotted in a saturation ternary diagram as presented in Figures 5.22 to 5.24. Relative permeabilities of water and gas were assumed equal to the corresponding values in two-phase experiments as outlined in Stone's method.

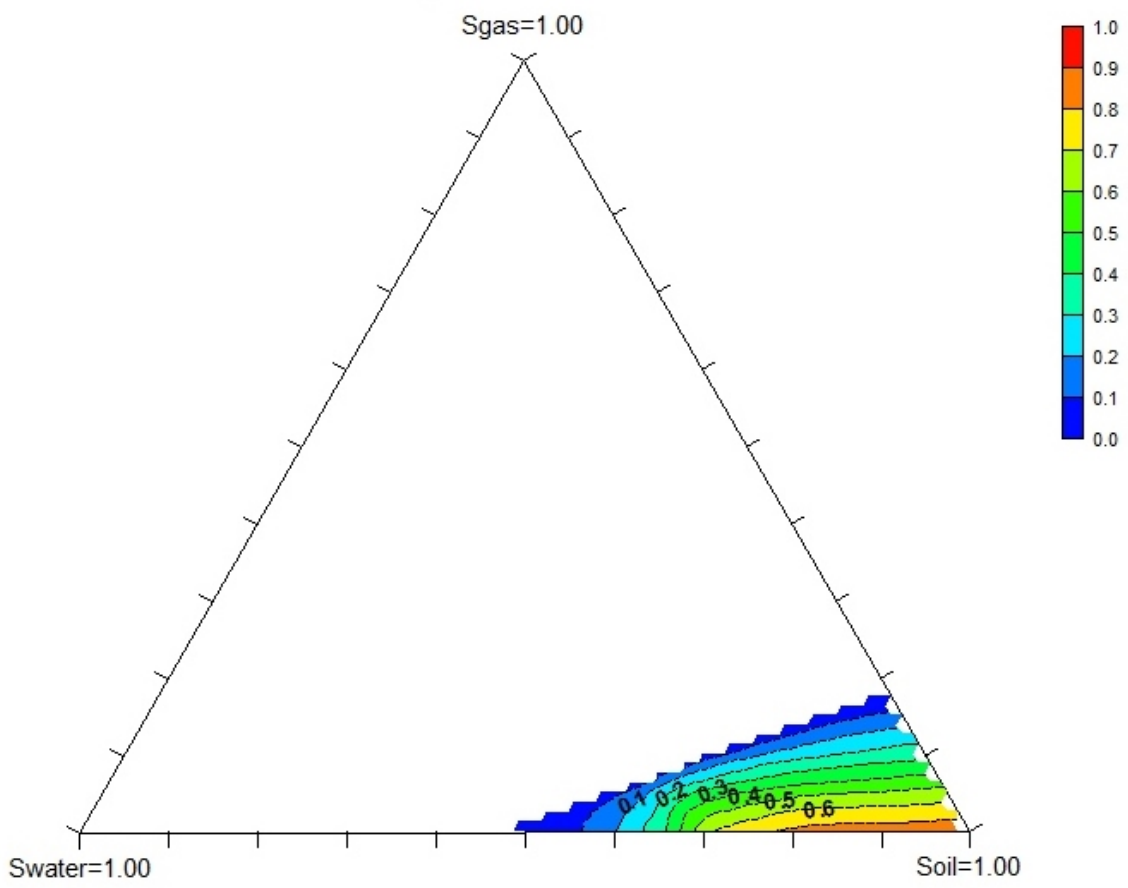


Figure 5.22 Three-phase relative permeability of oil calculated by Stone's first model

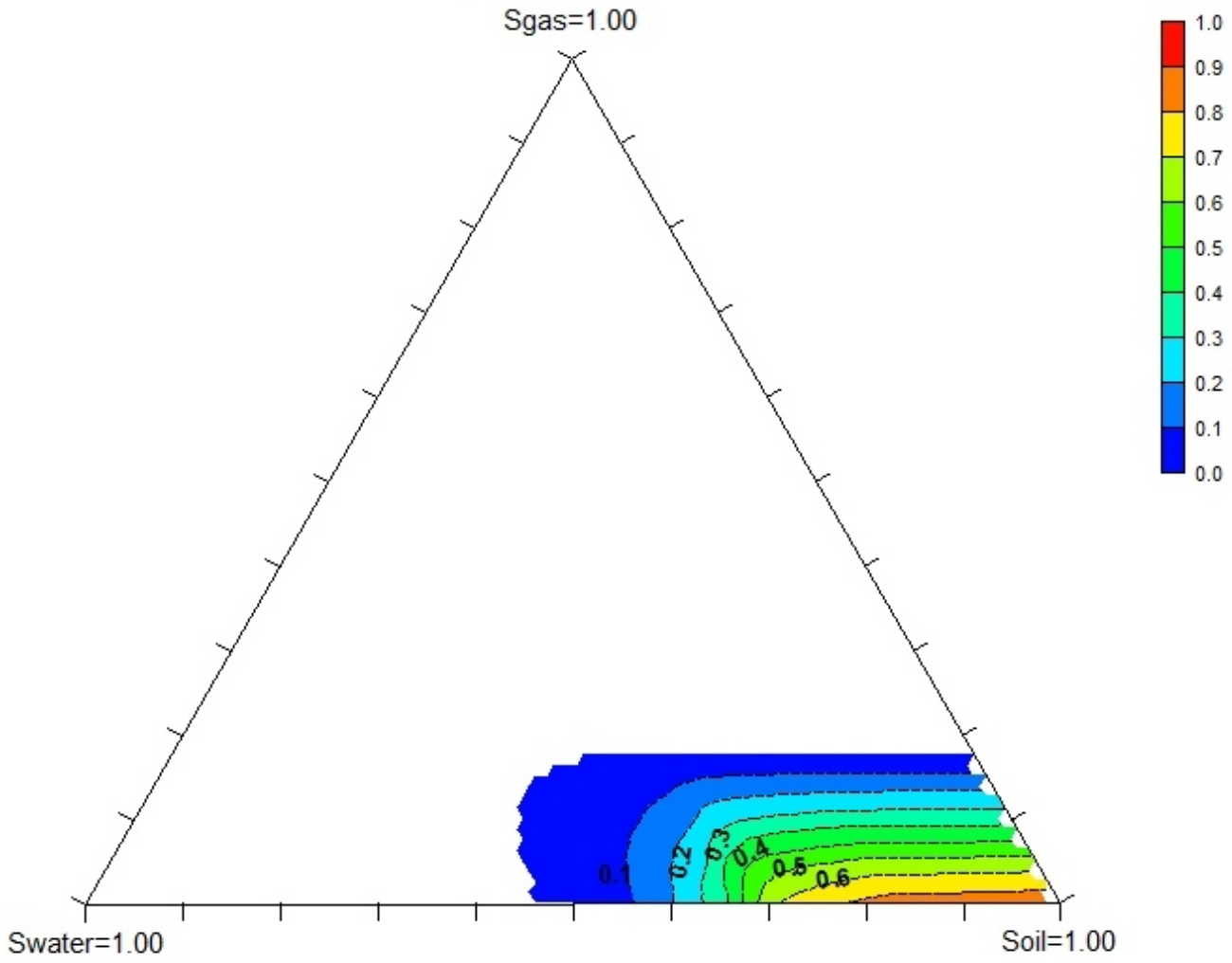


Figure 5.23 Three-phase relative permeability of oil calculated by Stone's second model

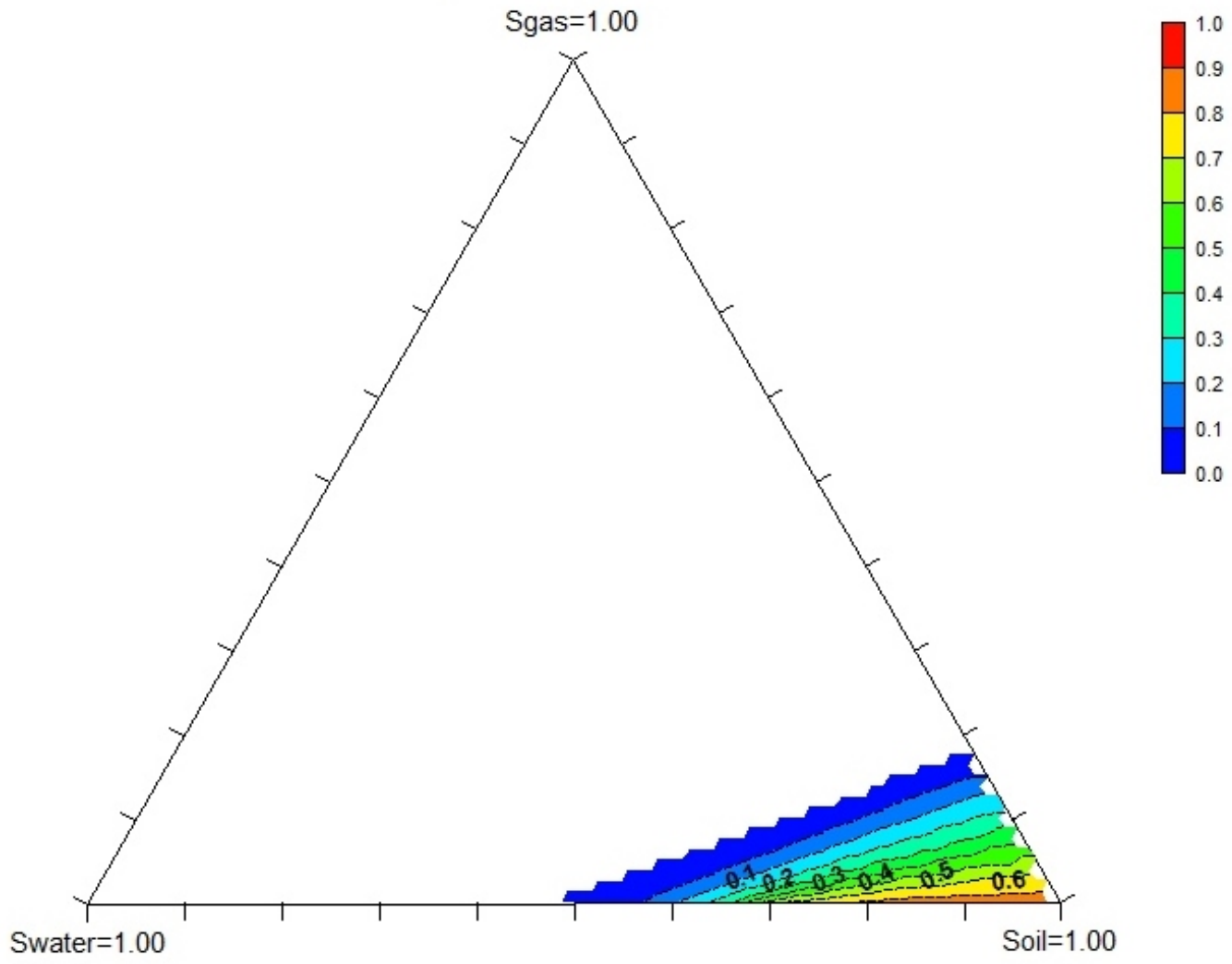


Figure 5.24 Three-phase relative permeability of oil calculated by Baker's interpolation method

Injection flow rates and production pressure history were treated as input to the simulator and the model predictions for liquid and gas production and injection pressures were determined. The results are presented in Figures 5.25 to 5.30.

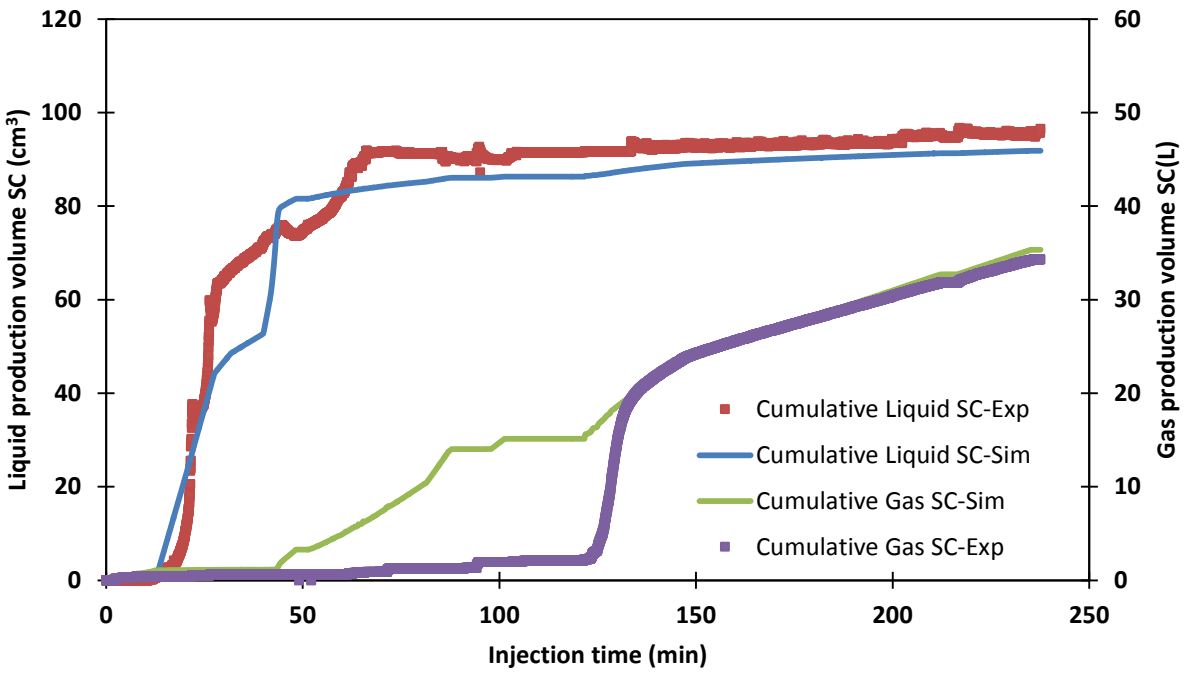


Figure 5.25 Prediction of produced liquid and gas in three-phase system using the Stone's first model to calculate the oil relative permeability

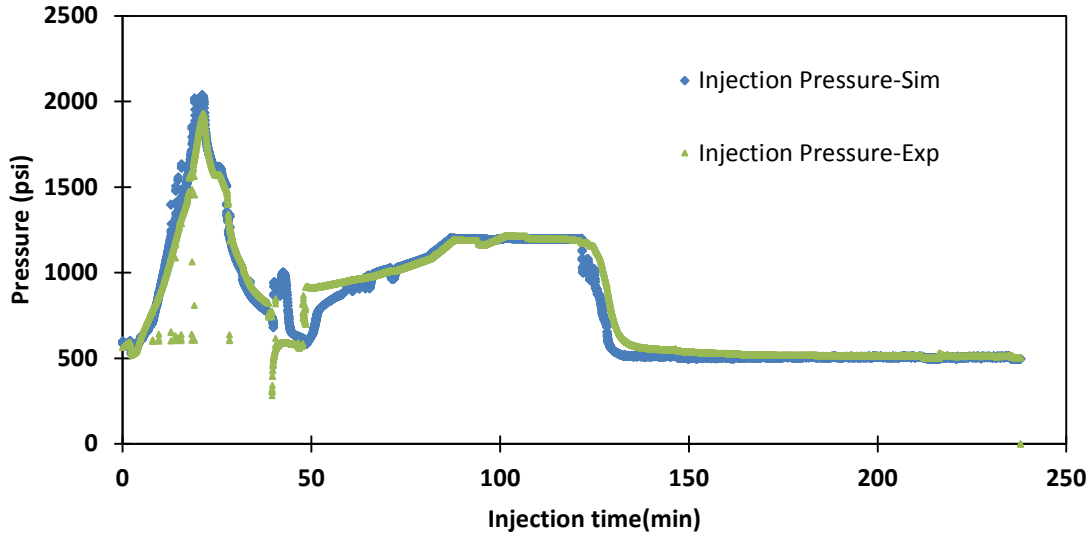


Figure 5.26 Prediction of injection pressure in three-phase system using the Stone's first model to calculate the oil relative permeability

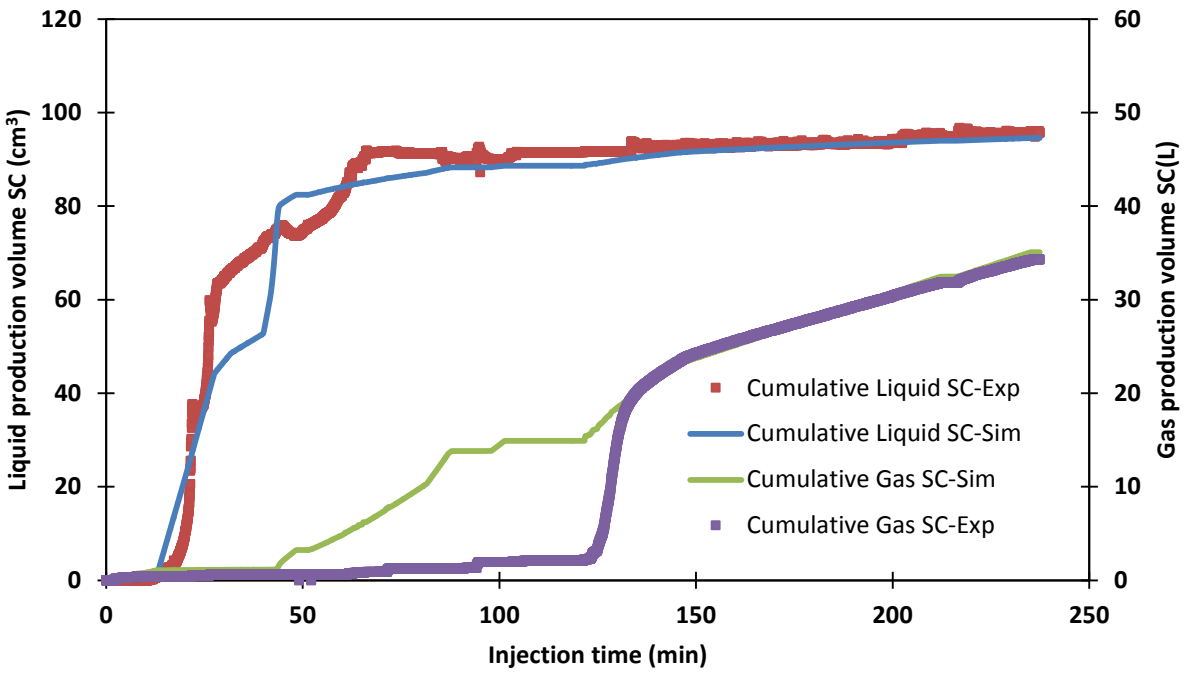


Figure 5.27 Prediction of produced liquid and gas in three-phase system using the Stone's second model to calculate the oil relative permeability

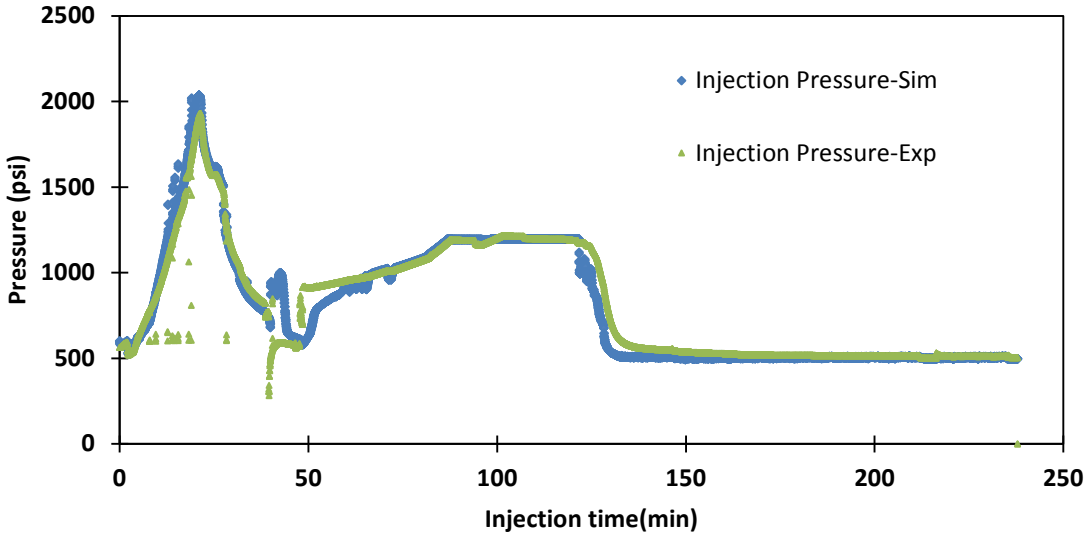


Figure 5.28 Prediction of injection pressure in three-phase system using the Stone's second model to calculate the oil relative permeability

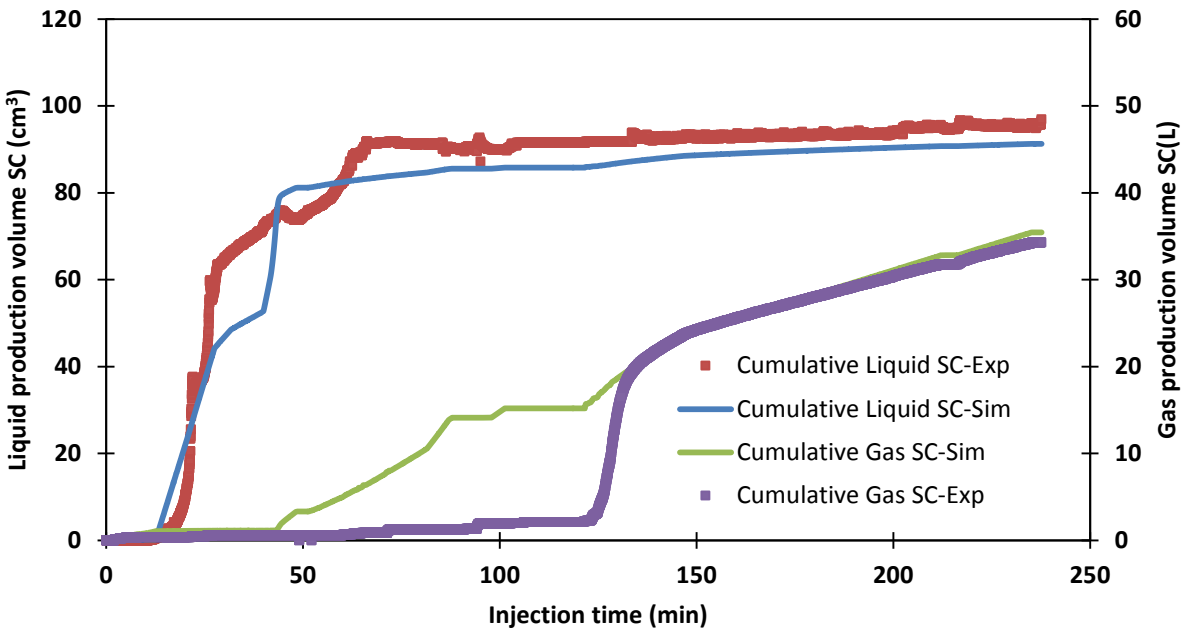


Figure 5.29 Prediction of produced liquid and gas in three-phase system using the Bakers interpolation model to calculate the oil relative permeability

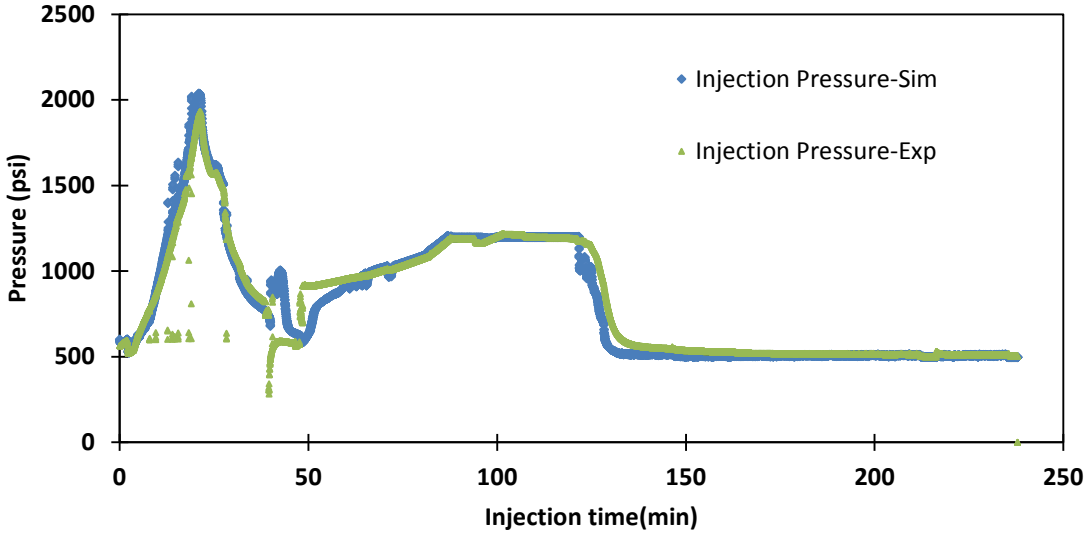


Figure 5.30 Prediction of injection pressure in three-phase system using the Bakers interpolation model to calculate the oil relative permeability

Predicted liquid productions in all three models showed some deviations from experimental values at early stages of the experiment however at later stages the predictions were closer. Stone's second model generated the best prediction for the produced liquid compared to the other two models. Predicted amount of produced gas showed significant deviation at the middle part of the experiment even though the final predicted values were in good agreement with the experimental data. Predictions of produced fluids from all investigated models are plotted in Figure 5.31 and 5.32 for comparison.

Predicted injection pressures from all models did not show significant deviation from experimental values and overall no significant difference were shown by different models.

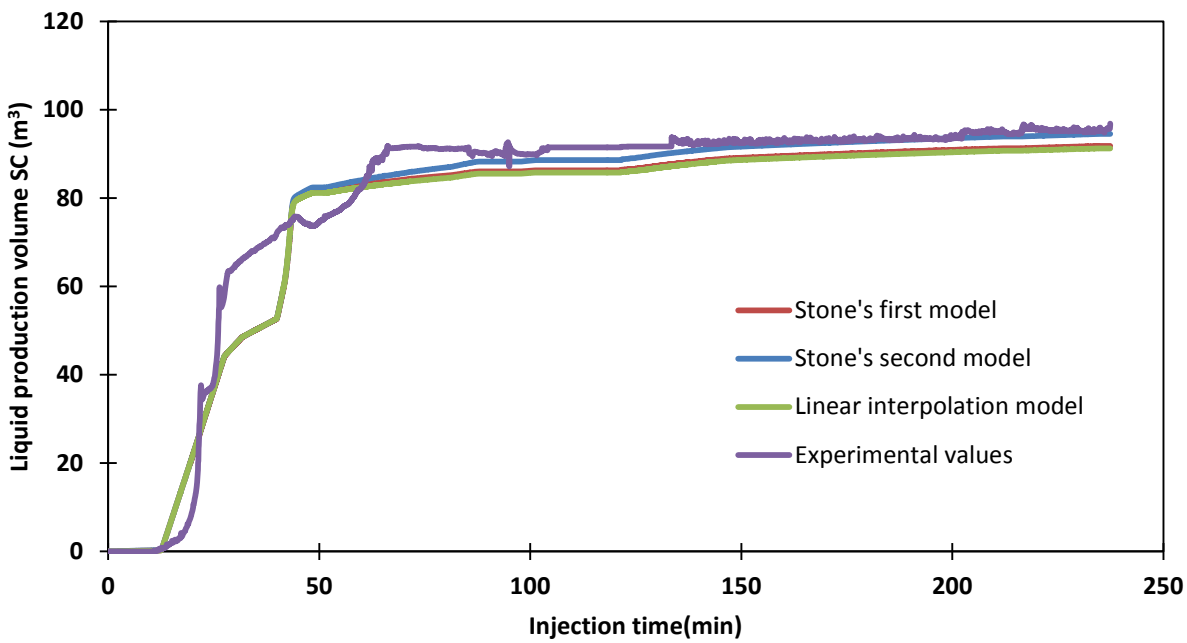


Figure 5.31 Comparison of the predicted values for produced liquid

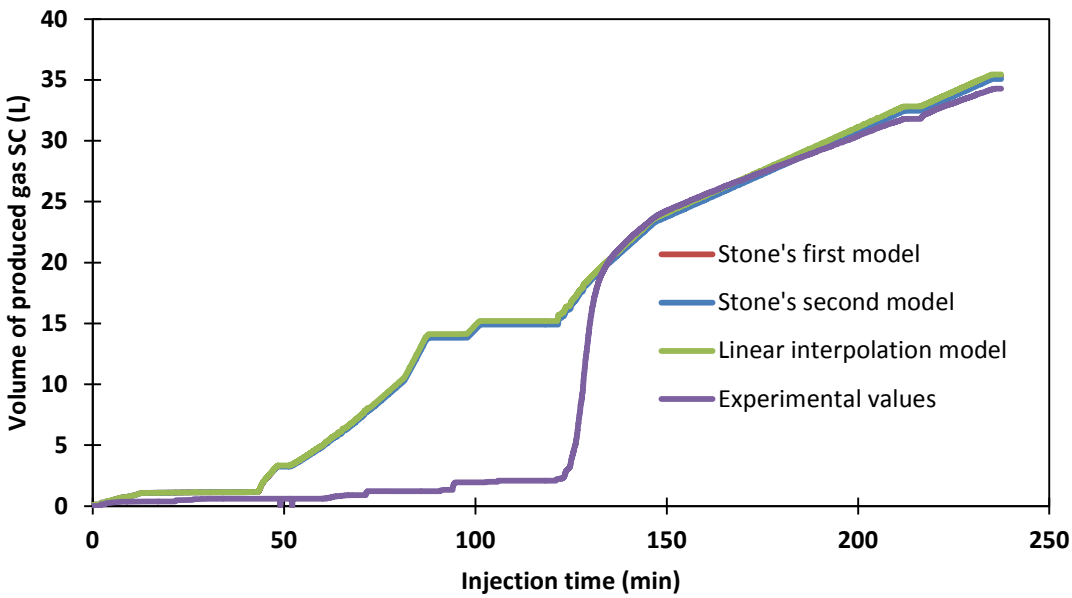


Figure 5.32 Comparison of the predicted values for produced gas

Overall, among the three-phase models which were investigated, the Stone's second model produced the closest results for fluid production. This implies that despite the simple form of the three-phase relative permeability models which were used in calculating the three-phase oil relative permeabilities, the predicted results were in reasonable agreement with experimental data provided that the appropriate two-phase relative permeabilities were employed. As outlined by Stone (1970), in three-phase flow the direction of saturation change for two-phase water/oil and liquid/gas should follow similar paths. The more similar are these directions, the more accurate will be the calculated three-phase oil relative permeability data. Even though it is not feasible to employ this rule for the total part of a complicated hysteresis accounting even for a portion of it would likely generate better approximation.

The order of the injected fluids in the three-phase experiment (Experiment No.5) in the current study includes injection of a slug of oil followed by a slug of water and eventually flooding by gas. As the boundary two-phase water/oil experiment which has the most similar saturation change pattern, the two-phase imbibition water/oil experiment (Experiment No.2) was selected and the corresponding relative permeabilities for water/oil was treated as input for all of the three-phase models. As the boundary values for liquid/gas, the relative permeabilities which were calculated in Experiment No.4 were used. Therefore in all three-phase models, the water relative permeability was assigned to be the calculated water permeability in Experiment No.2 and the gas relative permeability is the same as the calculated gas relative permeability in Experiment No.4.

# CHAPTER 6: CONCLUSION AND RECOMMENDATIONS

## 6.1 Summary

A series of core flood experiments were conducted on an unconsolidated core composed of cleaned Athabasca sand matrix and relative permeabilities of the involved phases were determined. Athabasca bitumen was used as the oil phase and distilled water and nitrogen were used as water phase and gas phase. Dynamic displacement and steady state methods were employed for water/gas experiments while for experiments which involve oil, the history match technique was used to determine relative permeabilities.

An experimental apparatus was designed and fabricated to run core flood tests for two-phase and three-phase water/gas/oil. During the course of this study several modifications and improvements were made on the experimental setup aiming at more accurate raw data by reducing the error sources.

The following situations were investigated in this study:

- Water/gas experiments were conducted on the Athabasca sand pack to study the relative permeability behaviour of water and gas in a typical heavy oil bearing formation which exists in Alberta.
- Drainage water/gas relative permeabilities were determined by using both unsteady-state and steady-state methods. For the imbibition process, only end point saturation and relative permeability were determined.
- To investigate the possible effect of temperature, all water/gas experiments were conducted at three different temperatures of 23 (room temperature), 40 and 80$^{o}$C.

- Oil/water experiments were conducted at 80$^{o}$C starting with a primary drainage process followed by imbibition process and secondary drainage. The goal was to assess the possible hysteresis effects on oil/water relative permeability
- The physical model and fluid model were built into a reservoir simulator. Density and viscosity data for oil were used to build the fluid model. Oil/water relative permeabilities were determined by using the history match technique.
- A secondary drainage process in which the core reaches the residual water saturation, was followed by gas injection till no further liquid production. Relative permeability of gas/liquid was determined through a history match technique.
- Three-phase flow was studied by first injecting a slug of oil into a gas flooded core. Then a slug of water was injected which was followed by continuous gas injection to simulate the three-phase flow inside the sand pack.
- Stone's first and second model and Baker's linear interpolation model were used to calculate the three-phase oil relative permeability in three-phase flow experiment. Two-phase imbibition water/oil and gas/liquid relative permeabilities were used as input for three-phase models to calculate the oil three-phase relative permeability.
- Main contribution of this study include the results for water/gas experiments as there are very few published data on the characteristics of relative permeabilities of water/gas in a sand-pack. The next major contribution is the behaviour of two-phase relative permeabilities in drainage process as well as finding an unusual behaviour for imbibition process. Introducing a modified version of Sigmund-McCaffery model for oil relative permeability in drainage process and setting up a three-phase displacement for heavy oil/water/gas system are other contributions of this study.

## 6.2 Conclusions

- In water/gas experiments, despite a common belief about high gas relative permeability, the relative permeability of gas turned out to be very low compared to the water relative permeability.
- Increase of temperature affects the end point saturations and end point relative permeability of both gas and water in drainage and imbibition processes. For a drainage process residual water saturation decreases at higher temperatures while end point relative permeability of gas gains higher values. However during the imbibition process, endpoint water saturations move toward higher values and water end point relative permeability increases.
- Overall, except for saturations near the end points, no significant shift in water relative permeabilities were observed by increasing temperature to higher values. However gas relative permeability was shifted up slightly at higher temperatures.
- In oil/water drainage experiments, resulting relative permeabilities from history match technique, were fitted to some of the available models in literature. Among the examined models the relative permeability model proposed by Sigmund and McCaffery (1979) produced a good fit for water relative permeability but showed relatively poor fit for oil relative permeability. By applying a minor modification in proposed model for oil, the quality of fit was improved significantly.
- Among the examined models, non of them were able to fit the determined shape of the relative permeability of oil in imbibition process.

- Overall, for oil/water systems, drainage end point relative permeability of water was around two orders of magnitude lower than the end point oil relative permeability.
- Calculated relative permeabilities for the imbibition process indicated a strong hysteresis effect on oil relative permeability to the extent that the oil relative permeability curve passes through an inflection point and changes its slope.
- Hysteresis was found to exist in water relative permeability when the direction of water saturation changes during imbibition and drainage process.
- Overall, the individual phase relative permeability was higher when its saturation was increasing than when decreasing.
- Comparison of the calculated oil/water relative permeabilities with available data in literature showed both similarity and deviation. While the shape of the water relative permeabilities were convex for either directions of saturation change, oil relative permeabilities were concave for drainage and a mixed pattern for imbibition. This shape complies with some similar published works while it contradicts with others.
- Residual oil saturation was close to the typical values which were reported by different authors even though the calculated residual water saturation in the current study is lower than the corresponding values in literature.
- Predicted values for oil and water production were in good agreement with experimental results for all drainage and imbibition oil/water experiments.
- Gas/liquid relative permeabilities for gas injection into an oil-flooded core, showed low gas relative permeability compared to the liquid relative permeabilities by around two orders of magnitude. These relative permeabilities resulted in a close match for the

produced liquid even though the gas production was slightly over predicted at higher gas saturations.

- In three-phase oil/water/gas experiments, two-phase water/oil and liquid/gas relative permeabilities were used to calculate the three-phase oil relative permeabilities through employing the built-in three-phase models in CMG STARS. Among the three examined models, Stone's second model produced the best prediction for liquid production and late time gas production even though the prediction of all of the models showed a significant deviation from experimental gas production during the early and middle time of the flood. Results for predicted injection pressures by all models did not show a significant difference and overall they were in close agreement with experimental values.
- Calculation of three-phase relative permeabilities from a combination of two-phase relative permeability may produce reasonable results provided that the two-phase relative permeabilities were chosen in accordance with the direction of saturation change in three-phase flow as much as feasible. Having a set of accurate two-phase relative permeabilities are crucial to get the best possible prediction from three-phase models which use a combination of two-phase data to estimate the three-phase relative permeabilities.

### 6.3 Recommendations for future work

Based on the observations made during the course of this study the following recommendations are made:

- To gain a better insight into the actual behaviour of relative permeabilities within the high temperature zone which exists downstream of the combustion front during i*n situ* combustion, one must conduct high temperature floods. Especially to replicate the steam zone which is preceded by a hot water bank, a steam flood would produce more accurate insights into the relative permeability behaviour in a typical *in situ* combustion process.
- During a typical *in situ* combustion process, the gas phase is a flue gas which consists of various components such as nitrogen, carbon dioxide, carbon monoxide and oxygen. During a core flood experiment, using a gas phase which consists of real flue gas components, would generate more complexity however it would generate more realistic replication of a real combustion process.
- Running a history match on available field data to determine relative permeabilities after having preliminary insight from the current results, would help to gain a more realistic understanding of relative permeability behaviour.
- Direction of saturation change has very significant impact on relative permeability of the various phases moving in a porous medium. Investigating other existing saturation hysteresis which exists in a typical combustion or hybrid process would produce a better replication of these processes.
- Three-phase relative permeability models which rely on two-phase data to calculate the three-phase relative permeabilities, are simple tools to have an initial estimate of the hard-to-determine three-phase relative permeabilities. Using three-phase flow models other than Stone's models, is required in order to better match the fluid production and pressure drop.

## REFERENCES


Adams, D. M. *Experiences With Water Flooding Lloydminster Heavy-Oil Reservoirs*. Journal of Petroleum Technology, 34, 08, 1982

*Athabasca Oil Sands*, SPE Reservoir Engineering Journal Volume 5, Number 1, February 1990, Pages 25-32.

Aziz, K., and Settari, A., *Petroleum Reservoir Simulation*, Applied Science Publishers Ltd., London, 1979

Baker, L. E., *Three-Phase Relative Permeability Correlations*. SPE Enhanced Oil Recovery Symposium, 16-21 April, Tulsa, Oklahoma, 1988

Bennion, D. B., Sarioglu, G., Chan, M. Y. S., Hirata, T., Courtnage, D., and Wansleeben, J., *Steady-State Bitumen-Water Relative Permeability Measurements at Elevated Temperatures in Unconsolidated Porous Media*., Annual Technical Meeting, May 9 - 12, Calgary, Alberta, 1993

Bennion, D. B., Thomas, F. B., Schulmeister, B. and Ma, T., *A Correlation of the Low and High Temperature Water-Oil Relative Permeability Characteristics of Typical Western Canadian Unconsolidated Bitumen Producing Formations,* Canadian International Petroleum Conference, 13-15 June, Calgary, Alberta, 2006

Bentsen R.G., *Conditions under which the Capillary Term may be Neglected*, JCPT, PP 25-30, 1978

Buckley, S. E. and Leverett, M. C., *Mechanism of fluid displacement in sands* ,Trans. AIME, 146,107, 1942

Closmann, PJ. Waxman, M.H. and Deeds, C.T., *Steady-State Tar/Water Relative Permeabilities in Peace River Cores at Elevated Temperature*, Paper SPE 14227, 60 Anniversary Technical Conference and Exhibition, Las Vegas, Nevada, Sep. 22-25, 1985

Curvers, J. and van den Engel, P., *Gas Chromatographic Method for Simulated Distillation up to a Boiling Point of 750°C Using Temperature-Programmed Injection and High Temperature Fused Silica Wide-Bore Columns*, J. High Resolution Chromatography, 12, 16-22, 1989

Donaldson, E.C and Dean, G.W., *Two- and Three-Phase Relative Permeability Studies,* US Bureau of Mines, Report No. 6826, 1966

Fayers, F. J., and Matthews, J. D., *Evaluation of Normalized Stone's Methods for Estimating Three-Phase Relative Permeabilities*, SPE Journal, 24, 02, 1984

Frizzell, D.F., *Analysis of 15 Years of Thermal Laboratory Data: Relative Permeability and Saturation Endpoint Correlations for Heavy Oils*, paper SPE 20528 presented at the SPE Annual Technical Conference and Exhibition, 23-26 September, 1990, New Orleans, Louisiana

Greaser G.R. and Shore R.A., *Steam Flood Performance in the Kern River Field*, SPE/DOE 8834, presented at the 1980 SPE/DOE Joint Enhanced Oil Recovery Symposium, Tulsa, April 20-23

Honarpour M., Koederitz L. and Harvey A.H., *Relative Permeability of Petroleum Reservoirs*, CRC Press, Inc, 1986, ISBN 9780849357398

Johnson, E. F., Bossler, D. P., and Naumann, V. O., *Calculation of Relative Permeability From Displacement Experiments*, Trans. AIME, 216, 310, 1959

Kyte, J.R. and Rapoport, L.A., *Linear Water Flood Behaviour and End Effects in Water Wet Porous Media*, Trans. AIME 213, pp 423-426, 1958.

Leung L.C., *Numerical Evaluation of the Effect of Simultaneous Steam and Carbon Dioxide Injection on the Recovery of Heavy Oil* , Journal of Petroleum Technology, 35, 09, 1983

Leverett, M. C., *Capillary Behavior in Porous Solids*, Trans. AIME, 142, 152, 1941

Leverett, M.C., *Flow of Oil-Water Mixtures through Unconsolidated Sands*, Trans., AIME 132, 381-403, 1939

Maini B.B. and Batycky J.P., *Effect of Temperature on Heavy Oil/Water Relative Permeabilities in Horizontally and Vertically Drilled Core Plugs*, Journal of Petroleum Technology, Vol. 37, No. 9, pp 1500-1510, 1985

Maini B.B. and Okazawa T., *Effect of Temperature on Heavy Oil-Water Relative Permeability of Sands*, Journal of Canadian Petroleum Technology, May 1987

McCaffery, F. G. and Bennion, D. W., *The Effect of Wettability on Two-Phase Relative Permeabilities*. Journal of Canadian Petroleum Technology, 10, 42, 1974

Moore, R.G., Ursenbach, M.G. and Mehta, S.A., *Air Injection in Heavy Oil Reservoirs-A Process Whose Time Has Come (Again)*, presented in CIPC Conference, 2007, Calgary, Alberta, Canada

Morse, R. A., Terwilliger, P. L., and Yuster, S. T., *Relative Permeability Measurements on Small Samples,* Oil and Gas J. , 46, 109, 1947

Polikar, M., Farouq Ali, S.M. and Puttagunta, V.R., *High-Temperature Relative Permeability's for Athabasca Oil Sands,* SPE Reservoir Engineering, 5, 01, 1990

Saraf, D. N. and Fatt, I., *Three-Phase Relative Permeability Measurement Using A Nuclear Magnetic Resonance Technique For Estimating Fluid Saturation*, Soc. Pet . Eng. J. 9 ,235. 1967

Saraf, D. N. and McCaffery, F. G., *Two- and Three-Phase Relative Permeabilities: A Review*, Petroleum Recovery Institute Report #81-8, Calgary, Alberta, Canada, 1982

Sarem, A.M., *Three-Phase Relative Permeability Measurement by Unsteady State Method*. Trans. AIME, 237, 199-205, 1966,

Sayegh, S. G. and Maini, B. B., *Laboratory Evaluation Of The $CO_2$ Huff-N-Puff Process For Heavy Oil Reservoirs*, Journal of Canadian Petroleum Technology, 23, 03, 1984

Settari, A. and Raisbeck, J.M., *Analysis and Numerical Modeling of Hydraulic Fracturing During Cyclic Steam Stimulation in Oil Sands*, Journal of Petroleum Technology, Volume 33(11), 2201-2212, 1981

Sigmund P.M. and McCaffery F.G., *An Improved Unsteady-State Procedure for Determining the Relative-Permeability Characteristics of Heterogeneous Porous Media*, SPE Journal, Feb 1979, 15-28.

Stone H.L., *Probability Model for Estimating Three-Phase Relative Permeability*, Journal of Petroleum Technology, 2, 214, 1970.

Stone, H.L., *Estimation of Three-Phase Relative Permeability and Residual Oil Data*, Journal of Canadian Petroleum Technology, 12, 53, 1973.

Tang, G.Q. and Firoozabadi, A., *Gas and Liquid-Phase Relative Permeabilities for Cold Production from Heavy Oil Reservoirs,* SPE Annual Technical Conference and Exhibition, 3-6 October, Houston, Texas, 1999

Treiber, L. E., Archer, D. L. and Owens, W. W., *A Laboratory Evaluation of the Wettability of Fifty Oil Producing Reservoirs*, SPE Journal , 12,6, 1972

Waxman, M.H., Closmann, PJ. and Deeds, C.T., *Peace River Tar Flow Experiments Under In Situ Conditions*, paper SPE 9511 presented at the 1980 SPE Annual Technical Conference and Exhibition, Dallas, Sept. 21-24.

Welge H. J . R. *A Simplified Method for Computing Recovery by Gas or Water Drive*, Trans .AIME 195, 91, 1952.

## APPENDIX 1: EQUATIONS OF BUILT-IN THREE-PHASE RELATIVE PERMEABILITY MODELS IN CMG STARS

CMG STARS was employed in current study to simulate the core flood experiments and to determine the relative permeabilities of two-phase water/oil and gas/liquid by history match technique. Three-phase oil permeabilities were determined by using the built-in models which are available in STARS. The built-in models include Stone's first and second model and Baker's linear interpolation model. The equations which were involved in Stone's models were summarized in this section by using the manual of STARS (CMG STARS manual, 2012).

### Stone's first model

Three-phase oil relative permeability can be calculated by using the Stone's first model. This model combines the two-phase oil-water and liquid-gas relative permeabilities to determine the three-phase oil relative permeability and it requires two assumptions:

1- Connate gas saturation is zero $S_{gc} = 0$
2- Minimal oil saturation $S_{om}$ varies between $S_{orw}$ and $S_{org}$. This option is available only when $S_{wc}$ is included in the liquid saturation.

The following correlations are used to calculate the three-phase oil relative permeability

$$k_{ro} = k_{row} * k_{rog} * S_{eo} / (k_{rocw} * S_{el} * (1 - S_{ew}))$$

$$S_{eo} = (S_o - S_{om}) / (1 - S_{wc} - S_{om})$$

$$S_{ew} = (S_w - S_{wc}) / (1 - S_{wc} - S_{om})$$

$$S_{el} = 1 - S_g/(1 - S_{wc} - S_{om})$$

For two extreme cases of $S_g = 0$ and $S_w = S_{wc}$, the equation reduces to two-phase data and in order to fulfill this condition $k_{rocw} = k_{row}(S_w = S_{wc}) = k_{rog}(S_g = 0)$ to ensure that $k_{ro} = k_{row}$ when $S_g = 0$ and that $k_{ro} = k_{rog}$ when $S_w = S_{wc}$.

The "minimal" value of the oil saturation which is denoted by $S_{om}$, is calculated by a linear function proposed by Fayers and Matthews (1984):

$$S_{om}(S_g) = (1 - a(S_g)) * S_{orw} + a(S_g) * S_{org},$$

where

$$a(S_g) = S_g / (1 - S_{wcrit} - S_{org})$$

**Stone's Model II (modified)**

According to Stone's second model it is assumed that in the three-phase system the gas relative permeability is a function of gas saturation only and it is equal to the gas relative permeability in the two- phase liquid/gas system. In the same manner the water relative permeability is equal to the two-phase water/oil system and it depends only on water saturation.

The three-phase oil relative permeability is calculated using the modification of Settari and Aziz (1979). When liquid phase contains $S_{wc}$ :

$k_{ro}$= $k_{rocw}$ * ( ($k_{row}/k_{rocw} + k_{rw}$) * ($k_{rog}/k_{rocw} + k_{rg}$) - $k_{rw}$ - $k_{rg}$)

where

$k_{rocw}$= $k_{row}(S_w=S_{wc}) = k_{rog}(S_g=0)$ to ensure that $k_{ro} = k_{row}$ when $S_g = 0$ and that $k_{ro} = k_{rog}$ when $S_w = S_{wc}$.

For the case that liquid phase does not contain $S_{wc}$:

$k_{ro}$= $k_{romax}$ * ( ($k_{row}/k_{romax} + k_{rw}$) * ($k_{rog}/k_{romax} + k_{rg}$) - $k_{rw}$ - $k_{rg}$)

where

$k_{romax}$= $k_{row}(S_w=0) = k_{rog}(S_g=0)$ to ensure that $k_{ro} = k_{row}$ when $S_g = 0$ and that $k_{ro} = k_{rog}$ when $S_w = 0$.